



National Library
of Canada

Bibliothèque nationale
du Canada

Canadian Theses Service

Services des thèses canadiennes

Ottawa, Canada
K1A 0N4

CANADIAN THESES

THÈSES CANADIENNES

NOTICE

The quality of this microfiche is heavily dependent upon the quality of the original thesis submitted for microfilming. Every effort has been made to ensure the highest quality of reproduction possible.

If pages are missing, contact the university which granted the degree.

Some pages may have indistinct print especially if the original pages were typed with a poor typewriter ribbon or if the university sent us an inferior photocopy.

Previously copyrighted materials (journal articles, published tests, etc.) are not filmed.

Reproduction in full or in part of this film is governed by the Canadian Copyright Act, R.S.C. 1970, c. C-30.

**THIS DISSERTATION
HAS BEEN MICROFILMED
EXACTLY AS RECEIVED**

AVIS

La qualité de cette microfiche dépend grandement de la qualité de la thèse soumise au microfilmage. Nous avons tout fait pour assurer une qualité supérieure de reproduction.

S'il manque des pages, veuillez communiquer avec l'université qui a conféré le grade.

La qualité d'impression de certaines pages peut laisser à désirer, surtout si les pages originales ont été dactylographiées à l'aide d'un ruban usé ou si l'université nous a fait parvenir une photocopie de qualité inférieure.

Les documents qui font déjà l'objet d'un droit d'auteur (articles de revue, examens publiés, etc.) ne sont pas microfilmés.

La reproduction, même partielle, de ce microfilm est soumise à la Loi canadienne sur le droit d'auteur, SRC 1970, c. C-30.

**LA THÈSE A ÉTÉ
MICROFILMÉE TELLE QUE
NOUS L'AVONS REÇUE**

THE UNIVERSITY OF ALBERTA

APPLICATION OF ^{31}P NMR TO A STUDY OF TUMOR METABOLISM

BY

C

CYNTHIA ARLENE STEWART

A THESIS

SUBMITTED TO THE FACULTY OF GRADUATE STUDIES AND RESEARCH
IN PARTIAL FULFILMENT OF THE REQUIREMENTS FOR THE DEGREE
OF MASTER OF SCIENCE

DEPARTMENT OF APPLIED SCIENCES IN MEDICINE

EDMONTON, ALBERTA

FALL 1986

Permission has been granted to the National Library of Canada to microfilm this thesis and to lend or sell copies of the film.

The author (copyright owner) has reserved other publication rights, and neither the thesis nor extensive extracts from it may be printed or otherwise reproduced without his/her written permission.

L'autorisation a été accordée à la Bibliothèque nationale du Canada de microfilmer cette thèse et de prêter ou de vendre des exemplaires du film.

L'auteur (titulaire du droit d'auteur) se réserve les autres droits de publication; ni la thèse ni de longs extraits de celle-ci ne doivent être imprimés ou autrement reproduits sans son autorisation écrite.

ISBN 0-315-32298-5

THE UNIVERSITY OF ALBERTA

RELEASE FORM

NAME OF AUTHOR	CYNTHIA ARLENE STEWART
TITLE OF THESIS	APPLICATION OF ³¹ P NMR TO A STUDY OF TUMOR METABOLISM
DEGREE FOR WHICH THESIS WAS PRESENTED	MASTER OF SCIENCE
YEAR THIS DEGREE GRANTED	FALL 1986

Permission is hereby granted to THE UNIVERSITY OF ALBERTA LIBRARY to reproduce single copies of this thesis and to lend or sell such copies of this thesis for private, scholarly, or scientific research purposes only.

The author reserves other publication rights, and neither the thesis nor extensive extracts from it may be printed or otherwise reproduced without the author's written permission.

(SIGNED) *C. Stewart*

PERMANENT ADDRESS:

85 Gormley Avenue
Toronto, Ontario
M4V 1Y9.

Dated *June 11* 1986.

THE UNIVERSITY OF ALBERTA
FACULTY OF GRADUATE STUDIES AND RESEARCH

The undersigned certify that they have read, and recommend to the Faculty of Graduate Studies and Research, for acceptance a thesis entitled APPLICATION OF ^{31}P NMR TO A STUDY OF TUMOR METABOLISM submitted by CYNTHIA ARLENE STEWART in partial fulfilment of the requirements for the degree of MASTER OF SCIENCE.

..... *Peter S. Fues*
Supervisor

..... *A. H. Barrett*

..... *Richard G. Snyder*

..... *Brian D. Sykes*

Dated *June 11* 1986.

To Don, who was good enough to wait.

ABSTRACT

A number of investigators have employed ^{31}P NMR spectroscopy to monitor cellular metabolism in vivo. A major weakness of previous investigations is the accurate assignment of the acquired spectrum to a specific region within the organ or tissue.

Work described in this thesis substantially overcomes this weakness by making use of surgical exposure on the one hand and refinements in the focusing of rf excitation and acquisition on the other. Having established the veracity of the NMR localization techniques, it then became possible to develop a tumor model and evaluate the response to metabolic insults in a far more precise way than had previously been possible using ^{31}P NMR spectroscopy.

The experimental strategy for identifying the localized region of NMR signal exploited a combined approach employing depth pulse localization sequences (13) with radiofrequency surface coils, in addition to proton superposition images of the sensitive volume. The superposition images produced by the surface coil excitation pulse sequences and by conventional imaging sequences using a circumscribing coil enabled us to "see" and to calibrate the region of tissue from which our spectra were obtained.

Employing the kidney model originally described by P. Gullino et al (54), Walker sarcoma 256 cells were implanted in the rat kidney just under the capsule and were maintained ~~in vivo~~-isolated. After approximately 15 days, the tumor cells replaced most of the kidney tissue resulting in a tumor mass connected to the host only by the vascular pedicle. The kidney/tumor was surgically exposed for NMR measurements with the surface coil placed directly adjacent to the kidney or tumor.

The data, showing the time course for the changes in the relative concentrations of ^{31}P metabolites and pH, were obtained at a depth of 2-4mm from the surface of the kidney/tumor. The spectra obtained from this depth were correlated with histological studies which indicated the extent of tumor growth.

The experimental protocol consisted of the comparison of in vivo ^{31}P NMR spectra for normal rat kidney with those from a tumor model in the rat kidney as a function of various influences. For example spectra were obtained from a rat kidney implanted with tumor cells at various stages of tumor growth. The effect of chemotherapy and ischemia on tumor energy metabolism were examined and compared to similar effects on normal kidney.

Production of ischemia in the normal rat kidney resulted in a decrease in ATP levels, with a corresponding increase in P_i and decrease in renal pH,

with recovery to control values within thirty minutes. The kidney implanted with tumor cells when rendered ischemic demonstrated a decrease in pH and ATP levels with no subsequent recovery to control values. Progressive tumor growth typically resulted in an acidotic shift in pH, an increase in Pi and a decrease in the high energy phosphates. Treatment with cyclophosphamide resulted in a reversal of the spectral characteristics to a more "aerobic like" state, i.e. an increase was observed in tumor pH and in the relative concentrations of ATP, PCr, and PME, together with a slight decrease in Pi when compared with spectra obtained prior to the treatment.

ACKNOWLEDGEMENTS

I wish to thank my supervisor Dr. P.S. Allen for his guidance and support throughout this project, and also for his time spent reviewing this thesis. I have gained much from his experience in scientific research and writing.

Also many thanks to Dr. D.P. Boisvert for his expert instruction in the surgical techniques in addition to his helpful insights into my research.

I owe much debt to Chris Hanstock who guided me through the initial stages of this project, assisted with most of the experiments, and wrote the pulse programs. He was a constant source of inspiration, and ideas, and kept me amused during marathon NMR sessions with his wonderful sense of humor.

A special thanks to Andrew Lunt who was always ready to lend a helping hand with frequent instrumental and software problems.

Technical assistance from Dan Doran was greatly appreciated.

I am also grateful to Fred Brauer for reading the manuscript and offering constructive criticisms.

I can't begin to thank the remaining members of the group who have also helped me in various ways both scientifically and socially; Erich Treiber, Steven Knudsen, Dan Gheorghiu, Manuel Castro, Craig Land, Dave

Philips, Bill Allen, and Evan Peers.

Many thanks to Perry d'Obrenan for his assistance in the preparation of the figures contained in this thesis, and to Sylvia Crowell for typing the figure legends.

Financial support provided by the Alberta Heritage Foundation for Medical Research in the form of a studentship is gratefully acknowledged.

TABLE OF CONTENTS

CHAPTER	PAGE
-1. INTRODUCTION	
1.1. ³¹ P NMR spectroscopy	1
1.1.1 Theory	2
1.1.2 Longitudinal and transverse relaxation	8
1.1.3 Chemical shielding	16
1.1.4 Indirect spin-spin coupling	19
1.1.5 Assignment	20
1.1.6 Concentration	24
1.1.7 Measurement of intracellular pH	27
1.2 The application of <u>in vivo</u> ³¹ P NMR to study energy metabolism	31
1.3 Cellular energy metabolism	35
1.4 Tumor energy metabolism	43
1.5 Tumor model	51
1.6 NMR localization techniques	55
1.6.1 DEPTH pulse sequences	60
2. METHODS	
2.1 NMR techniques	65
2.2 Determination of intracellular pH by ³¹ P NMR	69
2.3 Preparation of tumor cells	72
2.4 Kidney isolation and tumor implantation	73
2.5 Production of ischemia in the rat kidney	74
2.6 Chemotherapy	74
2.7 Histology	75

CHAPTER	PAGE
3. RESULTS AND DISCUSSION	
3.1 Development of the tumor model	76
3.2 Investigation of the spatial localization characteristics of depth pulse sequences.	80
3.3 Determination of saturation factors to apply to <u>in vivo</u> ^{31}P NMR spectra.	90
3.4 Monitoring untreated tumor growth in the rat kidney by ^{31}P NMR spectroscopy.	102
3.5 Monitoring ischemia in normal rat kidney by ^{31}P NMR spectroscopy.	122
3.6 Monitoring ischemia in the rat kidney implanted with tumor cells by ^{31}P NMR spectroscopy.	133
3.7 Monitoring tumor response to chemotherapy by ^{31}P NMR.	139
4. CONCLUSIONS	148
REFERENCES	153

List of Tables

Table		Page
1.1	Types of component pulses used in a depth pulse sequence together with their individual effects.	64
3.1	Longitudinal relaxation times reported for ^{31}P metabolites <u>in vivo</u> (sec).	96
3.2	Mean and standard deviation for the saturation factors.	99
3.3	Changes in the ATP/Pi intensity ratio and pH with tumour growth.	115

LIST OF FIGURES

Figure		Page
1.1	Vector representation of the nuclear magnetic moments.	5
1.2	Precession of nuclear magnetic moments about B_0 .	5
1.3	Representative chemical shift values.	18
1.4	Assignment of resonances in the ^{31}P NMR spectrum of Walker sarcoma cells implanted in the rat kidney.	22
1.5	Chemical structures of phosphate metabolites detected by ^{31}P NMR.	33
1.6	ATP production from glycolysis and oxidative phosphorylation.	37
1.7	Schematic representation of the cycle of ATP production and utilization.	42
1.8	Examples of the differences in the relative concentration of ^{31}P metabolites in different tissues.	52
1.9	Surface coil images of the distribution of signal intensity generated by a single pulse relative to the rf coil.	58
1.10	Plots of ^{31}P NMR signal intensity versus pulse length.	62
2.1	Pulse sequence employed to obtain surface coil images.	68
2.2	The chemical shifts of the ^{31}P NMR signals of 10mM ATP in the presence of 5mM MgCl_2 plotted as a function of pH.	70
2.3	Variation of chemical shift of inorganic phosphate (P_i) with solution pH at 37° .	71

Figure		Page
3.1	Plots of signal intensity of the PO_4 phantom sample (1cm from the surface coil) versus pulse length for a single pulse and depth pulse sequences $2\theta(+X); \theta; 2\theta(+x, +y)$, and $2\theta(+x); \theta; [2\theta(+x, +y)]_2$.	82
3.2	Surface coil images demonstrating the ability of the depth pulse sequence $2\theta(+x); \theta; [2\theta(+x, +y)]_2$ to narrow the excitation bands in the sample.	84
3.3	Calibration of the penetration depth for the 8 X 10mm ^{31}P surface coil.	86
3.4	Demonstration of suppression of high flux signals (270° and 450°) using depth pulse sequence $(\theta/5); (\theta/3); \theta(+X); AQ(+)$.	87
3.5	Surface coil images demonstrating the ability of the depth pulse sequence $(\theta/3); \theta/5; \theta(+X); AQ(+)$ to suppress high flux signals (270° and 450°).	89
3.6	Superimposed images of a transverse section of the abdomen and exposed kidney indicating the region (2mm depth) from which the ^{31}P spectra were obtained.	92
3.7	Superimposed images of a transverse section of the abdomen and exposed kidney indicating the region (just along the surface of the kidney) from which the ^{31}P spectra were obtained.	94
3.8	Signal intensities obtained for ^{31}P metabolites in the rat kidney employing the depth pulse sequence $(\theta/3); (\theta/5); \theta(+X); AQ(+)$ with repetition intervals of 1.0 sec and 20 sec.	101
3.9	Changes in ^{31}P metabolites with tumor growth (2-4mm depth).	103
3.10	Histological section of normal rat kidney and rat kidney one day after implantation with tumor cells.	105
3.11	Histological sections of rat kidney 3 days and 6 days after implantation of tumor cells	108

Figure		Page
3.12	Histological sections of rat kidney 9 days and 15 days after implantation of tumor cells.	112
3.13	Variation in intracellular pH with tumor growth.	113
3.14	Variation in the NTP_{β}/P_i ratio of the Walker sarcoma with tumor growth.	116
3.15	Time course of the changes in ^{31}P metabolites in the rat kidney (2-4mm depth) during ischemia and recovery.	125
3.16	Changes in the signal intensity of the ATP and Pi resonances during ischemia and recovery.	126
3.17	Changes in intracellular pH in the normal rat kidney during periods of ischemia and recovery.	128
3.18	^{31}P spectra of rat kidney to show changes in metabolite concentrations at different depths from the surface coil.	130
3.19	^{31}P spectra of rat kidney at different depths below the surface of the kidney following infarction.	134
3.20	Changes in the ^{31}P metabolites in the rat kidney implanted with tumor cells during ischemia and recovery.	136
3.21	Changes in the intracellular pH in the rat kidney implanted with tumor cells during ischemia and recovery.	137
3.22	Time course of the changes in ^{31}P metabolites in the rat kidney implanted with tumor cells after administration of a single dose of cyclophosphamide (150mg/kg I.V.).	142
3.23	The NTP_{β}/P_i ratio of Walker sarcoma as a function of time after treatment with cyclophosphamide (150mg/kg I.V.).	143
3.24	Variation in pH of the tumor after treatment with cyclophosphamide.	144

ABBREVIATIONS

ADP	Adenosine diphosphate
AMP	Adenosine monophosphate
ATP	Adenosine triphosphate
BCNU	1.3. bis(2chloroethyl)-1-nitrosourea
CPMG	Carr-Purcell-Meiboom-Gill
DNA	Deoxyribonucleic acid
DNP	Dinitrophenol
DRESS	Depth resolved surface coil spectroscopy
EGF	Epidermal growth factor
FADH	Flavin adenine dinucleotide
FID	Free induction decay
GPC	Glycerolphosphorylcholine
GPE	Glycerolphosphorylethanolamine
HE	Hematoxylin-eosin
HPLC	High pressure liquid chromatography
ISIS	Image selected <u>in vivo</u> spectroscopy
LDH	Lactate dehydrogenase
NADH	Nicotinamide adenine dinucleotide
PBS	Phosphate buffered saline
PC	Phosphorylcholine
PCr	Phosphocreatine
PD	Phosphodiester
PE	Phosphorylethanolamine
Pi	Inorganic phosphate
PME	Phosphomonoesters

rf Radiofrequency
RNA Ribonucleic acid
S/N Signal to noise ratio
SPARS Spatially resolved spectroscopy
 T_1 Spin-lattice relaxation time
 T_2 Spin-spin relaxation time
TCA Tricarboxylic acid cycle
TE Time to echo
TR Repetition time
UDPG Uridine diphosphoglucose
VSE Volume selective excitation

1. INTRODUCTION

1.1 ^{31}P NMR SPECTROSCOPY

For the past four decades nuclear magnetic resonance (NMR) spectroscopy has been widely used to provide information about processes at the atomic level. The magnetic resonance spectra contain a great deal of information about molecular structure, molecular interactions and about molecular motion. In recent years advances in instrument design have resulted in the application of NMR to investigations of cellular and tissue metabolism. In NMR studies of intact tissue relatively little molecular structural information is obtained from the signals. Instead, the spectra provide a means of identifying the presence of certain metabolites, evaluating their concentration and intracellular environment, and by monitoring the change in signal intensity with time, it is possible to follow the interconversions of the various metabolites. NMR has emerged as a novel method for studying the metabolism and, through production of NMR images, the anatomical structure of intact biological systems.

1.1.1 THEORY

Nuclear magnetic resonance is a branch of spectroscopy. In general terms, spectroscopy can be described as the study of the nature of the energy levels of material systems and of the transitions induced between them on absorption or emission of electromagnetic radiation (62). The energy absorbed or emitted by the sample is detected, and the output of the detector is displayed as a function of the frequency of the radiation or in the case of NMR, the magnetic field. This output display is referred to as the spectrum. More specifically, NMR spectroscopy involves the magnetic energy of the nuclei when they are placed in a magnetic field and the transitions that occur after absorption of radiofrequency radiation. The frequencies characteristic of NMR are in the radiofrequency region of the electromagnetic spectrum (typically in the range 1-500MHz) (42).

^{31}P nuclei possess a nuclear spin $I=1/2$, where I is the nuclear spin quantum number, and as a result are magnetic dipoles. When placed in a static, uniform, magnetic field (B_0) they orient themselves into one of two allowed orientations (parallel or anti-parallel) to the applied magnetic field. These two orientations correspond to two energy levels, the energy difference (ΔE), between which is:

$$\Delta E = \{h\gamma/2\pi\}B_0 \quad (1)$$

where h is Planck's constant, B_0 is the magnetic field strength, and γ is the nuclear gyromagnetic ratio which is a constant characteristic of each individual nuclear species (38). In thermal equilibrium the nuclei are distributed among the energy levels according to a Boltzman population-distribution. The population of the lower energy level is in excess because for this classical distribution, the probability of occupying an energy level decreases monotonically and exponentially with increasing energy.

Although the features of NMR are rigorously explained only by a quantum mechanical model, a number of properties can be visualized through a classical treatment which gives results equivalent to the quantum mechanical model. This is particularly true of the equation of motion of the net magnetization.

For a single nuclear spin system we can represent the nuclear magnetic moment by a vector. Since in the NMR experiment the sample contains a large number of magnetic nuclei, this ensemble of identical magnetic moments can be represented by the vector resultant of the collection of individual vectors. The nuclei in each of the two energy levels will give rise to a resultant magnetization vector either parallel or antiparallel to B_0 along the z axis. In thermal equilibrium there is an excess of nuclei in the lower energy state parallel to

This excess population can be represented by a net resultant magnetization vector (\vec{M}) parallel to B_0 along the z axis (38) (Fig 1.1(a)). By convention the direction of the field is taken to be the z direction. As a result of the torque ($\vec{M} \wedge \vec{B}$) exerted on the magnetic moments by the applied magnetic field B_0 , the magnetization vector will precess about the direction of the field (Fig 1.2(a)). According to the Larmor theorem, the magnetic moments will precess at an angular frequency $\omega_0 = \gamma B_0$. This is known as the Larmor frequency and is identical to the resonance frequency derived from quantum theory (38).

A convenient concept for describing the motion of the magnetization is that of the rotating frame of reference. The resonant rotating frame refers to a co-ordinate system which rotates about B_0 in the same direction and at the same frequency as that at which the nuclear moments precess. By analogy with the laboratory frame which has co-ordinates x, y, and z, the coordinates of the rotating frame are labeled x', y' and z'. The z axes in the laboratory frame and the rotating frame are equivalent, therefore the x' and y' coordinates rotate about the z axis (Fig 1.2(b)). In the transformation to the resonant rotating frame of reference, the magnetic moments which are precessing in the laboratory frame will appear stationary in the rotating frame. It is also found under the condition

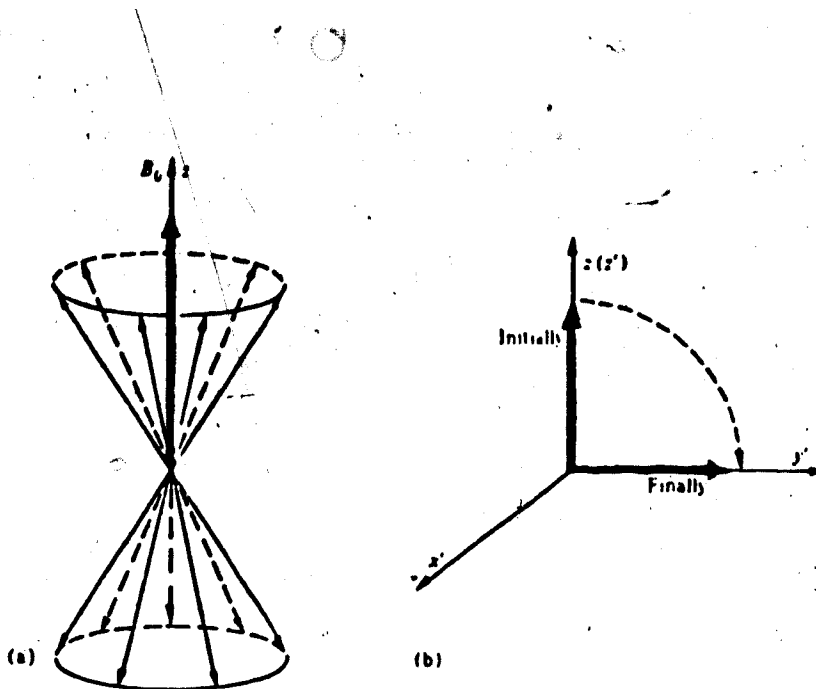


Fig. 1.1 (a) Vector representation of the nuclear magnetic moments precessing about B_0 and the resultant magnetization M along the z axis. (b) A 90° rf pulse applied along the x' axis which results in rotation of the magnetization M through 90° onto the y' axis.

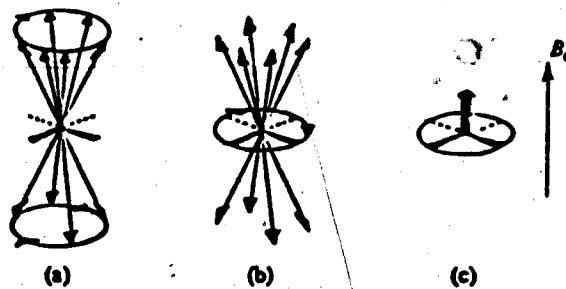


Fig. 1.2 (a) Precision of nuclear magnetic moments about B_0 : (b) Magnetic moments stationary in the rotating frame: and (c) the resultant magnetization.

when the rotating frame rotates at the Larmor frequency that the effective static field along the z axis of the rotating frame is zero. The magnetization M therefore effectively experiences a zero magnetic field.

The resultant magnetization M undergoes changes in orientation and magnitude as a result of perturbations of the nuclear spin system. Application of a radiofrequency (rf) field B_1 of frequency ω_0 perpendicular to the main field B_0 , causes the precession of M about B_1 with an angular frequency $\omega_1 = \gamma B_1$ (38). In the resonant rotating frame this rf field (B_1) will appear stationary, and is the only apparent field experienced in the rotating frame.

In the vector diagram the effect of this field on the spin system is such that the equilibrium magnetization M_0 rotates away from the z axis toward the y' axis through an angle θ , where

$$\theta = \gamma B_1 t_p \quad [2]$$

If the B_1 field is applied only for a time t_p such that the magnetization will rotate through an angle of 90° ($\theta = \pi/2$ rad),

$$\pi/2 = \gamma B_1 t_{90} \quad [3]$$

This is known as a 90° pulse (38) (Fig. 1.1(b)).

Similarly a 180° pulse occurs after a time $t_{180} = \pi/\gamma B_1$ sec, when the nuclear magnetization will have precessed through 180° . Application of the 180° pulse is equivalent to an inversion of the populations of the

energy levels, therefore M_z is now aligned along the $-z$ axis. When B_1 is turned off the spin system will tend to return to thermal equilibrium by means of a process that will be described in section 1.1.2.

The same rf coil that is used to transmit the B_1 field can also be used to detect the resulting signal. This signal arises because any component of the magnetization, which is left in the xy plane following termination of the B_1 field, will experience a torque due to the static field B_0 , which will make it precess in the xy plane. This rotating magnetization will cause a time dependent magnetic field to thread the rf coil and therefore induce an electromotive force (emf) in that coil. The induced emf is amplified and processed to produce the NMR signal. The magnitude of M_{xy} determines the strength of the observed free induction signal. Because of relaxation processes to be described in the next section this signal will decay and is therefore given the name free induction decay or FID. The NMR signal (FID) is collected as a function of time. In order to obtain the NMR spectrum in which signal intensity is plotted as a function of frequency, the time domain data must be converted to its equivalent frequency domain representation. This can be achieved by resorting to a mathematical device known as Fourier transformation. Fourier transformation enables a quantity that varies with time to be analyzed in terms of its frequency

components (62).

1.1.2 LONGITUDINAL AND TRANSVERSE RELAXATION

In an ideal case where all nuclei experience the same applied magnetic field and do not interact with each other or their environment, after perturbation by the rf pulse, the magnetization vector would precess around the z axis indefinitely. Because of interactions at the atomic level, the magnetization vector will undergo two distinct processes, longitudinal and transverse relaxation. Longitudinal relaxation concerns the recovery of the nuclear spin system back to thermal equilibrium ie. the recovery of the magnetization M along the z axis. This recovery is often exponential in time and is characterized by a time constant T_1 (3). The second process, transverse relaxation, describes the irreversible decay of the magnetization in the xy plane, and is characterized by an exponential time constant T_2 . Both of these processes, T_1 and T_2 , result from the interaction of the nuclear magnetic moments with the fluctuating local magnetic fields (B_L) generated by their environment (3). The time scale of the fluctuations determines their relative contributions to the two types of relaxation. All mechanisms that contribute to longitudinal relaxation can also contribute to transverse relaxation (38).

LONGITUDINAL RELAXATION

A number of physical mechanisms may contribute to the T_1 relaxation process. In most cases the magnetic dipole-dipole interaction is the dominant relaxation mechanism (38). In order to re-establish the thermal equilibrium populations, transitions between the nuclear magnetic energy states are required. Another magnetic field (B_L) oscillating at the Larmor frequency will induce these transitions. Nuclei experience fluctuating local magnetic fields (B_L) due to magnetic moments of nuclei in other molecules. These fields are rendered time dependent by molecular motion. Components of this time dependent field fluctuating at the resonant frequency will induce transitions which restore the spin system to thermal equilibrium (3). The distribution of frequencies representative of the motion of a randomly tumbling molecule can be expressed in terms of a Debye spectral density $J(\omega)$

$$J(\omega) = \tau_c / (1 + \omega^2 \tau_c^2) \quad [4]$$

where τ_c is a correlation time for the tumbling motion (42). Longitudinal relaxation is most efficient when $\tau_c = 1/\omega_0$, i.e. when the average frequency of molecular motion equals the Larmor frequency. When a relaxation transition occurs nuclear spin energy is exchanged with the kinetic energy of molecular motions, the result being that the spin system is now in thermal equilibrium with

the lattice.

Bloch and others assumed that longitudinal relaxation could be treated as a first order process and postulated that the variation of the net nuclear magnetization M_z in the presence of the applied magnetic field could be described in terms of a first order differential equation. The return of M_z to its equilibrium value M_0 can be described by the following equation (38):

$$dM_z/dt = \{M_0 - M_z\}/T_1 \quad [5]$$

TRANSVERSE RELAXATION

Transverse relaxation characterizes the decay of the magnitude of the M_{xy} magnetization following perturbation by the rf pulse. As a result of interactions between nuclei and from applied magnetic field inhomogeneities, the nuclei experience small variations in the local magnetic field (3). These variations give rise to a distribution of precessional frequencies of the magnetic moments. Some will rotate faster and some slower in the resonant rotating reference frame. In this reference frame there will be a "fanning out" of the xy magnetization vector as the component nuclear moments get out of phase with each other, which results in the decay of the nuclear signal (38). The greater the frequency spread the more rapidly M_{xy} decays. The dephasing of the nuclear moments as they precess leads to a corresponding broadening of the resonance in

the NMR spectrum. Transverse relaxation therefore involves processes that cause a broadening of the resonance linewidths. ~~The~~ natural linewidth at half height ($\Delta\nu_{1/2}$) is given by (42):

$$\Delta\nu_{1/2} = 1/\pi T_2 \quad [6]$$

Although T_2 can be thought of as a characteristic dephasing time for the xy magnetization components, not all dephasing can be said to be due to intrinsic T_2 processes. Intrinsic T_2 processes are mechanisms that describe the decay of the magnetization that is irreversible (3). The decay of the magnetization in the presence of a static magnetic field distribution, ΔB , can be recovered with an appropriate pulse sequence. Since ΔB does not change with time, the dephasing and rephasing will be exact. Static field inhomogeneities give rise to this recoverable dephasing (3). Since it is reversible it is not an intrinsic T_2 process. If the local magnetic field, B_L , changes location with time, the dephasing rates of all the components of the magnetization change. All memory of the dephasing will be lost. Rephasing will be perfect only if the field in which the dephasing and rephasing occurs in is constant in time. Since B_L is changing the decay of the magnetization in this case is irreversible. Mechanisms that give rise to intrinsic T_2 processes are the same mechanisms that give rise to T_1 processes, e.g. dipole-dipole interaction, but the manner in which they work is somewhat different (3).

The decay of the M_{xy} magnetization to zero can also be described by a first order differential equation as postulated by Bloch, namely (38)

$$dM_{xy}/dt = -M_{xy}/T_2 \quad [7]$$

MEASUREMENT OF T_1 AND T_2

Nuclear spin relaxation times T_1 and T_2 are measured using different radiofrequency pulse sequences. For example, longitudinal relaxation (T_1) is usually measured with an inversion recovery sequence; $180^\circ - \tau - 90^\circ$. (38). Application of the 180° pulse inverts the z magnetization so that it is along the negative z axis. Longitudinal relaxation then occurs during the interval τ allowing the z magnetization to recover towards its equilibrium value M_0 . In order to detect the amount by which M_z has recovered a 90° inspection pulse is applied after the time τ , and the subsequent NMR FID signal is recorded. The sequence $180^\circ - \tau - 90^\circ$ is repeated several times, each with a different value of τ , in order to determine the decay rate of M_z (38). T_1 can then be obtained from a plot of $\ln(M_0 - M_z(\tau))/2M_0$ versus τ which yields a straight line of slope $-1/T_1$ (42).

A method of determining T_2 employs a spin-echo pulse sequence ($90^\circ - \tau - 180^\circ$) which has been modified by Carr and Purcell (1954) to minimize the problem of molecular diffusion, and again by Meiboom and Gill (1958) to compensate for imperfections in the 180° pulses (38). The final sequence, known as the Carr-Purcell-Meiboom

-Gill (CPMG) sequence, provides the best method for determination of T_2 .

In the initial sequence $90^\circ-\tau-180^\circ$, the 90° pulse tips the magnetization into the xy plane in the rotating frame (38). The magnetization then precesses about the z axis. As a result of inhomogeneity in the applied field B_0 , some spins will precess faster or slower than others. After a certain time all coherence of the xy magnetization vector will be lost and the signal will have decayed to zero (42). If at a time τ after the 90° pulse a 180° inversion pulse is applied along the x' axis the spin distribution will be rotated 180° about the x' axis. Instead of spreading apart, the components of the magnetization now move together and will arrive at the -y axis at the same time (42). This results in the formation of an echo at a time 2τ after the initial 90° pulse. In the absence of transverse relaxation the echo would have the same amplitude as the initial signal from the 90° pulse (38). However, the magnitude of the magnetization decreases during the time 2τ due to processes responsible for transverse relaxation in the time T_2 . The echo amplitude therefore depends on T_2 . In principle, T_2 can be estimated by repeating the pulse sequence $90^\circ-\tau-180^\circ$ for different values of τ and plotting the decay of the echo amplitude versus τ . For each new value of τ it is necessary to wait approximately 5 times T_1 to allow the whole spin system to return to

thermal equilibrium (38).

The above sequence repetition will not necessarily yield a precise T_2 due to the effect of molecular diffusion in the inhomogeneous magnetic field. Diffusion causes the nuclei to move from one part of the inhomogeneous magnetic field to another which leads to a reduction of the echo amplitude. Refocusing of the echo will be perfect only if the field in which dephasing and refocusing occurs is constant in time (3). As a result of molecular diffusion the amplitude of the echoes of successive sequences does not decay in a manner determined solely by spin-spin interactions (38). The effect of diffusion can be reduced by modifying the spin-echo sequence so that a train of echoes is produced ($90^\circ - \tau - (180 - 2\tau)n$), the amplitude of which will decay with the characteristic time constant T_2 (42). The advantages of this Carr-Purcell method are first, there is a considerable saving of time since the train of echoes may be obtained with a single sequence and second, the diffusion effect is minimized since the time between pulses (τ) can be decreased, thereby allowing less time for molecular diffusion (62).

An additional problem in the measurement of T_2 using the above sequence is the inaccuracy of the 180° pulses, and the fact that these imperfections are cumulative (38). This problem can be overcome by applying the 180° pulses along the $+y'$ axis of the rotating frame rather

than about the +x' axis (38). In this case the spin distribution will be rotated 180° about the y' axis. The pulse imperfections are now not cumulative. All even numbered echoes will rephase back on the y axis and therefore will have the correct amplitude, all odd echoes will rephase slightly above the xy plane and therefore have a slightly reduced amplitude since the signal is detected in the xy plane (38).

Few measurements of T_1 of ^{31}P metabolites in intact tissue have been reported. (1,70,86,101). Those reported fall in the range of 0.5 to 5.0 sec and are dependent on the tissue of origin and the experimental parameters employed (43). The conventional method for determining T_1 is the application of an inversion recovery pulse sequence as described above. The use of this sequence for the determination of ^{31}P relaxation times in vivo using a surface coil is fraught with technical difficulties. As a result of the inhomogeneous B_1 field generated by the surface coil, the actual tip angles are not identical at all points within the sample (67). For the accurate determination of T_1 it is essential that the entire sample be subjected to an accurate 180° pulse. This problem can be overcome by employing a solenoidal coil which surrounds the organ/tissue of interest and provides a homogeneous B_1 field over the sample volume, thus ensuring more spatially uniform tip angles. The time required to

acquire a data set for the determination of ^{31}P T_1 in vivo is considerably long (≥ 8 hours) and therefore requires repeated administration of anaesthetic to the animal. The possibility of alterations in the concentration of ^{31}P metabolites during the course of the experiment must therefore be taken into consideration.

Measurements of T_2 in vivo are somewhat easier to obtain. As for the measurement of T_1 , it is essential that the entire sample be subjected to the same rf pulse strength. Employing the solenoidal rf coil (which provides a homogeneous B_1 field) with the CPMG pulse sequence which compensates for imperfections in the 180° pulse, in vivo T_2 can be determined. In the T_2 experiment a train of n echoes may be obtained in a single sequence thereby offering a considerable saving of time.

1.1.3 CHEMICAL SHIELDING

The local magnetic field at a particular nucleus differs from the applied field B_0 by an amount that depends on the electronic structure of the molecule within which that nucleus is situated (62). The small additional local field which the nucleus experiences is the result of unbalanced electronic currents in the atomic orbitals, induced by the applied field B_0 . It is found that under such circumstances the effective field at the nucleus can be represented by:

$$B_{r.f.} = B_0 (1 - \sigma) \quad [8]$$

where σ is a shielding constant that describes how much the local environment shields the nucleus from the main field in a linear fashion to yield the effective field actually felt by the nucleus (62). Since the magnitude of σ depends on the environment of the nucleus, identical nuclei in different chemical environments give rise to spectral lines at different frequencies. Fig 1.3 illustrates the chemical shift range of some phosphorus compounds commonly found in vivo. The separation of these resonance frequencies from a fixed reference frequency is called the chemical shift. Since the magnitude of the chemical shift is dependent upon the applied field, chemical shifts are reported in dimensionless units, namely parts per million defined as

$$\delta = (\nu_A - \nu_{r.f.}) / \nu_0 \times 10^6 \quad [9]$$

where ν_A is the resonance frequency of the signal of interest, $\nu_{r.f.}$ is the resonance frequency of the reference compound, and ν_0 is the spectrometer operating frequency (62). ^{31}P chemical shifts will obviously vary with all the environmental factors which affect the configuration of electronic orbitals such as temperature, ionic strength, pH, and the presence of divalent cations ex. Mg^{2+} (21). Changes observed in the chemical shift of in vivo ^{31}P spectra therefore provides important information on the nature of and alterations in the intracellular and extracellular environment.

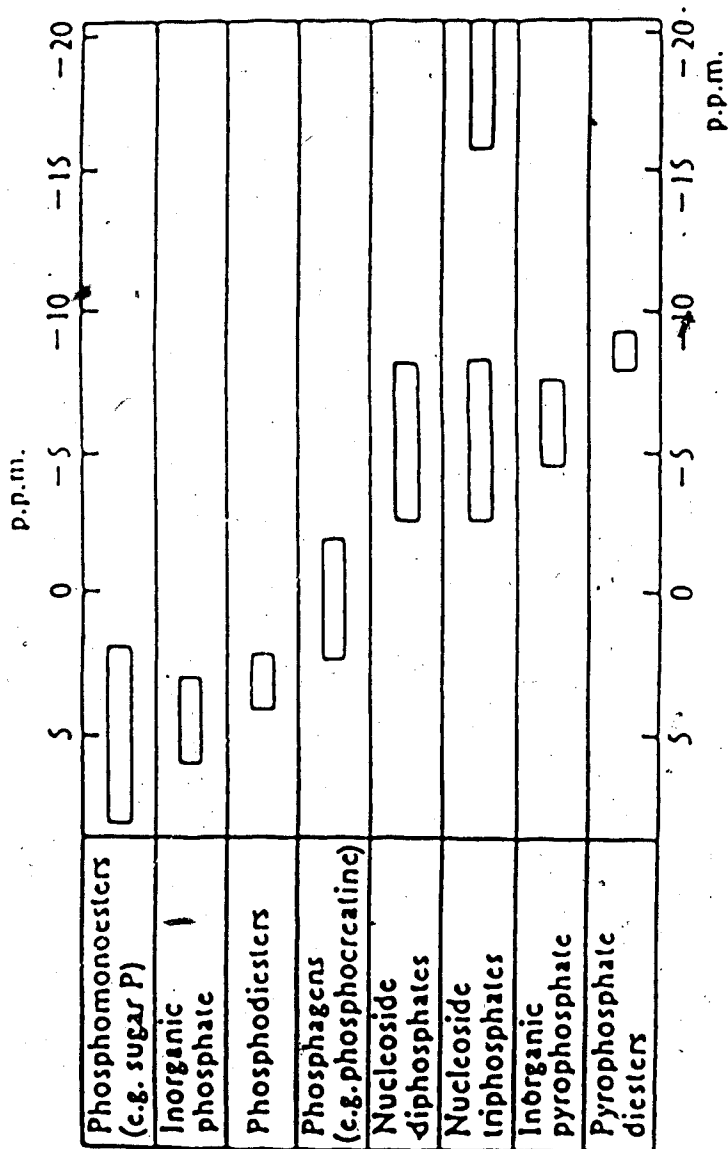


Fig. 1.3 Representative ^{31}P chemical shift values. Chemical shift range of some phosphorous compounds commonly found in vivo. The chemical shifts are reported relative to phosphocreatine which was assigned the value 0.00 ppm. (Adapted from reference 42).

1.1.4 INDIRECT SPIN-SPIN COUPLING

In some spectra a splitting of the spectral lines occurs as the result of a small interaction between the neighbouring nuclei known as indirect spin-spin coupling which gives rise to doublets or even multiplets. This coupling is described in terms of the coupling constant (J) which is found to have values in the range of 1-200Hz (42). This constant is characteristic of the molecule because the coupling interaction is the transmission of information about the spin state of one nucleus to another via the bonding electrons. Indirect spin-spin coupling is independent of the applied field B_0 and is usually a short range interaction extending over only two or three bonds. An example of indirect spin-spin coupling can be seen in a high resolution spectrum of adenosine triphosphate (ATP). The spectrum contains three chemically shifted groups of spectral lines corresponding to the α , β , and γ phosphates of ATP. The α and γ phosphates in ATP are split into doublets because they each sense the two possible spin states (parallel and anti-parallel to the field) of the β phosphate. The β phosphate is split into a triplet corresponding relative orientational possibilities of the spins of both the α and γ phosphates, namely both parallel, both antiparallel and the combination of parallel and antiparallel, the last possibility having

twice the probability of the other two.

In general coupling is observed in high resolution spectra and only rarely in in vivo spectra due to the broad resonances obtained in the latter circumstances.

1.1.5 ASSIGNMENT

Two important aspects of the interpretation of the NMR spectrum are the assignment of the resonances and the measurement of the relative or absolute concentration of the metabolites. Assignment of the different peaks of an in vivo ^{31}P NMR spectrum is normally done by comparing it with spectra from simple solutions of phosphorous compounds, or from perchloric acid extracts of tissue (43). The initial assignment of the observed resonances requires the accurate measurement of the chemical shifts and a knowledge of the range of possible chemical shifts for the expected metabolites. The chemical shift of a given metabolite can be affected by the intracellular environment. Since this environment is not known with any certainty, comparison of the phosphorus compounds in solution alone is not sufficient.

The tentative assignments obtained from solutions can be confirmed by freeze-clamping of the tissue followed by perchloric acid extraction, subsequent chemical analysis, and identification of the metabolites present by NMR, HPLC, and automated phosphorous analysis (34). NMR spectra of the extracts yield much narrower

resonances than those observed in intact tissue. The most definitive method of assignment using extracts is to record their spectra as a function of pH, before and after addition of the proposed metabolite (43). If the additional signal always coincides with the resonance of interest this provides additional evidence that the assignment is in fact correct (43).

In most tissue spectra the assignment of the resonances of ATP, PCr, and Pi is not ambiguous (43). Resonances in the phosphomonoester and phosphodiester region are more difficult to assign due to the many compounds of this type present in tissue that resonate in this region (43). Fig. 1.4 shows a typical ^{31}P in vivo spectrum of Walker sarcoma cells implanted in the rat kidney. The distribution of compounds can be arranged into three main regions.

The phosphomonoester region observed in the chemical shift range $\delta=8.0-6.0$ ppm, (measured relative to PCr) consists primarily of resonances from sugar phosphates (SP). The following glycolytic intermediates have resonances in this chemical shift region: glucose-6-phosphate, fructose-6-phosphate, fructose-1-6-diphosphate and AMP (39). Recently Evanochko et al (34) reported that the main constituents of the PME region in a RIF tumor was phosphoethanolamine (PE) and phosphocholine (PC) rather than glycolytic intermediates.

The chemical shift of inorganic phosphate (Pi) can

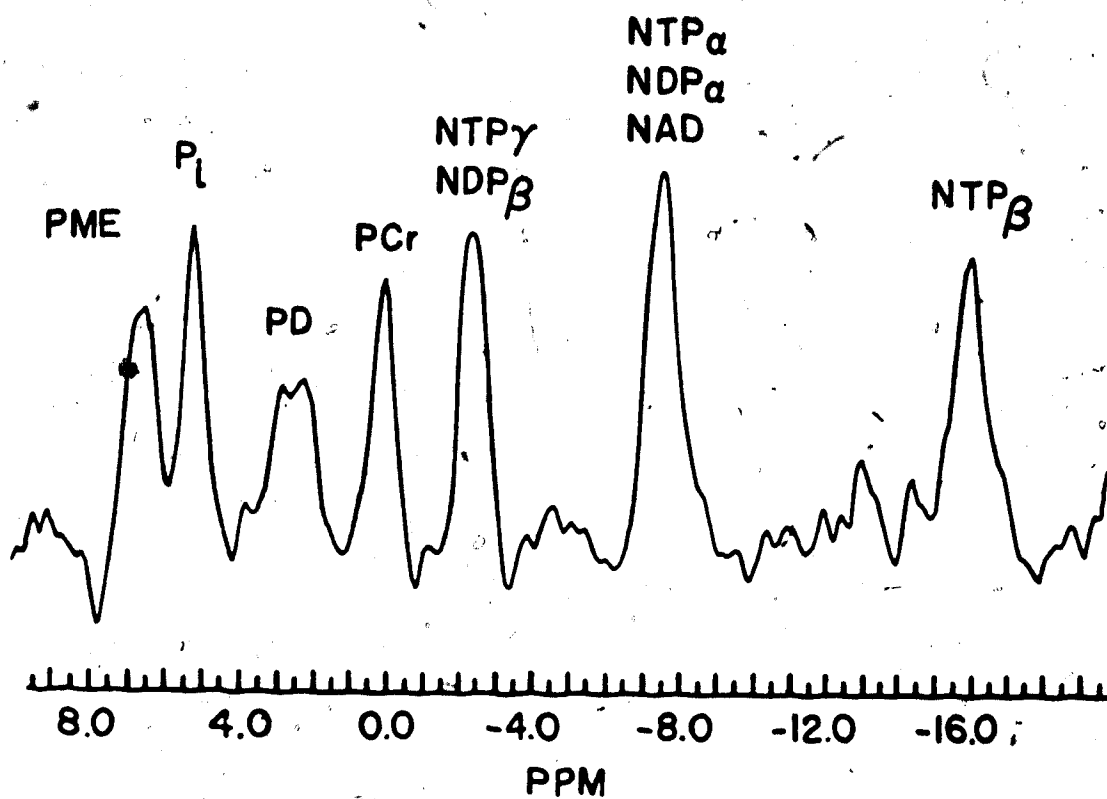


Fig. 1.4 Assignment of resonances in the ^{31}P NMR spectrum of Walker Sarcoma cells implanted in the rat kidney. The chemical shifts were expressed relative to phosphocreatine (PCr) which was assigned the value 0.00 ppm.

vary from $\delta=5.4$ to 3.5 ppm due to its sensitivity to intracellular pH.

The main constituents of the phosphodiester region (PD) ($\delta=3.0-2.0$ ppm) are the lipid derivatives glycerolphosphorylethanolamine (GPE) and glycerolphosphorylcholine (GPC) (22), although Cohen et al have assigned a diphosphodiester peak at $\delta=-12.3$ to -11.9 ppm in human lung cancer cells as uridine diphosphoglucose (UDPG) (25).

The phosphocreatine (PCr) resonance occurs at 0 ppm by definition because it is often used as an internal reference.

The high energy phosphates are observed between 0 and -16 ppm. The three resonances on the high field side of PCr have been attributed to nucleoside triphosphates (NTP), nucleoside diphosphates (NDP), and reduced and oxidized nicotinamide dinucleotides NAD and NADP. The peak at $\delta=-2.5$ ppm consists of contributions from the γ phosphate of NTP and the β phosphate of NDP, that at $\delta=-7.70$ from the α phosphate groups of NTP, NDP, and NAD. The NTP- β phosphate gives rise to a unique resonance at the high field of the spectrum $\delta=-16$ ppm. All nucleotide triphosphates contribute to these three resonances. Due to the fact that in most tissue samples ATP comprises $\geq 50\%$ of the nucleotide pool, the resonances are often assigned solely to ATP (34). ^{31}P NMR measures only ^{31}P metabolites that are in rapid molecular motion in the

cytoplasm, therefore ATP bound to membranes or ^{31}P metabolites present in macromolecules such as phospholipids, nucleic acids, and phosphoproteins are not NMR visible. As a result they do not appear in the ^{31}P spectra of living tissue.

1.1.6 CONCENTRATION

The relative concentrations of the NMR visible metabolite pools can be determined, in principle, from the areas under their respective resonances, since these areas are proportional to the number of nuclei that contribute to them. In practice, however, quantification of metabolites is difficult. There are several reasons for this. NMR is relatively insensitive, the lower limit for NMR visibility of the metabolites is $\geq 1\text{mM}$, and many of the resonances overlap (ex. ATP and ADP and NAD). The differences in the metabolite concentrations obtained by ^{31}P NMR measurements and by currently accepted standard enzymatic and chemical assays can result from a number of sources. The major difference between the two methods is that the biochemical method measures total metabolite concentrations, whereas NMR measures only metabolites that are in rapid molecular motion in the cytoplasm (43). The techniques differ with respect to the way they reflect metabolites strongly bound to macromolecules within the cell. In general, the NMR technique usually yields slightly higher values for ATP and PCr, but lower

values for ADP and AMP when compared to analytical techniques (112). This is because metabolites such as ADP and AMP may be bound to protein or cellular membranes therefore yielding a lower NMR visible concentration of ADP and AMP detected by NMR than by biochemical methods (10). Another factor which must be considered is the speed of the freezing period in the biochemical technique. It has generally been acknowledged that the speed of halting metabolism is critical to prevent post mortem changes in metabolite levels. The high energy phosphates are particularly susceptible to degradation, which may yield artificially high levels of ADP and Pi by the biochemical method.

For accurate quantification it is also necessary that the resonances are not saturated, i.e., their areas must correspond to a thermal equilibrium population distribution and this can be brought about by ensuring that the time between perturbations of the spin system must be greater than five times the longest spin-lattice relaxation time (T_1) present in the sample. Resonances in tissue spectra typically have T_1 values in the region of 0.5-5.0sec (43). To speed up acquisition time and to optimize the signal to noise (S/N) ratio, rf pulses are normally applied at time intervals approximately equal to the T_1 values of the resonances. Since the different phosphorous compounds have different T_1 values, the signal to noise ratio cannot be optimized for all

resonances. Under these conditions the relative areas of the individual resonances are reduced by factors determined by their T_1 values and by the tip angle and the interval between successive pulses (43).

Dawson et al (28) corrected for this phenomena by comparing intensities in muscle at a rapid pulse rate and also at one that allowed full relaxation. The relative concentration of NMR visible ATP, PCr, SP, Pi and PD pools were then arrived at by multiplying the resonance areas obtained during rapid sequencing by 1.0, 1.25, 1.5, 1.8, and 1.3 respectively.

A second method for quantification is that of Burt et al (20). These authors inserted a capillary tube containing a compound that resonates at a chemical shift downfield from the tissue phosphates. Comparison of the ratio of the reference peak area to a solution of Pi of known concentration run under identical conditions to that of the tissue sample gives an effective concentration for the capillary. Using the corresponding ratio in the sample, metabolite concentrations could be obtained. With this method it is necessary to calibrate each metabolite against the capillary individually. This method also assumes the T_1 of the compound is the same in tissue as in solution, a situation which may not be entirely valid. Either method depends on the ability to measure the relative T_1 's of the resonances in the compound of interest. Quantitative calibration of

concentrations in absolute terms is also complicated by the fact that the exact volume that contributes to the signal cannot be accurately determined in-vivo and this presents a major obstacle (43).

One of the major shortcomings of ^{31}P NMR is the inability to quantify accurately the concentrations of the metabolites present.

1.1.7 MEASUREMENT OF INTRACELLULAR pH

The measurement of pH provides an important contribution to our understanding of in vivo metabolism. ^{31}P NMR is one of the best methods for measuring intracellular pH since the measurements can be made continuously and non-invasively. NMR was first used to measure intracellular pH by Moon and Richards (88) in 1973. Their measurements on red blood cells were based on the observation that 2,3-diphosphoglycerate and P_i generate NMR signals whose frequencies are sensitive to pH variations in the physiological range (pH~7.0). Although any resonance whose frequency is sensitive to pH can be used, inorganic phosphate is the most suitable since it is readily observable in the majority of in-vivo spectra and P_i has a pK_a in the physiologic region ($\text{pK}_a = 6.88$).

The pH of a solution is a measure of its hydrogen ion (H^+) concentration. The dissociation reaction for a weak acid is (76):

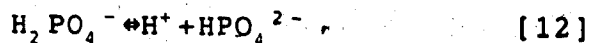


[10]

with an equilibrium constant K. The pK of an acid is the pH at which it is half dissociated, pH being related to pK by (76):

$$pH = pK + \log \left\{ \frac{[A^-]}{[HA]} \right\} \quad [11]$$

A number of dissociation reactions occur in biological phosphates. Inorganic phosphate exists as



at neutral pH (76). Each of the two phosphorus species has a unique electronic structure and therefore a unique chemical shift. There is a difference of 2.3ppm between the resonances of the two phosphorus species (39). Due to the fact that the 1H exchange between them is faster than the frequency difference between the two resonances, the observed spectrum consists of an exchange averaged single resonance, the frequency of which depends on the relative amounts of the two species (39). The frequency of the signal as a function of pH gives therefore a standard pH curve (43). The intracellular pH is obtained by measuring the chemical shift of the compound in vivo and determining from the standard pH titration curve to which pH this chemical shift corresponds. The accuracy of the method depends on the construction of titration curves of phosphorus solutions designed to mimic the intracellular environment. Typical titration curve solutions consist of 100mM KCl, 100mM NaCl, 10mM PCr, 5mM

ATP, 5mM MgCl₂, 10mM Pi (86). pH measurements are affected by temperature; therefore the sample temperature should be maintained at 37°C.

The chemical shift is usually expressed relative to PCr ($\delta=0.00$ ppm by definition) since the pK_a of PCr is about 4.6 and is insensitive to pH changes in the physiological region pH ~6.2-7.3 (86). The relationship between the pH and the measured chemical shift of Pi can be described by the following equation:(111).

$$pH = pK + \log(\delta_{obs} - \delta_{H_2PO_4^-}) / (\delta_{HPO_4^{2-}} - \delta_{obs}) \quad [13]$$

In order to calculate pH from this equation it is necessary to determine the values for the three constants pK, $\delta_{H_2PO_4^-}$, and $\delta_{HPO_4^{2-}}$. Samples are titrated to pH 4.0 and pH 10.0 ensuring 99.9% of the phosphorus is in the $H_2PO_4^-$ and HPO_4^{2-} forms respectively, the NMR spectra are obtained and the chemical shift recorded relative to PCr. Over the pH range 6.4 to 7.2, the chemical shift difference between PCr and Pi has an approximately linear dependence on pH. To establish the pK for a particular phosphorus compound samples are titrated in the range of their pK's (111). For the accurate determination of intracellular pH, it's necessary to determine the pK value of phosphorous metabolites in vivo (111). Due to the lack of knowledge on the composition of the intracellular media in intact cells, some uncertainty in the determined pK value cannot be excluded (111). Seo et al (111) demonstrated that the apparent pK value

for a solution of a given ionic strength can vary by 0.1 to 0.3 units depending on the type of dominant ion present in the solution. The authors compared the pK values obtained from titration of a 10mM K-phosphate buffer solution (pK 6.85) with that obtained from titration of muscle extract solutions (pK 6.75). This variation of 0.1 unit in the apparent pK results in an overestimate (or underestimate) of the intracellular pH by 0.11 pH units (111).

A number of factors other than pH can affect the chemical shift of P_i , the ionic strength of the solution, metal ion binding, temperature, and the binding of P_i to macromolecules (41). These factors may also contribute to errors in the estimates of intracellular pH.

Although ^{31}P NMR provides a convenient means of estimating pH, there are nevertheless some uncertainties. In general, there is good agreement between the NMR method and intracellular microelectrodes. The pH of the giant barnacle muscle cell was found to be 7.35 using ^{31}P NMR, and 7.25 using a microelectrode (41). Illingworth reported that glass electrodes can produce pH measurements that are in error by as much as 0.2 pH units or more (68). This may account for the fact that slight differences exist in pH titration curves quoted in the literature. Gadian has pointed out that accuracy of the NMR method is not better than ± 0.1 pH unit, however changes in pH have been reported by some authors who

claim an accuracy of better than 0.05 pH units (41).

1.2 THE APPLICATION OF IN-VIVO ^{31}P NMR SPECTROSCOPY TO STUDY ENERGY METABOLISM

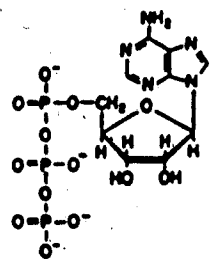
From a biochemical point of view the nuclei of interest for in vivo NMR studies are ^1H , ^{13}C , ^{15}N , ^{17}O , ^{31}P , and ^{23}Na . The three nuclei that represent the best compromise between NMR sensitivity and biochemical interest and abundance are ^1H , ^{13}C , and ^{31}P . The major drawbacks for the direct application of in vivo ^1H spectroscopic studies are first, that the spectra obtained are extremely complex since ^1H is the most prevalent atom in biomolecules, and secondly, that suppression sequences are required in order to observe signals from low concentrations of metabolites which are often hidden under the large water and fatty acid signals. The major problem with ^{13}C NMR is its low sensitivity and its low natural abundance (1.1%) therefore necessitating isotopic enrichment (43). In vivo ^{31}P NMR on the other hand has several advantages which have meant that most NMR studies on intact biological systems have concentrated on ^{31}P . For example, narrow resonances can be obtained which are well separated throughout a wide range of chemical shifts, about 30 ppm for biological phosphates. Although the sensitivity of ^{31}P is less than that of ^1H -NMR, it is

still, nevertheless, one of the more sensitive NMR nuclei. ^{31}P is the only naturally occurring isotope of phosphorous, therefore no isotopic enrichment is necessary. Several important phosphorylated metabolites are present in the cell at concentrations detectable by NMR ($\geq 1\text{mM}$), for example, adenosine triphosphate (ATP), phosphocreatine (PCr), inorganic phosphate (Pi), phosphomonoesters (PME) and phosphodiester (PDE) (Fig. 1.5) (39). Apart from the technical considerations, an important biological reason for choosing ^{31}P is due to the involvement of the above metabolites in cellular bioenergetics.

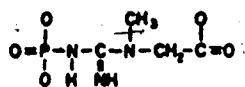
The conventional method for studying metabolism in living tissue requires rapid freezing to stop the chemical reactions, then acid extraction of the metabolites from the tissue and chemical analysis of the metabolites. This requires sacrifice of numerous animals at precisely timed intervals in order to reconstruct the time course for a given metabolic process. The metabolic picture obtained from studies of extracts is therefore a quasi-static one.

The main objectives in investigations of metabolism in living tissue are: first, to identify the molecules in the metabolic pathways and determine their chemical interactions, second, to determine the reaction rates, third, to determine the mechanism of control of these rates, and fourth, to understand the normal and abnormal

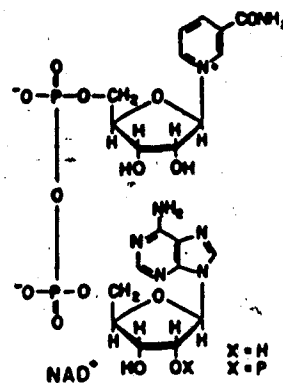
A. HIGH ENERGY PHOSPHATES



Adenosine triphosphate

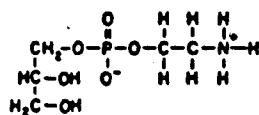


Phosphocreatine

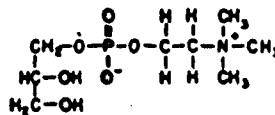


Nicotinamide adenine dinucleotide

B. PHOSPHODIESTERS

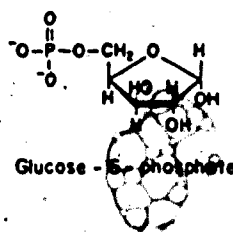


Glycerolphosphorylethanolamine

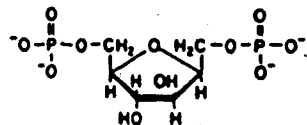


Glycerolphosphorylcholine

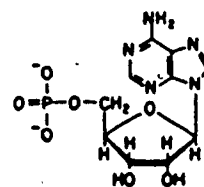
C. PHOSPHOMONOESTERS



Glucose-6-phosphate



Fructose 1-6 diphosphate



Adenosine monophosphate

Fig. 1.5 Chemical structures of phosphate metabolites detected by ^{31}P NMR.

operation of these controls in both normal and pathological tissue (67).

The advantages of using NMR to study metabolism, over the conventional biochemical techniques, are that it provides a noninvasive, nondestructive measure of certain tissue metabolites. The NMR measurements can be made repetitively from the same intact animal, permitting comparisons to be made between different metabolic states under a variety of conditions. The time course of changes in concentration of different metabolites can be followed; provided that the changes are slower than the time required for the accumulation of signals. Several investigators have used ^{31}P NMR to identify high energy metabolites in the heart (53), in skeletal muscle (20), in the kidney (110) and in brain (15). The kinetics of the metabolic interconversions can often be determined using the NMR technique of saturation transfer. Determination of the rate of ATP synthesis from Pi and ADP has been achieved for intact heart (81), brain (113), and kidney (40,75). The rate constants for the creatine kinase reaction ($\text{PCr} + \text{ADP} \rightleftharpoons \text{ATP} + \text{Cr}$) have been determined for rabbit brain (29) and skeletal muscle (69).

The kinetics of many enzyme reactions are affected by changes in intracellular pH (96). ^{31}P NMR also provides a means of estimating the intracellular pH. The measurement of pH contributes significantly to our

understanding of in vivo metabolism. Sehr (110) and Manganaro (79) have demonstrated the utility of ^{31}P NMR pH measurements to assess tissue viability for transplant purposes.

The unique power of NMR spectroscopy is its ability to be a non-invasive probe of tissue metabolism. Differences observed between the phosphorous spectrum in normal and in diseased states are being actively pursued for clinical applications.

1.3 CELLULAR ENERGY METABOLISM - GLYCOLYSIS AND RESPIRATION

Our knowledge of the major metabolic pathways of intermediary and energy metabolism were made possible largely through in vitro extraction and analysis of the cellular metabolites, and the use of radioisotopes as chemical tracers. Recent developments in NMR spectroscopy have resulted in the application of this non-destructive technique to investigations of energy metabolism in intact living systems. Initial investigations tended to confirm existing knowledge of bioenergetics, but this was important in establishing the validity of the NMR method.

In order to comprehend the information obtained from analysis of the in vivo ^{31}P spectrum, a knowledge of some important cellular processes is required. Chemical energy is provided to the living cell by two primary

biochemical pathways, glycolysis and oxidative phosphorylation. Glycolysis is the degradation of carbohydrates to produce energy in the form of adenosine triphosphate (ATP). Oxidative phosphorylation is the complex process of electron transport via a chain of respiratory enzymes to the electron acceptor oxygen which is directly coupled to the phosphorylation of ADP to ATP. These metabolic pathways are summarized in Fig. 1.6.

Glycolysis is of great importance to the cell, since the degradation of glucose releases the chemical energy inherent in the glucose molecule in the form of ATP. During glycolysis, glucose a 6 carbon molecule, is eventually degraded into two molecules of pyruvate, a 3 carbon molecule. For this process eleven enzymes are required which interconvert the glucose molecule into a number of sugar phosphate intermediates (Fig.1.6). The pentose phosphate shunt is the major alternative pathway to glycolysis (76). Glucose utilization through this pathway leads to the production of ribose-5-phosphate which is involved in the synthesis of nucleic acids (76). (Fig.1.6). The catabolic pathway of glucose, glycolysis, is opposed by the biosynthetic pathway of glucose production, gluconeogenesis. The rate and direction of these opposing pathways are determined by the concentration and activity of the key glycolytic enzymes, present together with the opposing key gluconeogenic enzymes (119).

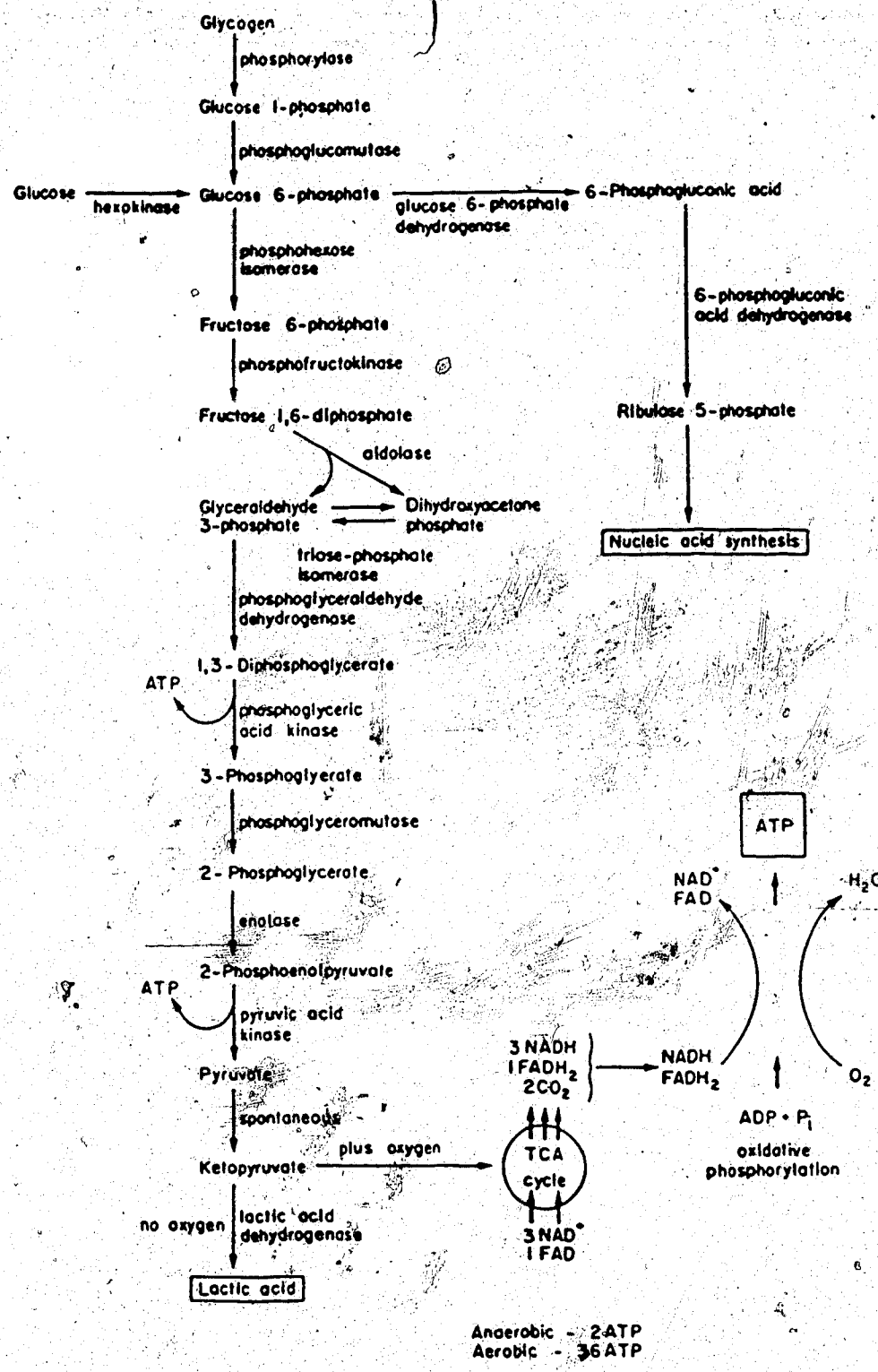


Fig 1.6 ATP production from glycolysis and oxidative phosphorylation. (Adapted from reference 76).

In the absence of oxygen (anaerobic glycolysis) two molecules of ATP are produced for every molecule of glucose degraded (39) (Fig 1.6). The end point of anaerobic glycolysis is the production of lactate from pyruvate. Lactate is not useful to the cell in terms of energy and due to its acidic nature causes a decrease in the intracellular pH (76).

Using various metabolic insults, Evans and Kaplan (35) demonstrated the ability of ^{31}P NMR to monitor changes in the glycolytic pathway. As expected the ^{31}P spectrum of HeLa cells (human cancer cells) incubated with iodoacetate exhibited an increase in the sugar phosphate levels and a decrease in ATP levels. Iodoacetate is an alkylating agent which inhibits the glycolytic enzyme phosphoglyceraldehyde dehydrogenase. Blockage of glycolysis at this early stage in the pathway leads to accumulation of glycolytic intermediates (mainly fructose 1,6,diphosphate) and prevents the replenishment of ATP (Fig. 1.6).

Reduction of oxygen to the cells resulted in a depletion of ATP levels with time and an acidotic shift of the P_i resonance which was attributed to the accumulation of lactate (35). ATP levels were observed to increase upon reoxygenation.

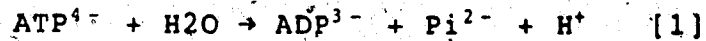
Cells metabolizing in the presence of oxygen (aerobic glycolysis) yield more ATP (36 molecules /molecule of glucose) than those metabolizing under

anaerobic conditions (2 molecules of ATP/molecule of glucose). Under aerobic conditions, pyruvate produced during glycolysis is converted to acetyl CoA and is further oxidized in the tricarboxylic acid cycle (TCA), which is the common pathway of oxidation of all fuel molecules in aerobic cells. The TCA cycle reactions produce the energy yielding compounds NADH (nicotinamide adenine dinucleotide) and $FADH_2$ (flavin adenine dinucleotide). During oxidative phosphorylation the electron carriers NADH and $FADH_2$ donate electrons to oxygen and are re-oxidized to NAD and FAD (76). This process is directly coupled to the phosphorylation of ADP to ATP (Fig 1.6). The energy release in the process of electron transport to oxygen is transformed into phosphate bond energy. The precise mechanism of this energy conversion is not known with any certainty.

Evans and Kaplan (35) also assessed the ability of ^{31}P NMR to monitor the effects of uncouplers of oxidative phosphorylation. Uncouplers of oxidative phosphorylation allow the electron transport to continue but prevent the phosphorylation of ADP to ATP. Administration of 2,4-dinitrophenyl (DNP) to HeLa cells resulted in a decrease in ATP levels with no increase in sugar phosphate levels indicating that the ^{31}P spectrum reflects the specific effect of DNP on oxidative phosphorylation.

The two biochemical pathways, glycolysis and oxidative phosphorylation, are responsible for the

regeneration of ATP. ATP is hydrolyzed to ADP and Pi whenever energy is required for metabolic processes such as biosynthesis, membrane transport, and muscle contraction (19).



$$\Delta G^\circ = -31.8 \text{KJ/mole}^{-1}$$

The equilibrium for this reaction lies far to the right. Phosphate compounds, such as ATP and PCr, are often referred to as "high energy phosphates" due to the large free energy for hydrolysis (ΔG°) for these compounds, -31.8KJ/mole for ATP, -43.1KJ/mole for PCr. In the above reaction (1) the energy released comes from the decrease in the electrostatic interactions which occurs when the terminal phosphate is cleaved. At neutral pH, ATP bears four negative charges that cause internal repulsion and thermodynamic instability. Cleavage to ADP and Pi is accompanied by the separation of negative charge which accounts in part for the large change in free energy. Resonance stabilization also contributes to the large ΔG° for hydrolysis (19).

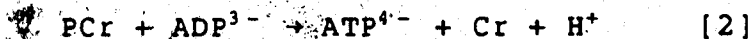
ATP concentrations vary widely among cell types and among species (19). The concentration may depend on physiological conditions, age, growth rate, stage of cell cycle, and other factors. In cultured cells, ATP concentrations have been reported to vary from 2.4 to 11 nmol/10⁶ cells. In tissue, concentrations of 4.7-7.8 umol ATP/gm wet wt has been reported for skeletal muscle,

and 4.5 $\mu\text{mol ATP/gm wet wt.}$ for heart (19).

Within cells, the ATP can be compartmented within mitochondria, nuclei, or other cellular organelles as well as bound to other cellular components. ^{31}P NMR will detect only ATP that exists free in the cytoplasm.

^{31}P NMR studies have confirmed biochemical reports that ATP exists in the cytoplasm as a Mg^{2+} complex (66).

Another high energy phosphate detectable by NMR is PCr. ATP is usually visualized as the primary form of chemical bond energy for direct utilization, whereas PCr is usually depicted as having a secondary role as a storage form for phosphoanhydride bond energy (19).



PCr acts as a reservoir for the reversion of ADP into ATP. The interrelationship between ATP, ADP, PCr, and Pi is summarized in Fig 1.7.

All metabolic reactions are closely integrated and coordinated. A number of control mechanisms regulate the key enzymes involved in the reactions in response to changing conditions in the cell. It is important to note that not all of these reactions occur within the same intracellular compartment. For example, glycolysis occurs in the cytoplasm while oxidative phosphorylation occurs in the mitochondria. For this reason metabolic control and its mechanism is best studied in the intact system. One of the main advantages of in vivo NMR spectroscopy can therefore be exploited to study

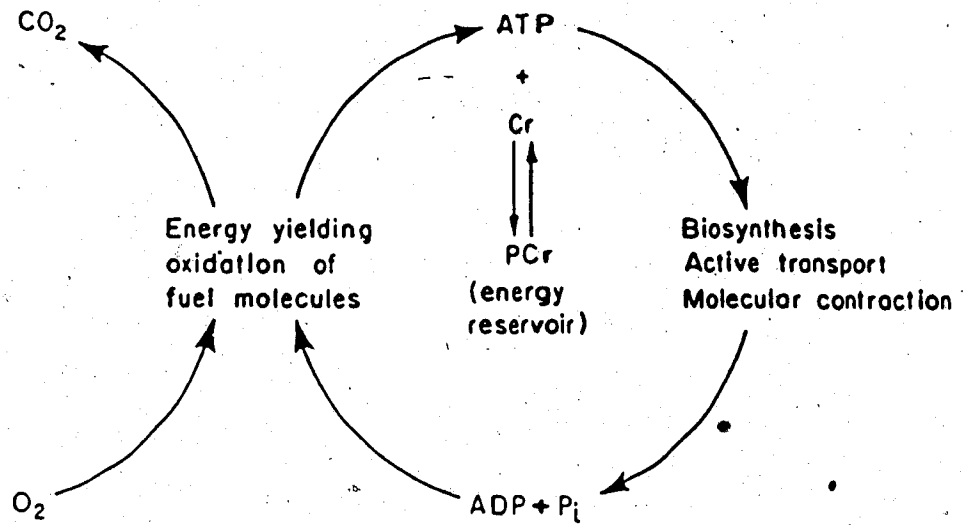


Fig. 1.7 Schematic representation of the cycle of ATP production and utilization. (Adapted from reference 19).

metabolism in normal and pathological states.

1.4 TUMOR ENERGY METABOLISM

For several years the biochemist has been studying the characteristics of cancer cells. In early studies it was hoped that a single biochemical abnormality would be found to account for the disorderly growth. It is clear now that there is no single difference between cancer tissue and the normal tissue of origin. In fact there are so many differences that precise relationships have become confused. Although no specific characteristic is common to all cancer cells, a certain number of properties can be attributed to them which permits the microscopic diagnosis of malignancy (106). Under the light microscope cancer cells appear to be more variable in size and shape. The most notable abnormalities are the nuclear and chromosomal aberrations. Cancer cells have large nuclei and in many cases are multi-nucleated. Rapid cell division results in increased incidence of mitotic figures and the presence of abnormal mitoses.

On a molecular level, the concentration of enzymes involved in DNA and protein synthesis are elevated in tumor cells which allows for the increased rate of mitosis and cell proliferation. In carbohydrate metabolism key glycolytic enzymes increase and the opposing gluconeogenic enzymes decrease in concentration, parallel with the rate of tumor growth (119). Tumor

cells produce a number of proteases which probably aid in their invasion of normal tissue. A lower serum requirement for tissue culture of tumor cells indicates that they can synthesize tumor growth factors which facilitate their growth in a toxic environment (ie. low oxygen, decreased nutrients and acidic pH) (106). In addition to these intracellular changes, the tumor cell membrane also exhibits changes in structure and permeability. Although these characteristics prevail the individual cells of a malignant tumor exhibit marked biochemical heterogeneity. Factors which account for the biochemical diversity exhibited by a tumor mass are the characteristics of the cell type of origin, the rate of tumor growth, and the extent of vascularization (46). In general a tumor mass consists of three regions of cells which differ with respect to their proximity to vascular capillaries. Close to the capillaries the tumor cells are adequately supplied with oxygen and nutrients. Beyond this aerobic cell layer are cells which are hypoxic but are still viable. Regions of the tumor more distant from vascular capillaries consist of poorly nourished anoxic necrotic cells. Cells in this region are often dead or dying existing mainly in extracellular fluid (26).

Another factor contributing to the biochemical heterogeneity of the tumor is the fact that the tumor mass does not consist solely of a population of homogeneous malignant cells but often contains

significant but variable amounts of host derived material (ex. connective tissue)(26). An established tumor mass therefore can be regarded as a complicated and highly variable ecosystem.

Researchers are still searching for "biochemical markers" or "spectroscopic markers" which will differentiate normal from cancerous tissue and thereby aid in the detection and diagnosis of malignancy.

One of the first applications of NMR to the study of malignant tissue was made by Damadian in 1971 (27). Using ^1H NMR he claimed to demonstrate longer longitudinal relaxation times (T_1) for protons in malignant tissue biopsies as compared to normal tissues. The lengthening of the T_1 was later attributed to increased tissue hydration. The distribution of cell water is known to be abnormal in tumor tissue. Tumors tend to be oedematous since they lack lymphatic vessels which aid in the drainage of extracellular fluid from the center of the tumor mass. Cell water is present in a bulklike state and in a state associated with macromolecules, the associated state having the shorter T_1 . The water associated with macromolecules is in rapid exchange with the free water pool. The observed T_1 is an average of the two environments. Changes in tissue water will therefore result in changes in the associated/free ratio of cell water and therefore an altered T_1 (67). These experiments suggested that proton relaxation times

can discriminate between normal and malignant tissue. However, this initial promise has not been fulfilled because of the substantial overlap of normal and tumor values due to biological variability.

Initial ^{31}P NMR investigations on the energy metabolism in malignant tissue were performed on tumor cell suspensions, (35), (93), (94), (122), and later progressed to intact tumor biopsy (24), (103) specimens and then to in vivo tumors (31), (33), (50), (51), (94). Analysis and interpretation of the results obtained from studies of cell suspensions was complicated by the use of a number of different cell lines and of the experimental protocols employed. Conflicting reports (59), (35), (93), concerning the presence or absence of a PCr resonance in the tumor cells could result from differences in the metabolic characteristics of the cell strain, tissue culture media composition, or the extent of oxygenation and perfusion.

Although metabolic information can be obtained by analysis of spectra of excised living tissue, numerous biochemical changes can occur within a few seconds of tissue excision. Also, a number of technical problems are encountered in attempting to maintain the excised tissue in an in-vivo like state. To obtain an accurate account of metabolic processes, ideally one should monitor metabolism of the tissue in vivo without surgical intervention.

The development of the surface coil by Ackerman et al (5) made possible the non-invasive, in vivo observation of tissue metabolism. In vivo ^{31}P NMR spectra have been reported for a variety of tumors of murine (77), rat (50), (51), (73) and human origin (90) (91). In 1981, Griffiths et al (50) reported the first investigation of a solid tumor in situ in a living animal. Walker sarcoma tumors were implanted into the inguinal region in Wistar rats. The tumor exhibited intense NTP, Pi, and PME resonances, weaker phosphodiesteres and no detectable PCr.

Ng et al (94) observed a considerable range of variations in the relative concentrations of the ^{31}P metabolites among different tumors and even among the same tumors examined in different hosts at different stages of growth. This is not altogether surprising, considering the variable metabolic states of the different cell types which comprise a solid tumor and the unpredictable growth of tumors. Histological examination of many tumors shows considerable variation in cell type and in the degree of differentiation from one part of the tumor to another. This variation in histological pattern is associated with considerable variation in biochemical activity (26). None of the tumors examined demonstrated a "unique" ^{31}P resonance characteristic. Evelhoch et al (37) also noted marked differences in the ^{31}P spectral characteristics of tumors that were identical in mass,

site and number of cells injected, and extent of tumor growth. Both groups suggest that the observed metabolic variability is a result of differences in tumor vascularization. Another factor which may contribute to the observed spectral differences is the method employed to acquire the ^{31}P NMR spectrum. NMR localization techniques were not implemented in these studies therefore the spectra may contain differential contributions from surrounding normal tissue. Other factors which affect energy metabolism and therefore may be reflected in the ^{31}P spectra are modifying host factors such as the nutritional state of the animal, or hormonal and metabolic differences between animals. Deutz (125) showed that the intensity of the ^{31}P NMR signals was not affected by the use of pentobarbital.

In the 1930's Warburg and his colleagues first suggested that cancer tissues are more anoxic than normal tissue, and that cancer tissues were characterized by a high rate of lactate formation under aerobic as well as anaerobic conditions (99). Anaerobic glycolysis therefore becomes the major source of the cancer cells' ATP. Warburg hypothesized that the dependence of tumor cells on anaerobic glycolysis for energy is a consequence of an impairment in the respiratory enzymes or coenzymes in the tumor cell, thus hindering oxidative phosphorylation (99). A number of investigators have demonstrated that many tumors contain a full complement

of respiratory enzymes, coenzymes, and mitochondria which appear normal morphologically and functionally and therefore are capable of producing ATP by oxidative phosphorylation (26). The observed increase in the rate of breakdown of glucose by tumor cells is to compensate for the lower yield of ATP per molecule of glucose. The anaerobic cell requires 36/2-18 times more glucose to be as efficient in ATP production as the aerobic cell. (76). Reliance of the tumor cell on anaerobic glycolysis leads to a production of a large amounts of lactate which results in a decrease in tumor pH.

Griffiths et al (51) attempted to demonstrate that administration of glucose to the Walker-Sarcoma tumor in vivo should enhance glycolysis and cause a further drop in tumor pH. Employing ^{31}P NMR, their attempt to show this effect failed. However, Evelhoch et al (36) succeeded in eliciting a decrease in tumor pH of RIF-1 tumors using a substantially larger intraperitoneal dose of glucose (four times those employed by Griffiths et al).

Analysis of the ^{31}P spectra as a function of tumor growth appears to support Warburg's hypothesis that tumors derive their energy from anaerobic glycolysis.

C. Ng et al (94) studied a series of subcutaneously implanted tumors. Initially, the ^{31}P spectrum indicated that the tumor cells appeared to have adequate blood flow and therefore adequate oxygen. The cells are

predominantly aerobic with most of the ATP being generated by oxidative phosphorylation. As the tumor grew a decrease in the blood supply resulted in an increase in the hypoxic fraction in the tumor. The dependence of the hypoxic cells on anaerobic glycolysis was reflected in a decrease in PCr with a corresponding increase in Pi and PME with little change in ATP levels. The intracellular pH had decreased slightly. To compensate for the lesser efficiency of this pathway for ATP synthesis, the tumor cells utilize PCr to maintain the high and approximately constant level of ATP. The decrease observed in the intracellular pH was attributed to the accumulation of lactic acid, the end product of anaerobic glycolysis. As tumor growth progressed, further depletion of the PCr reserve and decreased ATP resonances was observed along with an increase in PME. The increased rate of glycolysis has resulted in the accumulation of glycolytic intermediates. At advanced stages of growth only the Pi and PME peaks were observed. Cancer cells are characterized by a high rate of hydrolysis of ATP ($ATP \rightarrow ADP + Pi$). ATP has been hydrolysed to yield the predominant Pi resonance. The presence of the intense Pi peak at late stages of growth probably reflect accumulation of necrotic and metabolically inactive cells since by comparison dead tumors generally exhibited an intense Pi peak and a small residual PME peak (33).

Several investigators have reported substantial differences in the ^{31}P spectrum of normal tissue ex. muscle as compared with that of tumor tissue (as illustrated in Fig.1.8) and have suggested that these differences could provide a means of diagnosis of cancer in vivo. To date, a unique spectroscopic fingerprint for cancer has not been found. Although most tumors exhibit high levels of Pi and PME with low levels of high energy phosphates, this profile is only observed at late stages of tumor growth. The fact that these spectral characteristics are observed in normal tissue under moderately hypoxic conditions (100) suggests that it is unlikely that ^{31}P spectroscopy alone will prove useful as a diagnostic technique for tumor detection.

In the past, determining the tumor's metabolic pattern was difficult and time consuming. Recent developments in NMR have made it possible to assess rapidly several aspects of high energy phosphate metabolism, pH, and the relaxation times of tumors non-invasively.

1.5 TUMOR MODEL

Ideally for experimental studies, a tumor model should exhibit spectroscopic and biological properties that resemble those of a human tumor of clinical interest. The tumor should be suitable for in vivo and

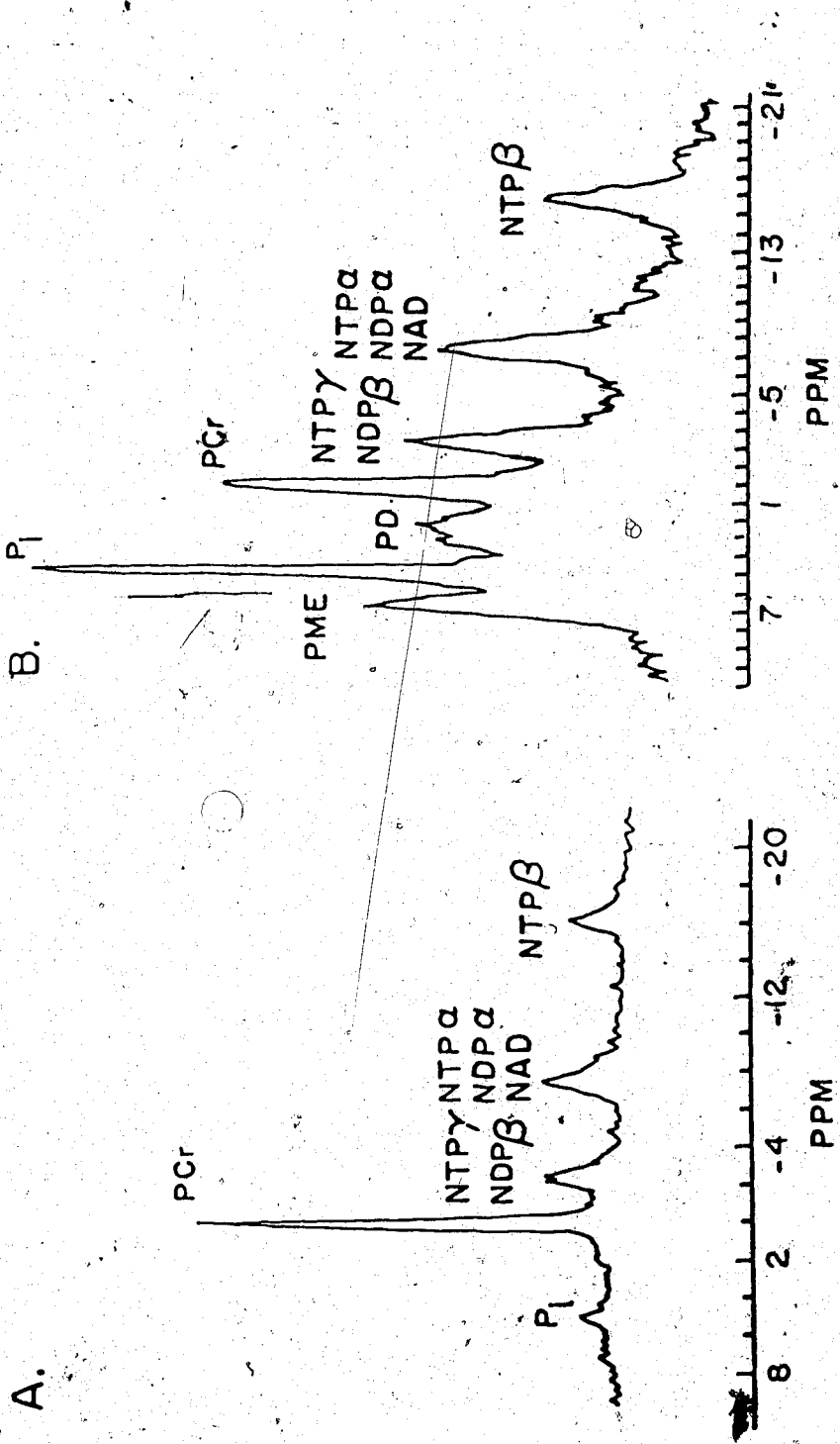


Fig. 1.8 Examples of the differences in the relative concentrations of ³¹P metabolites in different tissues. (A) rat flank muscle, (B) Dunning tumor propagated in the rat flank.

in vitro studies, responsive to therapeutic agents, have well documented histology, and be non-immunogenic and non-metastatic, at least until the very late stages of growth. Unfortunately, no tumor satisfies all these criteria (46).

The tumor model chosen for this investigation of tumor metabolism was the Walker sarcoma 256. Other investigators have employed this model (50), (51) to monitor tumor metabolism by ^{31}P NMR spectroscopy. The advantages of using the Walker sarcoma as an experimental tumor model are its rapid growth (10-14 days), its reproducibility, its sensitivity to chemotherapeutic agents, and the fact that it exhibits gross necrosis only at late stages of growth.

The Walker sarcoma is a malignant tumor which arose in a pregnant albino rat in 1928 in the laboratory of Dr. George Walker (102). Histologically, it is described as a mammary adenocarcinoma (102). The hormone independent carcinoma grows rapidly, invasively, and reproducibly. After subcutaneous implantation of a tumor slice ($\approx 5 \text{ mm}^3$) it is fatal to the host rat within 14-16 days when it has reached a size of approximately $8 \times 5 \times 5 \text{ cm}$ and weighs about 60g (102). This rapid growth and the release of proteolytic enzymes (proteases) by the tumor, destroys the vascular walls which results in a reduction of the blood supply to the tumor (47). As a consequence of this, a central necrotic region develops which is evident

from the seventh day of tumor growth (102). This region consists mainly of cell debris and extravasated erythrocytes. The periphery of the tumor is, however, still well vascularized. As the tumor grows the vascular density at and around the tumor periphery increases. The tumor can elicit new capillary growth from the host via the action of a tumor angiogenesis factor (47). These newly formed tumor vessels have a single layer endothelial wall which lacks a more resistant external coating (47).

The Walker sarcoma has remained relatively stable in its sensitivity to chemotherapeutic agents (102). The tumor is very responsive to alkylating agents (ex. cyclophosphamide) (30). Complete regression of the tumor can occur with sufficient dose and number of administrations of the drug (30).

Early NMR studies of tumor metabolism examined tumors implanted subcutaneously in the animal. No spatial localization techniques were employed in these experiments. A potential problem with that method was that the tumor was in direct contact with adjacent tissues and therefore the NMR spectrum acquired was likely to contain contributions from the surrounding tissue. To overcome this problem and to reduce the spectroscopic localization required, we have developed a tumor model in which tumor growth occurs isolated from the surrounding tissue. Employing the method originally

described by P. Gullino et al (54), Walker sarcoma cells ($\sim 10^6$) were implanted into the rat kidney just under the capsule. The kidney was then wrapped in parafilm to restrict tumor growth.

The rapidly growing and infiltrating tumor cells replaced most of the kidney tissue within 14-16 days, resulting in a tumor mass connected to the host only by the renal artery and vein. This feature provided considerable control over the administration of insults such as chemotherapy and ischemia.

1.6 NMR LOCALIZATION TECHNIQUES

The ability to monitor metabolism non-invasively by NMR was made possible by the development of radiofrequency surface coils for the excitation and detection of NMR. The surface coil is the most sensitive means of detecting low concentration metabolites within tissue close to the surface of the animal. Sensitivity is greatest close to the surface of the animal and rapidly decreases with increasing depth into the sample. One of the major technical problems is the detection of signals from metabolites at some depth below the surface without detecting regions closer to the coil. In order to monitor tumor metabolism in vivo one must overcome this problem of selectively acquiring NMR signals from the tumor, or a particular region of the tumor, and discriminate against similar signals arising from

surrounding tissue.

Early NMR studies of tumor metabolism examined tumors implanted subcutaneously in convenient anatomical locations in the animal (i.e., close to the surface) e.g. the tail or flank region. The NMR signal was detected using a single radiofrequency pulse for excitation from a region determined solely by the placement of the coil and its diameter. As a result of the inhomogeneous rf field generated by the surface coil, the detected signal arises from an approximately hemispherical region of the sample of diameter equal to the coil diameter. This method has been used in a variety of in-vivo NMR metabolic studies but does not provide adequate localization.

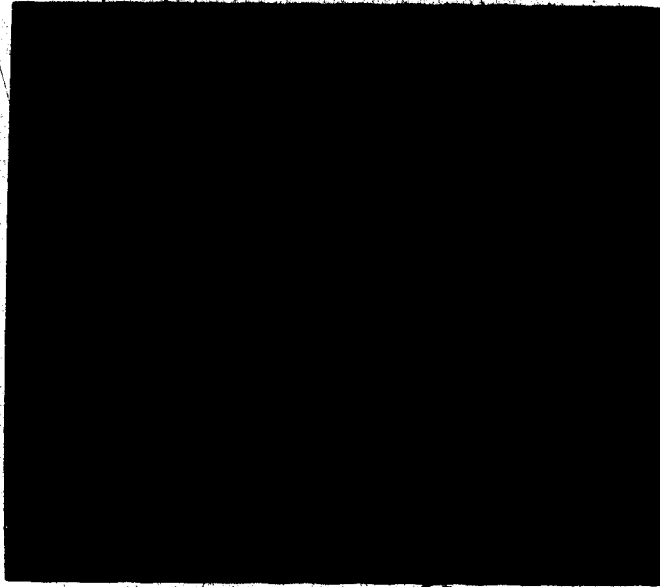
The sensitive regions generated in this way can be revealed experimentally. Using a slice phantom containing H_3PO_4 , a surface coil image was produced using a standard 2D-FT imaging sequence. The experimental parameters employed are described in Fig 2.1. Fig 1.9 (a) and (b) depicts the distribution of signal intensity relative to the rf coil. In fig 1.9 (a), progressing from the outer band inwards, the first bright band represents the region in the sample which experiences a 90° excitation pulse, the dark region of zero signal intensity corresponds to spins that experience a 180° pulse. The next bright band nearest the coil is that of spins experiencing a 270° pulse. In order to sample a region deeper into the tissue the pulse length is

Fig. 1.9

Surface coil images of the distribution of signal intensity generated by a single pulse relative to the rf coil.

- (a) The large curved region of bright intensity corresponds to the region in the sample that experiences a 90° excitation pulse ($\theta = 90^\circ$). The dark band of zero signal intensity corresponds to $\theta = 180^\circ$. The next small bright region nearest the surface coil corresponds to $\theta = 270^\circ$. The pulse length employed was 100 μsec .

- (b) An increase in the pulse length to 400 μsec results in the movement of the 90° excitation band further into the sample. In addition, high flux signal corresponding to $\theta = 270^\circ$, 450° and 630° regions of signal intensity can be observed, the 630° region being the closest to the surface coil.



increased. As a result, the 90° excitation band moves deeper into the sample, but this movement is accompanied by the appearance of additional regions producing high flux signals closer to the coil Fig 1.9. (b). The single pulse technique therefore provides a simple method of localizing on a selected region that is close to the surface of the sample but it is not possible to sample a deeper region without generating large signals near the coil. The spectra acquired are not therefore free of surface layer signals. Employing a surface coil with a single rf excitation pulse has the advantage of being easy to implement and provides moderate localization but the localized region is poorly defined and deeper regions of the body/animal are inaccessible.

Several techniques have been reported which claim to obtain spectra from discrete regions within an intact organ/tissue. These include topical magnetic resonance (TMR) (48), (49), Depth Pulse sequences (13), Depth Pulse sequences in conjunction with magnetic field gradients (12), Depth resolved surface coil spectroscopy (DRESS) (16), Volume selective excitation (VSE) (89) image selected in vivo spectroscopy (ISIS) (98), and spatially resolved spectroscopy SPARS (78). All of these methods offer improved localization over the single pulse method. We have implemented the phase cycled "depth pulse" localization sequences described by Bendall and Gordon (13) to acquire data from a specific region of tissue,

primarily because they do not require switched gradients. Depth pulse sequences are easy to implement, rapid, provide a well defined sensitive region, and have the ability to selectively monitor deeper regions of tissue. Ng and Glickson (95) demonstrated the improved localization afforded by the depth pulse technique by selectively acquiring signals from a necrotic region of a Dunn osteosarcoma.

1.6.1 DEPTH PULSE SEQUENCES

Depth pulse sequences have been designed to restrict signal response to within chosen ranges of tip angles. In order to remove the error signals obtained when using inversion recovery or spin-echo sequences with inhomogeneous rf fields, the rf pulses are phase cycled. The phase cycling leads to cancellation of contributions to the signal from spins that experience flip angles different from 90° , 270° , or 450° .

A series of pulse sequences can be constructed using the phase alternated inversion pulse $2\theta(+/-X)$, the excitation pulse θ , and the phase cycled refocusing pulse $2\theta(+/-X,+/-Y)$ in different combinations to yield the desired result (Table 1.1). Examples of depth pulse sequences are:

$$\theta; [2\theta(+/-X,+/-Y)]_2; AQ(+/-) \quad (1)$$

$$2\theta(+/-X); \theta; [2\theta(+/-X,+/-Y)]_2; AQ(+/-) \quad (2)$$

$$\theta/3; \theta/5; \theta(+/-X); AQ(+/-) \quad (3)$$

Progressive improvement in the localization afforded by the above sequences is illustrated in Fig. 1.10 which depicts ^{31}P NMR signal intensity versus pulse length. Curve (a) represents localization by a surface coil as a function of a single rf pulse, curves (b) and (c) are obtained with depth pulse sequences (1) and (2) respectively. Both sequences provide improved localization, i.e., narrowing of the 90° excitation band sequence (2) being better than sequence (1) due to the increased phase cycling. In both cases signals from high flux regions are still present. Curve (d) is obtained using depth pulse sequence (3) which suppresses the high flux signals resulting in a spectrum acquired from a certain depth without contributions from surface signals.

Prior to implementing the depth pulse sequence in vivo it is necessary to perform calibration experiments on phantom samples to determine the pulse length required to obtain a specific penetration depth.

Surface coil images of the sensitive volume produced by the excitation pulse sequence provide information on the distribution of signal intensity relative to the rf coil. The size, shape, and location of the observed volume can be varied by altering the coil diameter, rf pulse length, resonance offset, and sample position (36). The surface coil image is produced by applying the depth imaging sequence. The experimental parameters employed

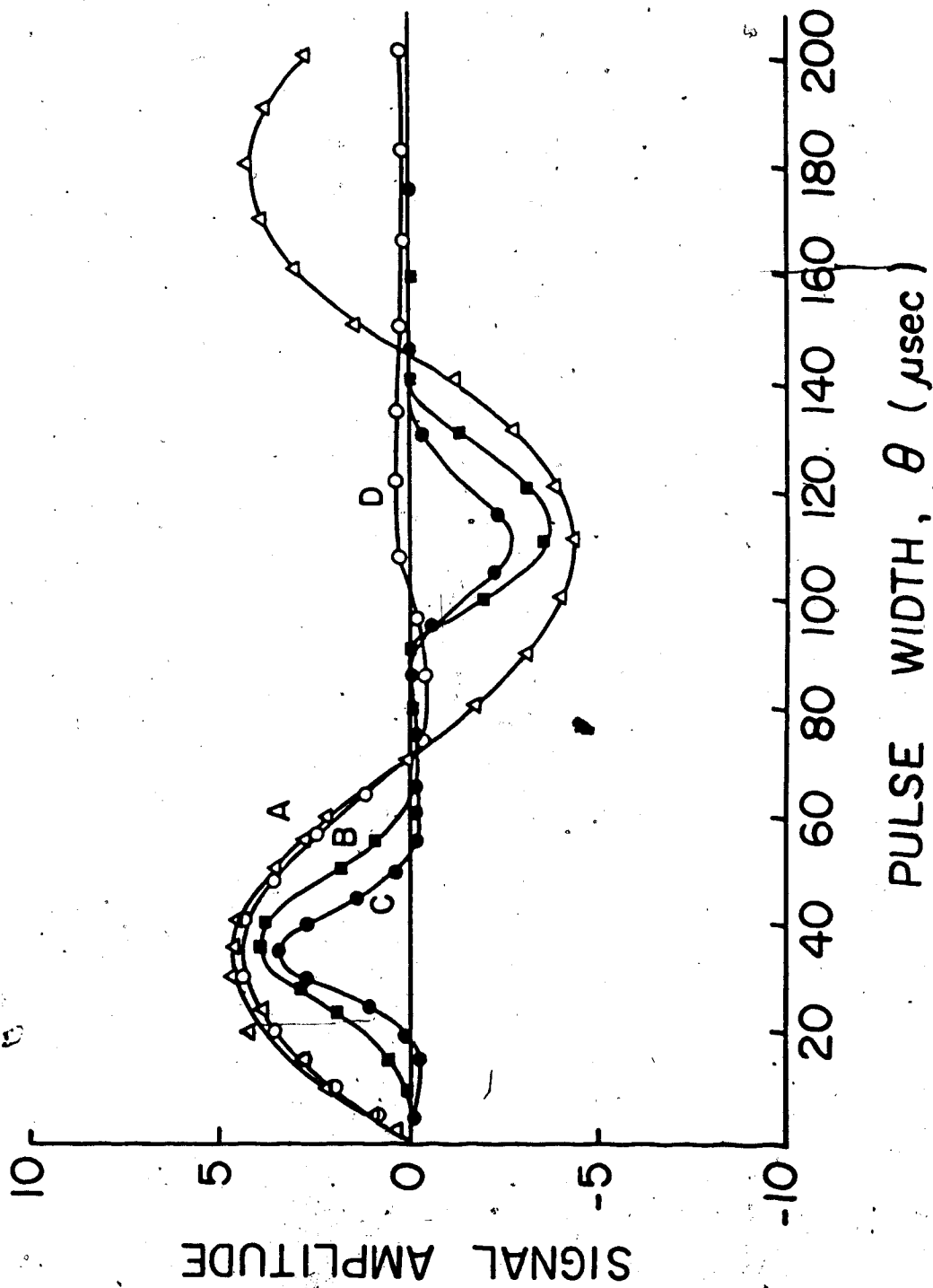


Fig. 1.10 Plots of ^{31}P NMR signal intensity versus pulse length for (A) a single pulse, (B) depth pulse sequence (1), (C) depth pulse sequence (2), and (D) depth pulse sequence (3). Adapted from reference (95).

sequence. The experimental parameters employed are described in Fig. 2.1. In order to "see" and to calibrate the region of tissue from which spectra are obtained, the surface coil image of the sensitive volume can be superimposed onto a transverse image of the animal produced by the circumscribing coil. The two images are combined by adding the two time-domain data sets together.

Depth pulse localization sequences are well suited to a study of tumor metabolism since, provided the tumor is large enough, spectral characteristics of a particular region of the tumor can be obtained.

The advantage of using the depth pulse sequence therefore is that it is easy to implement, rapid and provides a well defined sensitive region. Deeper regions of tissue can be monitored but with a reduction in signal intensity and with some reduction in control of the regional extremities due to the larger diameter of the surface coil.

TABLE 1.1 Types Of Component Pulses Used In A Depth Pulse Sequence Together with Their Individual Effects

<u>Pulse</u>	<u>Phase Cycling</u>	<u>Effect</u>
Excitation (Θ)	+X	90° excitation pulse at the center of the sensitive volume.
Inversion ($N\Theta$)	+/-X	where $N=2,4,6,8\dots$ results in narrowing of the excitation bands.
(Θ/N)	+/-X	where $N=3,5,7,\dots$ suppresses high flux signals from 270°, 450°, 630°.. regions respectively.
Refocusing (2Θ)	+/-X, +/-Y	narrows the excitation bands.

2. METHODS

2.1 NMR TECHNIQUES

NMR measurements were made at 37°C, using a 40 cm horizontal bore superconducting magnet operating at 2.35T, corresponding to a Larmor frequency of 40.55 MHz for phosphorus. The rats were anaesthetized with somnotol (65mg/kg I.P.) and secured on a calibrated plexiglass platform for accurate placement within the magnet. The body temperature of the animal was maintained at 37-38°C by forcing warm air from a hair dryer into the magnet bore to establish a warm atmosphere over the animal during the experiment.

A two turn 0.8cm x 1.0cm surface coil was used both to transmit and detect signals from the tissue. Spatial localization was achieved by employing a depth-pulse sequence (13) which contained the following pulses;

$\theta/3$; $\theta/5$; θ (+/-x); AQ (+/-)

The $\theta/3$ and $\theta/5$ pulses, phase cycled through +x and -x, suppress the contributions to the spectrum from regions in the sample whose spins would experience 270° and 450° tip angles in a one pulse experiment.

Spectra were obtained by Fourier transformation of accumulated FID'S signal averaged with a repetition interval of 1.0s for 512-1024 transients and obtained with a spectral width of 2500Hz. Each FID contained 2048 data

points/scan.

Relative concentrations were estimated from the intensity of the corresponding ^{31}P NMR resonances. Saturation factors of 1.7, 1.4, 2.0, 1.8, 1.5, 1.3, and 1.1 for the partial saturation of the phosphomonoester (PME), inorganic phosphate (Pi), phosphodiester (PDE), phosphocreatine (PCr), and the γ , α , and β phosphates of the ATP resonances were applied to the respective intensity values obtained. Assignments of resonances for the ^{31}P metabolites were made by comparison of the chemical shift obtained with those of published values.

A convolution difference routine was applied in order to remove resonances of broad linewidth. Line broadening functions of 75Hz and 15Hz were applied to the FID and the resulting spectra subtracted.

To maximize its homogeneity the magnetic field was shimmed using the proton signal from kidney water. This proton signal was detected with the ^{31}P probe tuned and matched to the ^1H frequency of 100.19MHz. The proton line width was typically 19-25Hz. The 90 degree pulse length was independently determined for each nucleus by positioning a 4cm glass sphere containing 85% H_3PO_4 on the opposite side of the coil to the sample, at an equivalent distance from the coil to the chosen region of interest within the sample.

^1H NMR images of the abdomen and surgically exposed kidney were obtained with a circumscribing rf coil using a

standard spin-echo 2D-FT imaging sequence. The spin echo imaging sequence consisted of a soft 90 degree slice-defining pulse followed by a 300 usec hard 180 degree refocusing pulse for the echo. The time interval between the echoes (TE) was 32 msec, the repetition time (TR) was 1.0 sec. Frequency encoding was determined by the field gradient in the X direction, phase encoding by the stepped field gradient in the Y direction (128 steps) and slice defining by the field gradient in the Z direction. All slices obtained were transverse slices through the kidney and abdomen. All gradient strengths were 0.5G/cm, and the slice thickness obtained was ~3mm.

Images of the "sensitive volume" generated by the depth pulse sequence were acquired using the surface coil with the depth pulse sequence in conjunction with the standard spin-echo imaging sequence. (Fig. 2.1).

The ^1H 180-degree hard pulse and 90 degree soft pulse were calibrated as previously described using a 4mm glass sphere containing H_3PO_4 and corresponded to the appropriate depth into the sample from which the ^{31}P spectra were obtained.

The combined surface coil and imaging coil images were obtained by adding the two time-domain data sets together prior to reconstruction of the image. The same X, Y, and Z gradient strengths were used for both images and therefore the two images were directly superimposable.

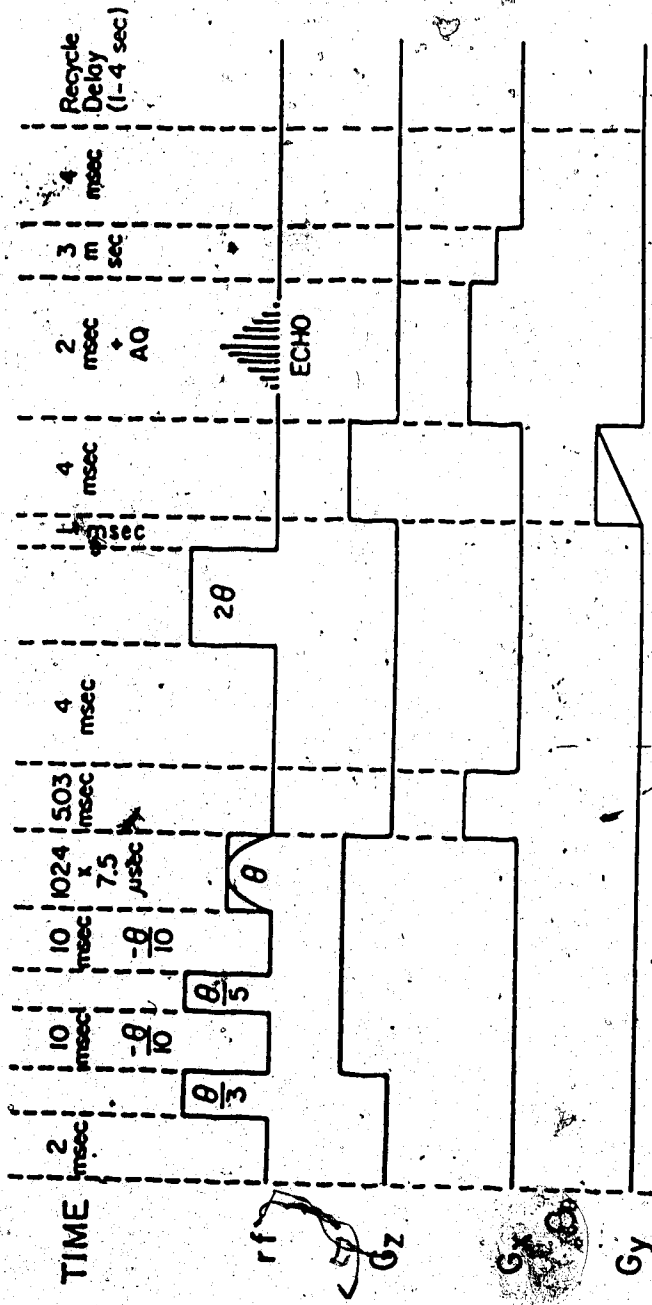


Fig. 2.1 Pulse sequence employed to obtain surface coil images. The 180° hard pulse and the 90° soft pulse were calibrated for each experiment corresponding to the depth into the tissue from which the 3lp data were obtained.

2.2 DETERMINATION OF INTRACELLULAR pH BY ^{31}P NMR

The apparent intracellular pH was estimated from the chemical shift of the Pi peak relative to PCr. This shift was calibrated with solutions of 120mM NaCl, 20mM PCr, 10mM ATP, 5mM Na_2HPO_4 , 5mM MgCl₂, titrated by addition of small aliquots of 0.1M HCl or 0.1M NaOH. The pH of the solutions was measured with a Fisher Accumet pH meter model 805 MP fitted with a glass electrode and calibrated with standard buffers (Fisher Scientific) of pH 4.0, 7.0, and 10.0 at 37°C. The PCr resonance, defined at 0.00 ppm, was used as an internal chemical shift reference. In cases where extremely small PCr peaks were present, 0.00 ppm was assumed from the α -ATP peak (δ -7.71) which we demonstrated to be relatively insensitive to changes in pH over the range pH 5.0 to pH 8.0 (Fig.2.2). The sample temperature was maintained at 37°C by placing the samples in a 37°C water bath prior to the acquisition of spectra and by controlling the magnet bore temperature with warm air from a hair dryer.

^{31}P spectra for the titration curve were obtained using the 0.8 x 1.0 cm surface coil under the following conditions: pulse length, 10 μ sec; spectral width, 2000Hz; time domain points, 8K; relaxation delay, 4.0 sec; number of scans, 24.

A standard pH titration curve depicting the variation of chemical shift of Pi with pH was constructed from the experimental results obtained. (Fig 2.3) An apparent pK

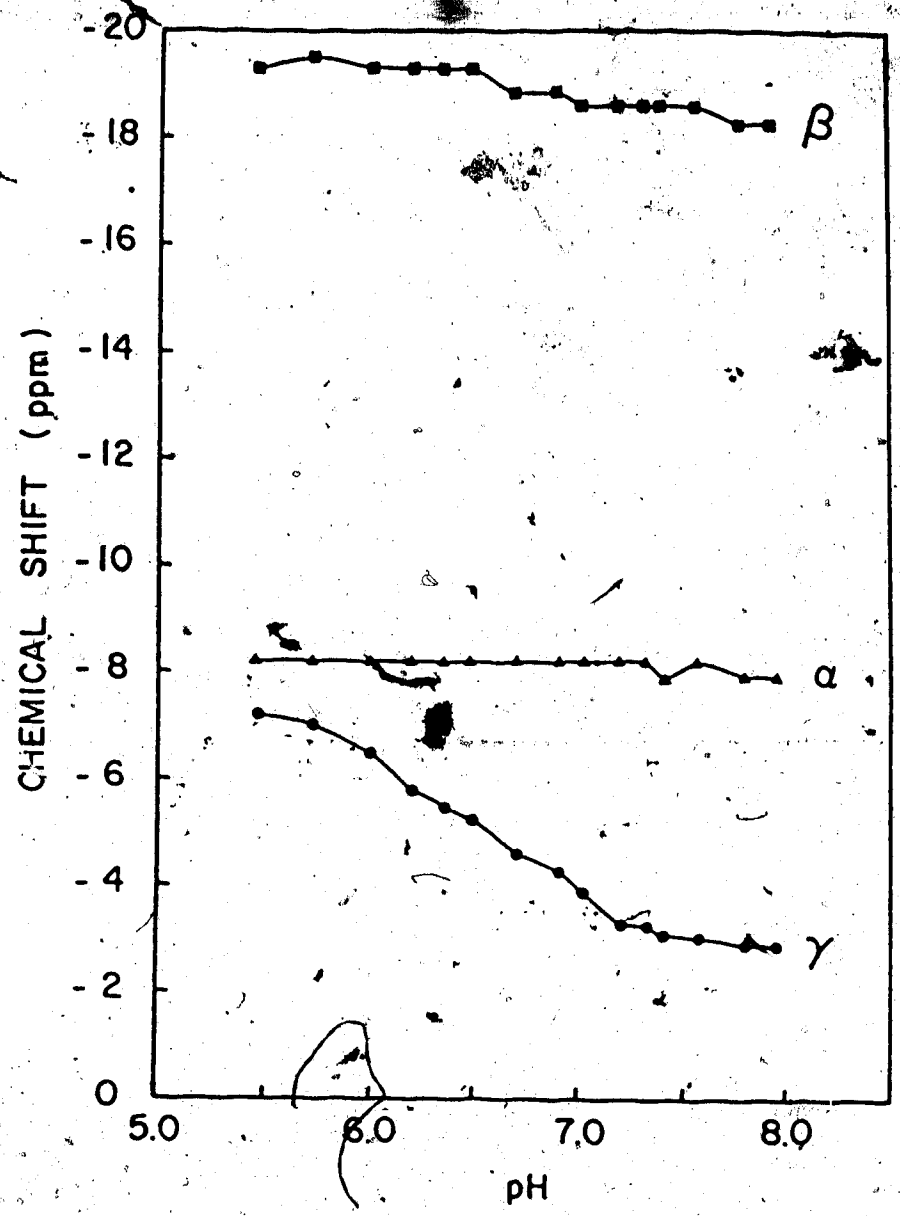


Fig. 2.2 The chemical shifts of the ^{31}P NMR signals of 10 mM ATP in the presence of 5 mM MgCl_2 plotted as a function of pH.

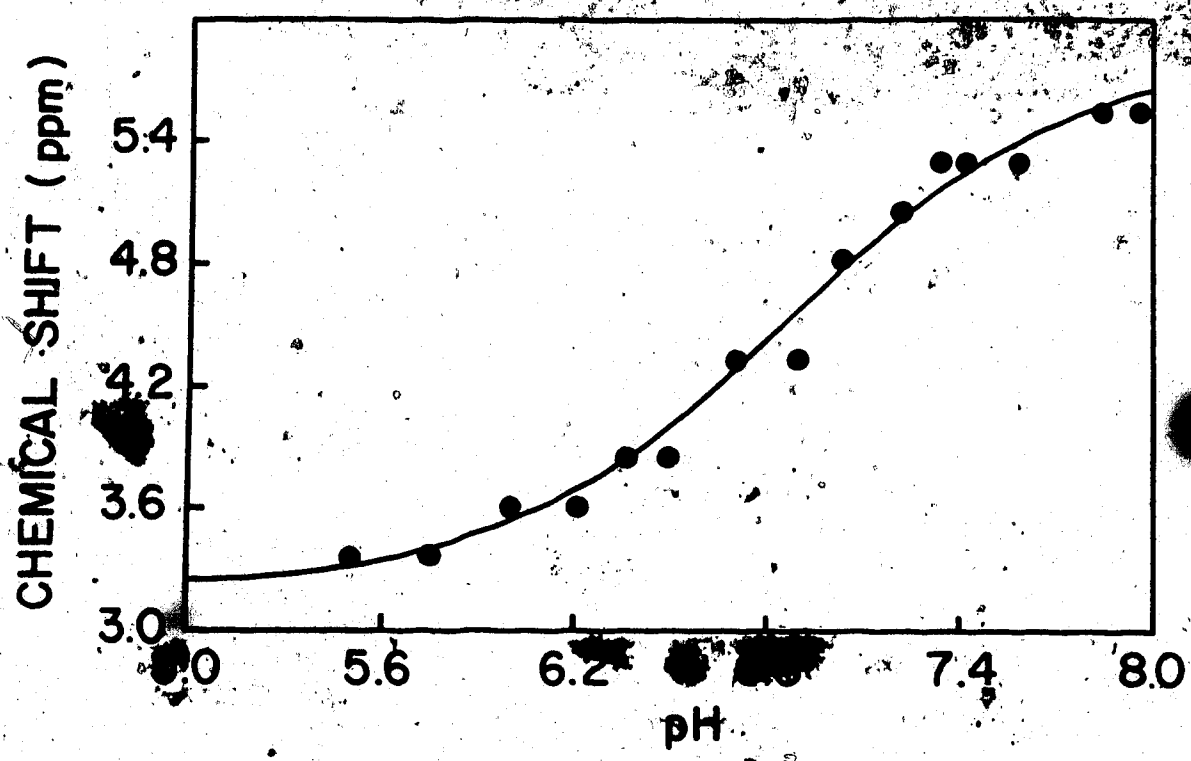


Fig 2.3 Variation of the chemical shift of inorganic phosphate (Pi) with solution pH at 37°C. The chemical shift is expressed relative to that of phosphocreatine (PCr). Solutions contained 20 mM PCr, 10 mM ATP, 120 mM NaCl, 5 mM Na₂HPO₄, 5 mM MgCl₂, and were titrated with 0.1 M NaOH or 0.1 M HCl.

for P_i of 6.80 was estimated from the curve.

The relationship between the pH and the measured chemical shift of P_i is described by the following equation:

$$pH = pK - \log \left(\frac{\delta_{obs} - \delta_{HPO_4^{2-}}}{\delta_{H_2PO_4^-} - \delta_{obs}} \right)$$

where δ_{obs} is the observed chemical shift of P_i , $\delta_{HPO_4^{2-}}$ and $\delta_{H_2PO_4^-}$ are the limiting chemical shifts at high (pH10) and low (pH4) pH. A pH chart was calculated (for a chemical shift range of 3.60-5.30 ppm) using the above equation. The values for the acidic and basic endpoints and the pK were determined to be $\delta_{HPO_4^{2-}} = 5.19$ ppm, $\delta_{H_2PO_4^-} = 5.72$ ppm, and $pK = 6.80$ respectively.

2.3 PREPARATION OF TUMOR CELLS

Walker carcinosarcoma 256 cells were obtained from Dr. A.J. Franko, of the Cross Cancer Institute, Edmonton, Alberta. Tumor chunks stored frozen in liquid nitrogen were thawed and implanted subcutaneously in the flanks of male Sprague Dawley rats weighing 180-250g. Rats were provided with rat chow and water ad libitum.

After a period of 10 days growth the tumors were excised and minced in phosphate buffered saline (PBS). A single cell suspension was prepared by trypsinization of the tumor cells using a final concentration of 0.1% trypsin. The sample was incubated with the enzyme for 30 minutes at 37°C. The reaction was stopped by the addition of cold media plus serum and filtered through sterile gauze. The

cells were then harvested by centrifugation at 1000 rpm for 20 minutes at 5°C. The pelleted cells were resuspended in approximately 5 ml of phosphate buffered saline.

2.4 KIDNEY ISOLATION AND TUMOR IMPLANTATION

Rat kidneys were surgically isolated and implanted with Walker sarcoma tumor cells by the method of P. Gullino et al (54). Rats were anaesthetised by intraperitoneal injection of somnotol (65mg/kg I.P.). A 2 cm incision was made in the lumbar region, the kidney was carefully isolated from the surrounding adipose tissue and pulled out through the abdominal muscle layer into the subcutaneous space. Care was taken to avoid damage to the renal pedicle. The abdominal muscle layer was partially sutured under the kidney to prevent the kidney from falling back into the abdominal cavity. Approximately ($\sim 10^6$) Walker Sarcoma 256 cells suspended in 100ul of culture medium were injected into the rat kidney just under the capsule. The kidney was then wrapped in an hour-glass shaped piece of parafilm and heat sealed to maintain the organ "tissue isolated". After approximately 15 days, the infiltrating and destructively growing tumor cells completely replace the kidney tissue leaving the tumor mass connected to the host by a single artery and vein.

2.5 PRODUCTION OF ISCHEMIA IN THE RAT KIDNEY

The kidney was isolated as described in section 2.4. The renal artery was isolated and a loop of 3-0 silk suture was threaded around the artery. The thread was knotted and fed through a 3 cm long piece of plastic capillary tubing. The tension of the tubing on the thread was sufficient to hold the capillary in place, tight against the artery, such that arterial flow could be stopped to produce a period of ischemia and then reestablished to allow the monitoring of the recovery.

2.6 CHEMOTHERAPY

Cyclophosphamide (500mg) was obtained from Bristol Laboratories of Canada. The drug was dissolved in 12.5ml of bacteriostatic water to a final concentration of 40mg/ml. After 9 days of tumor growth in the rat kidney a freshly prepared solution of cyclophosphamide (150mg/kg) was injected under direct vision into the femoral vein. Each animal received its dose as a single injection. NMR spectra were acquired 1 hr., 2 days, 4 days, and 5 days post injection. The effect of the drug on other tissues, namely muscle and normal kidney, was also examined.

2.7 HISTOLOGY

Healthy kidneys and kidneys containing tumors at various stages of growth were excised and fixed in 10% formaldehyde. After embedding in paraffin, 5 um sections were cut and stained with hemotoxylin-eosin (HE) according to routine methods. Photographs were produced from the microscope slides at a magnification of 4:1 or 10:1.

3. RESULTS AND DISCUSSION

The main objective of this project was to improve on previous experimental protocols for monitoring the bioenergetic state of normal and malignant tissue by ^{31}P NMR spectroscopy. In our approach to this problem emphasis has been in two areas; (a) the development of a tumor model and (b) implementation and evaluation of NMR localization techniques to ensure that the ^{31}P spectra acquired are from a well defined region of tissue.

With improvements in these areas, untreated tumor growth was monitored at various stages to provide information about the biochemistry and physiology of the tumor and to serve as a baseline for the analysis of the effect of chemotherapy and ischemia.

3.1 DEVELOPMENT OF THE TUMOR MODEL

Previous ^{31}P -NMR studies of tumor metabolism analysed tumors implanted subcutaneously in the host in convenient anatomical locations i.e., the flank or tail. In this instance, the invading tumor is in direct contact with surrounding tissue. One of our objectives was to develop a tumor model in which the margins of the tumor are well defined in order that tumor energy

metabolism could be monitored with minimum contamination from extraneous tissues. This was achieved by employing the method originally described by P. Gullino et al (54). Tumor cells were implanted into the kidney of a Sprague Dawley rat and the organ was wrapped in a parafilm pouch. In maintaining the tumor tissue isolated, the cellular contamination of the tumor by surrounding tissue is reduced. In order to minimize the spectroscopic localization required, the tumor although implanted into the rat kidney, was not buried in the abdominal cavity of the animal. The tumor was surgically exposed for the NMR measurements, thereby reducing the contribution to the NMR signals from muscle and adipose tissue.

Another important characteristic of this model is that the tumor grows in the parafilm pouch connected to the host by only the vascular pedicle (renal artery and renal vein). This feature provides considerable control over the administration of metabolic insults such as chemotherapy and ischemia.

Gullino et al (54) noted that in general the biological characteristics of tumors grown in this manner resembled tumors grown by subcutaneous implantation. On cross-section however, the tumor grown in the enclosed parafilm pouch appeared to have less extensive necrotic areas than the subcutaneous implants of equal size.

As the tumor cells infiltrated the kidney, the tumor mass attained a round or ovoid shape and varied in colour from a pale yellow to pink to dark red with the occasional appearance of white patches. The dark red regions are probably due to hemorrhage from the host organ after injection of the tumor cells which could not always be avoided. The white patches observed may be the result of infection.

About eight days after tumor implantation, a substantial amount (10-20ml) of fluid resembling plasma accumulated in the subcutaneous space between the skin and the parafilm pouch containing the tumor. Since a normal kidney wrapped in parafilm does not produce this excess fluid this can be interpreted as an effect of the tumor alone (54). Tumor growth in the rat kidney was considerably variable. The tumor/kidney wet weight examined 10 days after implantation of the tumor cells varied from 1.9-4.1g. The average diameter of the tumor at this stage of growth was 4cm.

Although growth of the Walker sarcoma cells is very rapid and destructive, the tumor implants of the kidney probably contain varying amounts of normal kidney tissue. Gullino et al (54) noted that at advanced stages of growth, histological examination revealed the presence of some intact glomeruli dispersed in the neoplastic tissue.

The problems encountered with this model were the

occasional onset of hemorrhage in the kidney after injection of the tumor cells, and the aggressive growth of the tumor which at late stages of growth often escaped the confines of the parafilm sack and spread to the surrounding abdominal tissue.

The tumor cells for injection into the rat kidney were first propagated in a rat flank for a period of 10 days. A single cell suspension for injection was then prepared by trypsinization of the excised tumor. This cell suspension contains a heterogeneous population of cells, some of which may not be capable of propagating the tumor. This may account for the fact that the success rate for tumor transplantation into the rat kidney was only 50-60%. Cell viability studies should have been performed to ensure tumor growth.

An unsuccessful attempt was made to decrease the 10 day waiting period for tumor growth by growing and maintaining the Walker sarcoma cells in tissue culture. A sample of the resuspended cells, added to tissue culture media and incubated for three days did not reach confluency. After a period of one week all tumor cells had died.

Although the Walker sarcoma model was employed throughout this study preliminary results on a second tumor model were obtained which had several technical advantages over the Walker sarcoma. Glioma cells obtained from Dr. Warren, University of Alberta,

Edmonton, Alberta, were capable of propagation in tissue culture and were therefore easily tested for cell viability prior to injection. Injection of this homogeneous population of tumor cells yielded a 100% success rate for tumor growth when implanted into the kidneys of Fisher 344 rats. The glioma is not as aggressive as the Walker sarcoma and tended to grow as a raised nodular mass on the surface of the kidney and was not observed to invade surrounding tissues at late stages of growth.

3.2 INVESTIGATION OF THE SPATIAL LOCALIZATION CHARACTERISTICS OF DEPTH PULSE SEQUENCES

In order to precisely define the origin of our spectroscopic data, NMR localization techniques were implemented, namely the depth pulse sequences described by R. Bendall (13). The spatial localization characteristics of these sequences were examined initially in vitro using phantoms containing 85% H_3PO_4 . The results obtained were compared with those obtained using a single rf excitation pulse. A 4 mm diameter glass sphere containing H_3PO_4 was placed 1 cm above the surface coil. Signal intensity was recorded as a function of pulse length for the following pulse sequences:

- a) a single pulse

b) $2\theta(+/-X); \theta; 2\theta(+/-X, +/-Y)$

c) $2\theta(+/-X); \theta; [2\theta(+/-X, +/-Y)]_2$

A plot of ^{31}P NMR signal intensity versus pulse length (Fig 3.1) for the single pulse (a) resulted in a sine curve. Plots for the depth pulse sequences yielded modified periodic curves, the maxima and minima being coincident with those of curve (a). As predicted from the theoretical curves of signal intensity versus pulse length (Fig 1.10), the depth pulse sequences produced a narrower localized region than the single pulse sequence. The narrowing of the widths of both the positive and negative segments of the curves represents a narrowing of the bands of excitation in the sample. DEPTH pulse sequence (c) producing the narrower region due to the increased number of steps in phase cycling. The signal intensity for the three curves produced by the above pulse sequences was found to decrease in the order $a > b > c$, this is a consequence of the inhomogeneity of the field generated by the surface coil.

Further demonstration of the improved localization afforded by the depth pulse sequences was provided by surface coil images of the sensitive volume produced by the pulse sequence (Fig 3.2). The images enabled us to "see" the narrowing of the bands of excitation when progressing from a single pulse to the depth pulse sequence (b) or (c).

Application of the depth pulse sequences in vivo

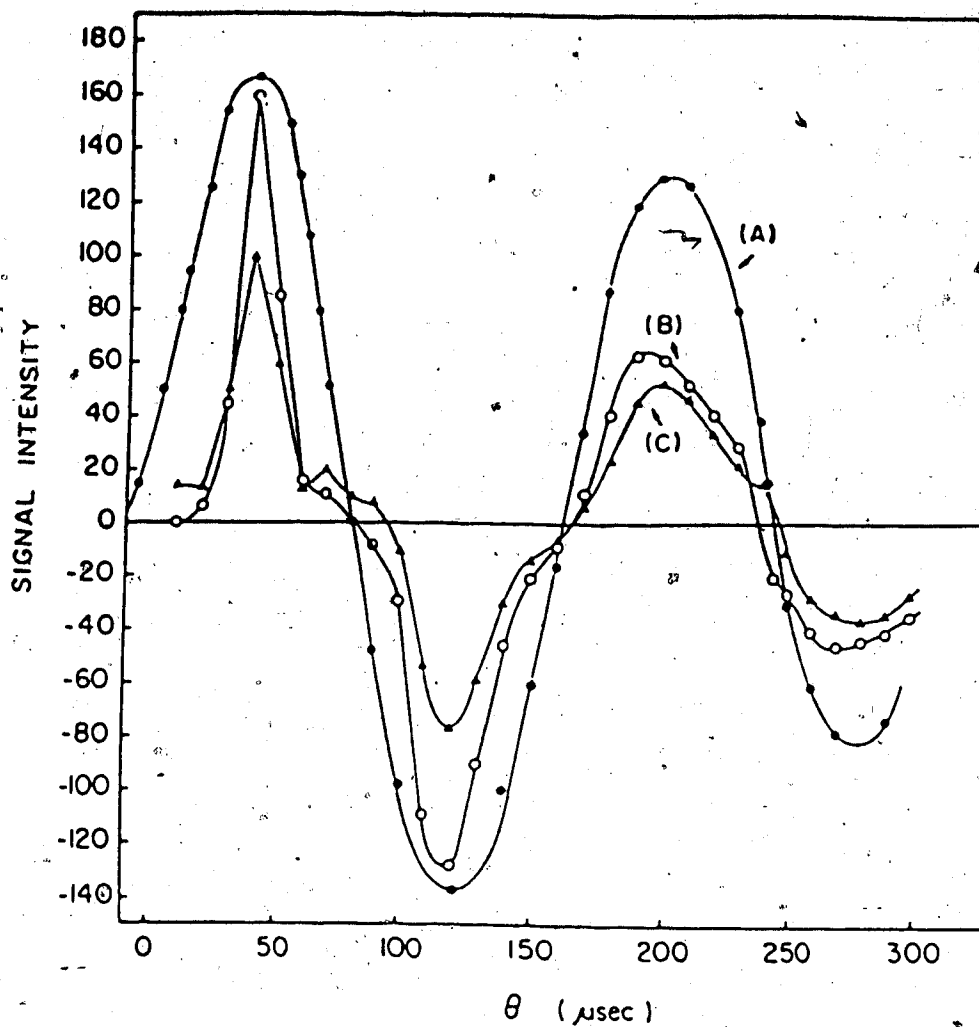
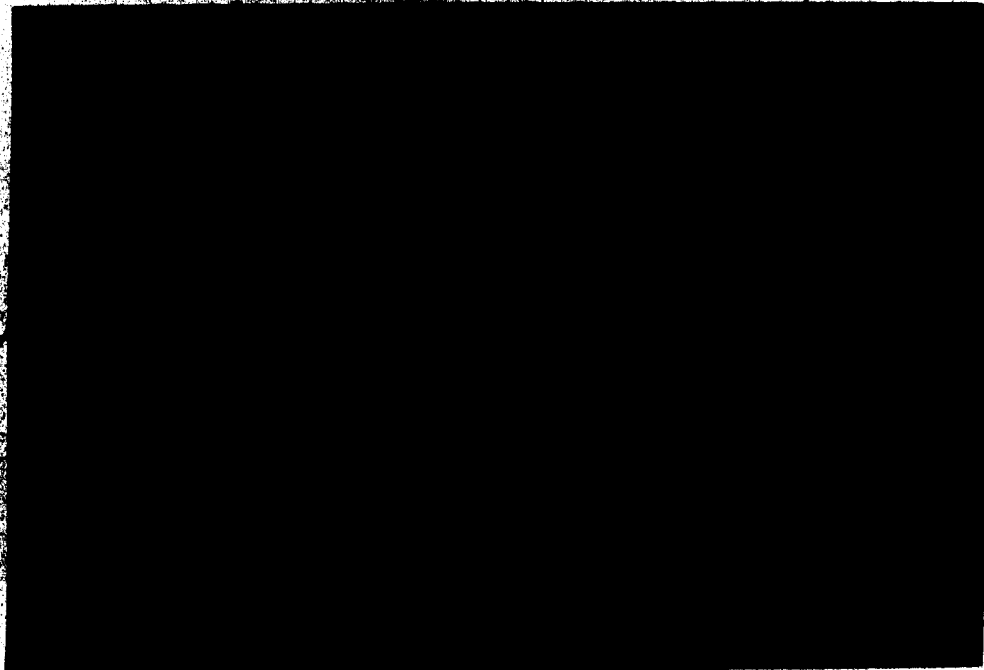


Fig 3.1 Plots of signal intensity for the H_3PO_4 phantom sample (1 cm from the surface coil) versus pulse length. (A) single pulse, (B) depth pulse sequence $2\theta(\pm x); \theta; 2\theta(\pm x, \pm y)$ (C) depth pulse sequence $2\theta(\pm x); \theta; [2\theta(\pm x, \pm y)]_2$.

Fig 3.2 Surface coil images demonstrating the ability of the depth pulse sequence to narrow the excitation bands in the sample.

a) Sensitive volume produced using a standard spin-echo pulse sequence. (90° - τ - 180° - τ -AQ). The ^1H 180° hard pulse was 800 μsec . The soft 90° pulse gain setting was 380.

b) Sensitive volume produced using the depth pulse sequence in conjunction with the spin-echo sequence DP- 90° - τ - 180° - τ -AQ (where DP=2 θ ; 2 θ). The ^1H 180° hard pulse was 800 μsec . The soft 90° pulse gain setting was 380.



requires calibration experiments to determine the pulse length and power amplifier gain settings for obtaining a particular penetration depth. A calibration curve of penetration depth (mm) versus pulse length was constructed using a 5 mm diameter glass sphere containing H_3PO_4 placed at various distances from the $0.8 \times 1.0 \text{ cm } ^{31}\text{P}$ surface coil (Fig 3.3). At each distance the ^{31}P 180° pulse, the ^1H 180° hard pulse, and the ^1H 90° soft pulse were determined. The power amplifier gain settings were 3.0, 3.5, and 3.5, respectively. The ^{31}P 180° pulse was determined for each experiment.

In order to penetrate deeper into a sample, the pulse length must be increased so that the 90° tip angle occurs at greater depths. A consequence of this is that regions of high flux signals (270° and 450°) are generated closer to the coil. These high flux signals can be suppressed to less than a few percent by employing the following DEPTH pulse sequence $\Theta/3; \Theta/5; \Theta(+/-X); AQ(+/-)$ as illustrated in Fig 3.4. This can also be demonstrated in the corresponding surface coil images in Fig 3.5. The above depth pulse sequence was employed to provide spatial localization for all in vivo ^{31}P NMR spectra reported in this thesis, unless otherwise indicated.

In order to determine the region of tissue from which our ^{31}P spectra were obtained, surface coil images of the sensitive volume generated by the depth pulse

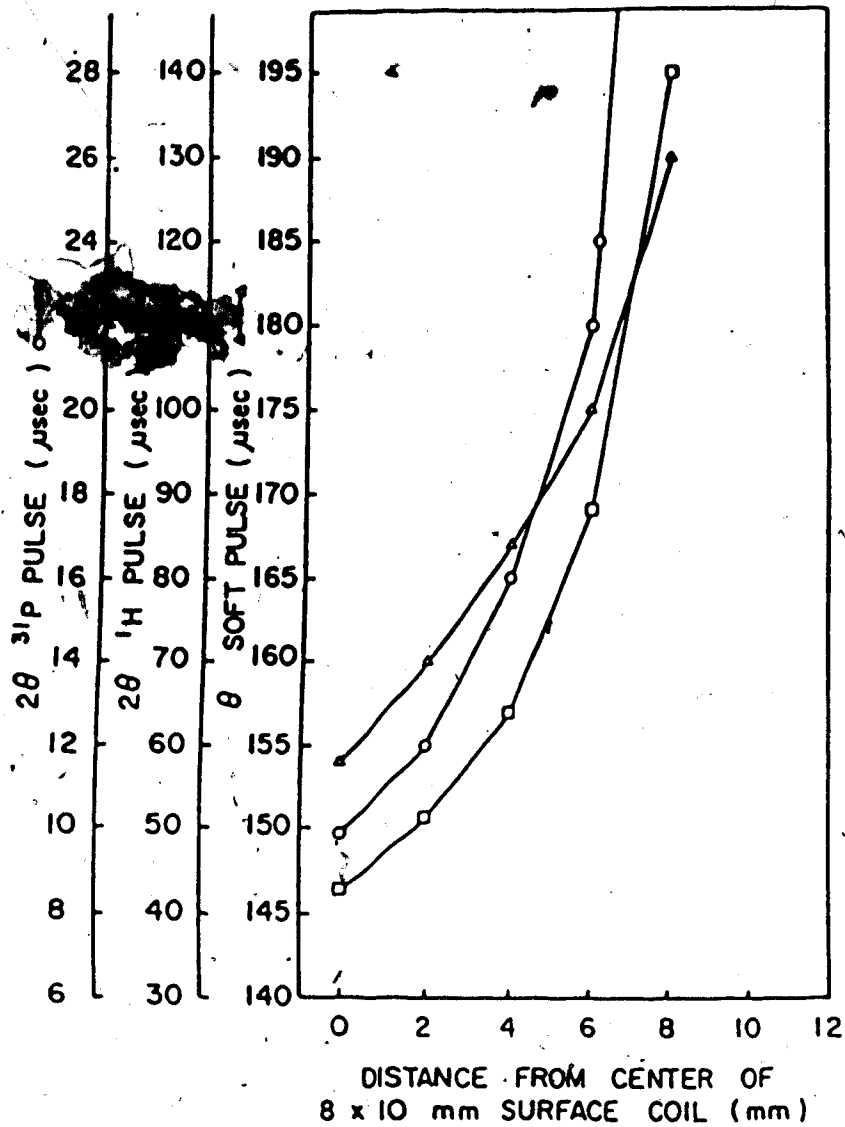


Fig. 3.3

Calibration of the penetration depth for the 8 x 10 mm surface coil. A 5 mm diameter sphere was placed at various distances from the center of the coil. The ^{31}P 180° pulse, ^1H hard 180° pulse, and the soft 90° pulse were determined for each distance. The power amplifier gain settings were 3.0, 3.5, and 3.5, respectively.

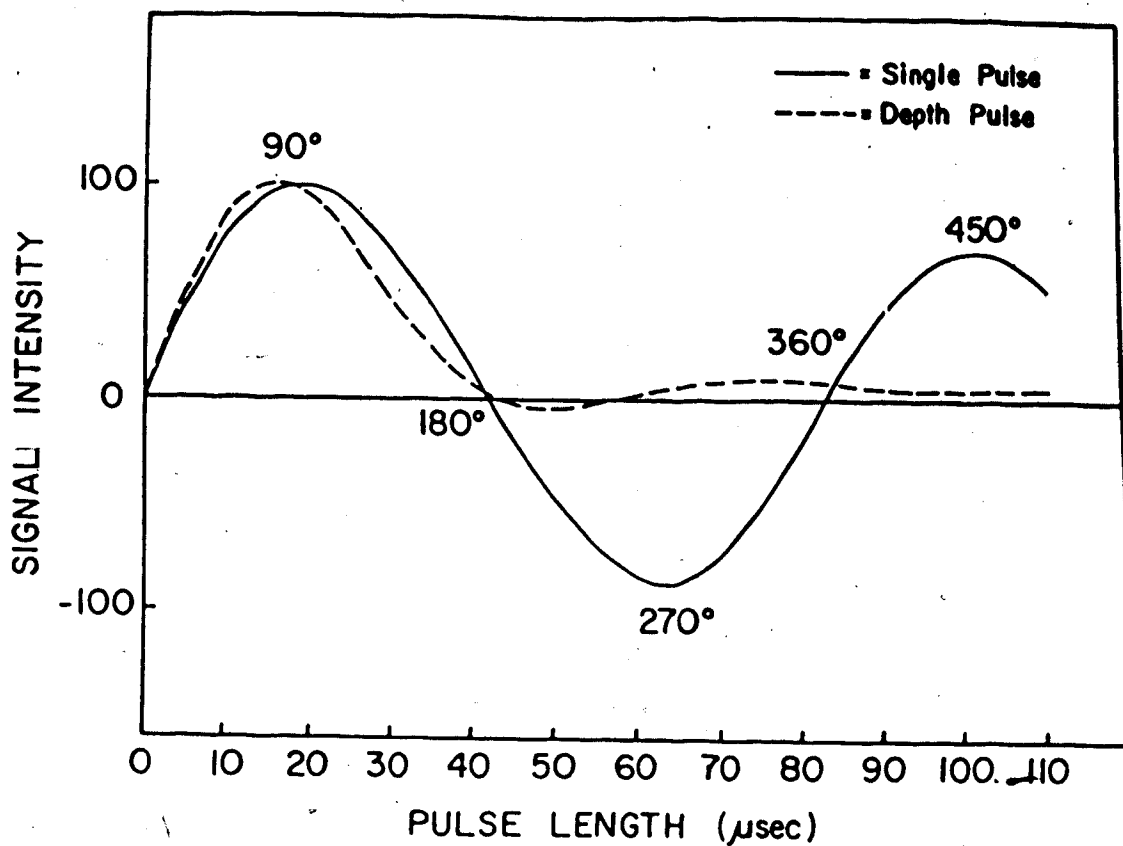


Fig. 3.4

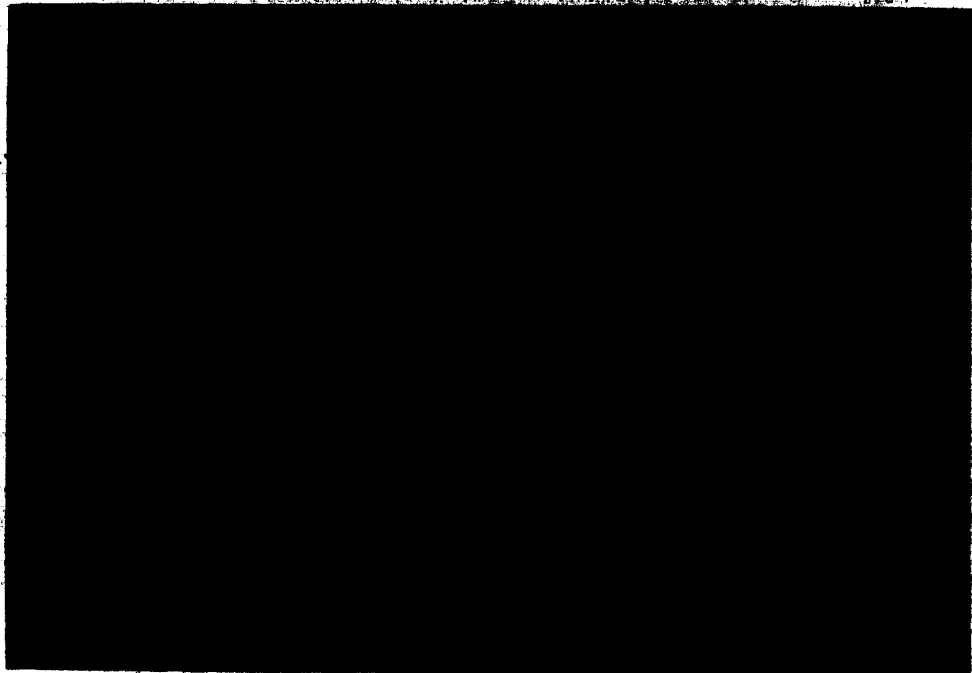
Demonstration of suppression of high flux signals (270° and 450°) using DEPTH pulse sequence $\theta/5$; $\theta/3$; $\theta(\pm x)$; AQ(+/-). A 4 mm sphere containing H_3PO_4 was placed 2 mm above the surface coil. Signal intensities were recorded as a function of pulse length using a single pulse (—), and the depth pulse sequence (----).

Fig. 3.5

Surface coil images demonstrating the ability of the DEPTH pulse sequence $\theta/3$; $\theta/5$; to suppress high flux signals (270° and 450°).

- a) Sensitive volume produced using a standard spin-echo pulse sequence: (90° - τ - 180° - τ -AQ).
The ^1H hard pulse was 800 μsec .
The soft 90° pulse gain setting was 380.

- b) Sensitive volume produced using the DEPTH pulse sequence in conjunction with the spin-echo sequence. DP- 90° - τ - 180° - τ -AQ (where DP = $\theta/3$; $\theta/5$)
The ^1H hard pulse was 800 μsec .
The soft 90° pulse gain setting was 380.



sequences were superimposed onto ^1H images (obtained with a circumscribing coil) of the abdomen and exposed kidney. The values for the 180° hard pulse, and 90° soft pulse used to generate the images corresponding to the region from which the ^{31}P spectra were obtained were determined from the calibration curves. Fig 3.6 and Fig 3.7 depict images of a transverse section through the rat abdomen and the exposed kidney. The regions of bright signal intensity in the kidney represent the regions from which the ^{31}P spectra were obtained. A 2θ ^{31}P pulse length of 12 usec corresponds to a penetration depth of 2mm into the rat kidney (Fig 3.6), (ie. $\theta=90^\circ$ at 2 mm) whereas the shorter pulse length, $2\theta=5$ usec, corresponds to excitation of the surface of the rat kidney (Fig 3.7).

3.3 DETERMINATION OF SATURATION FACTORS TO APPLY TO THE in vivo ^{31}P NMR SPECTRA

All in vivo spectra were acquired using the DEPTH pulse sequence $\theta/3; \theta/5; \theta(+/-X); AQ(+/-)$, with a repetition interval of 1.0 sec. In order to determine the relative concentration of a particular ^{31}P metabolite from the intensity of its resonance, the time between rf pulses must be at least five times the longest longitudinal relaxation time (T_1) in the sample. Due to the fact that the different ^{31}P metabolites have

Fig. 3.6 Superimposed images of a transverse section of the abdomen and exposed kidney indicating the region (2 mm depth) from which the ^{31}P spectra were obtained. The images were obtained using circumscribing and surface coils. The pulse length for the ^{31}P 2θ pulse was 12 μsec , that for the ^1H 2θ pulse was 51 μsec . These pulse lengths corresponded to a penetration depth of 2 mm from the centre of the surface coil to the centre of the region of excitation.

(b) Enlargement of the rat kidney in image (a).

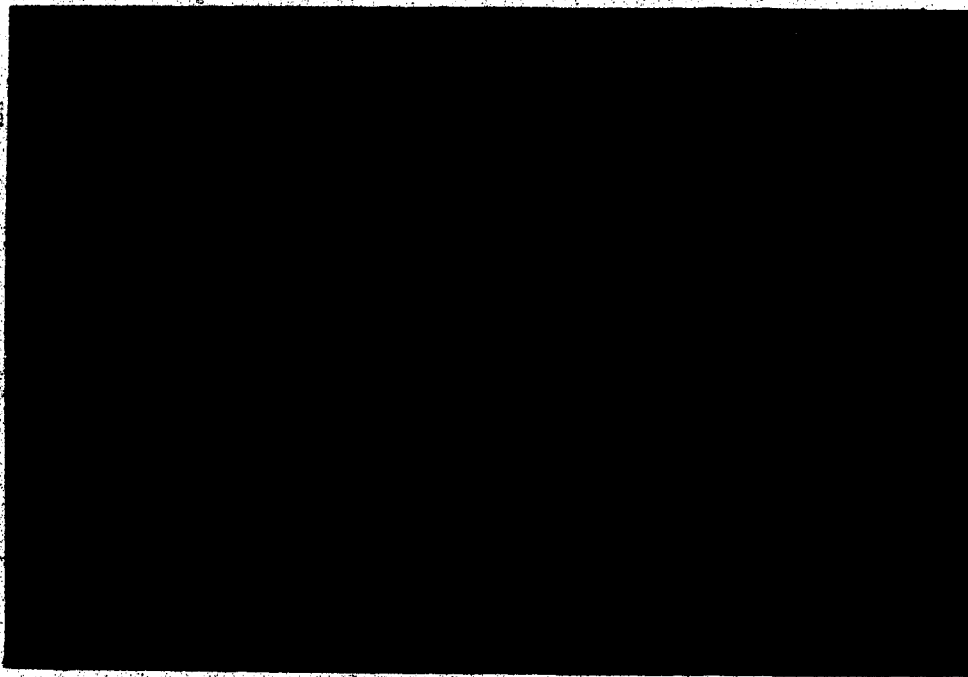
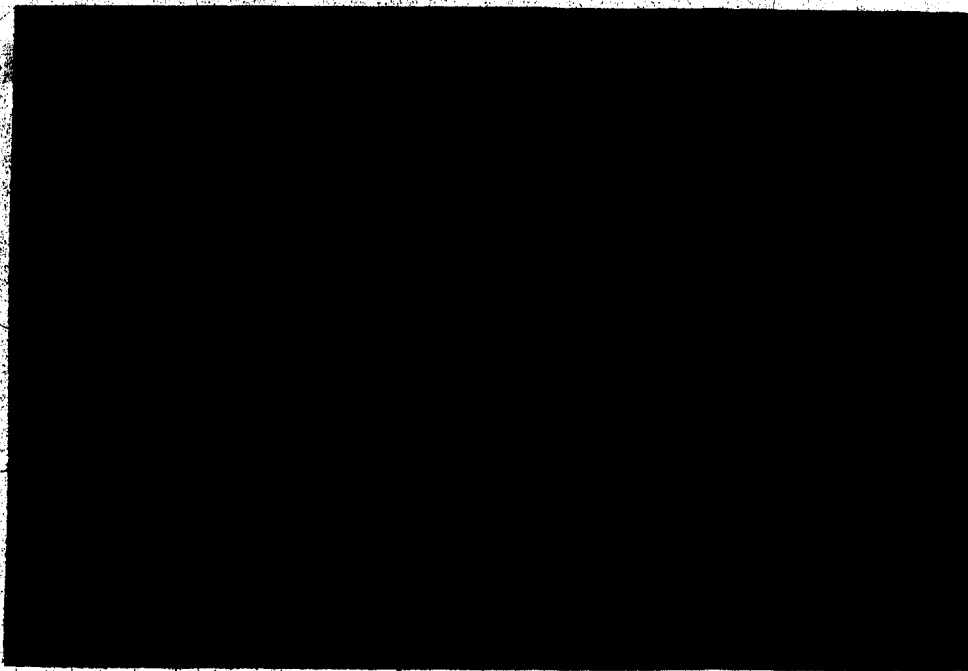
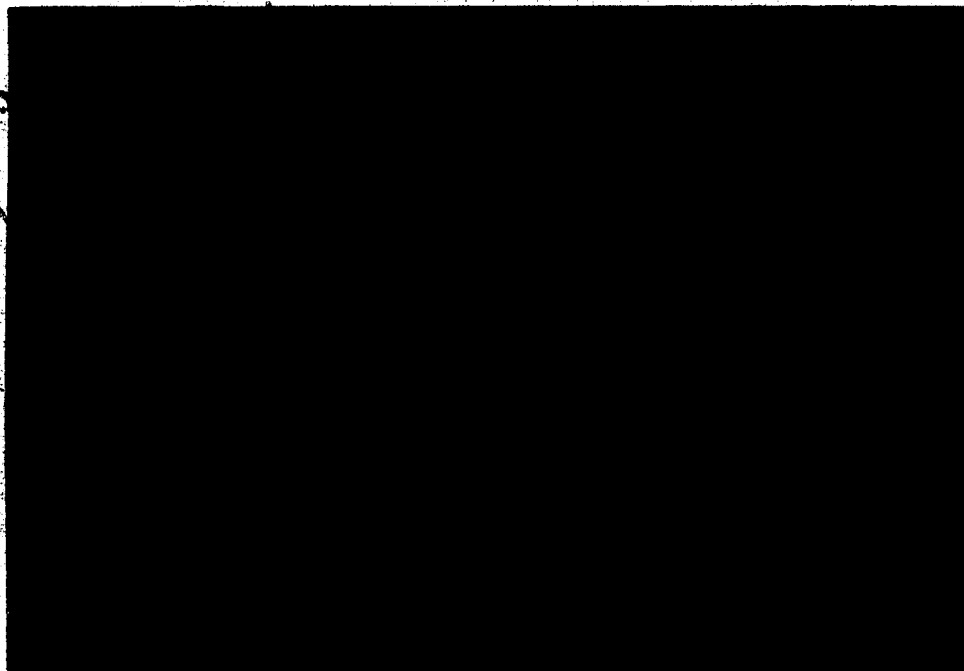
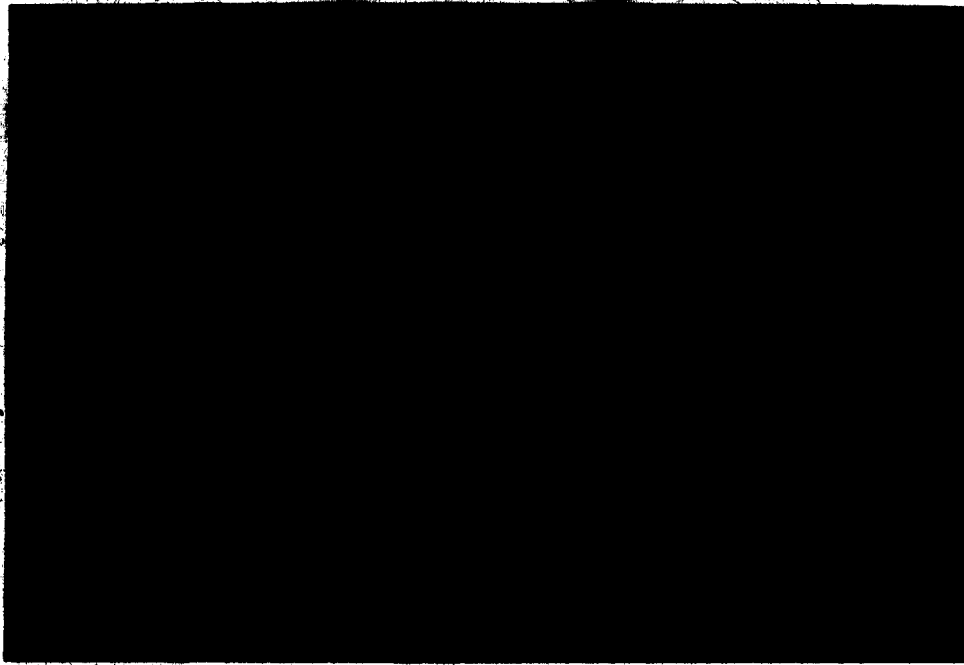


Fig. 3.7 Superimposed images of a transverse section of the abdomen and exposed kidney indicating the region just along the surface of the kidney from which the ^{31}P spectra were obtained. The images were obtained using circumscribing and surface coils. The pulse length for the ^{31}P pulse was 5 μsec , that for the ^1H pulse was 20 μsec . These pulse lengths corresponded to a penetration depth just along the surface of the rat kidney.

(b) Enlargement of the rat kidney in image (a).



different relaxation times (0.5-5.0 sec (43)), employment of a 1.0 sec repetition interval results in partial saturation of the resonances. The extent of the reduction in intensity of the different resonances is dependent on the T_1 value of that particular metabolite. Accurate quantification of metabolite levels requires the determination of the ^{31}P T_1 measurements of the resonances and calibration of the surface coil to determine the sample volume contributing to the NMR signal (82). Few T_1 measurements of ^{31}P metabolites in intact tissue have been reported. Meyer and Brown (86) determined the T_1 's for ^{31}P metabolites in perfused cat skeletal muscle, Irving et al (70) for rat muscle and rat muscle implanted with a mammary adenocarcinoma, Adams et al (1) for a subcutaneously implanted KHJJ mammary adenocarcinoma, and Rhodes et al for perfused kidney (101). Their results are listed in the Table 3.1.

The considerable variation that exists in the above T_1 values is probably due to the different tissues examined and pulse sequences employed. The ^{31}P T_1 's reported by Irving et al for the mammary adenocarcinoma implanted in the rat hind leg were obtained by placing the leg with the tumor into the probe. Therefore, these results include contributions from the rat muscle and adipose tissue and are not representative of the tumor alone.

TABLE 3.1 Longitudinal Relaxation Times Reported For
³¹P Metabolites in vivo (sec)

	SP	Pi	PD	PCr	ATP-γ	ATP-α	ATP-β
Meyer et al cat muscle ^a	/	4.6	/	3.1	1.3	1.1	1.0
Irving et al rat muscle ^b	/	/	/	5.1	3.7	2.7	2.7
Irving et al rat muscle with tumor ^a	6.5	2.0	/	4.6	2.7	3.1	5.2
Adams et al KHJJ tumor ^c	/	2.2	/	1.9	1.7	2.2	1.9
Rhodes et al perfused kidney ^d	0.8	1.1	2.5	/	0.8	0.8	0.8

^a determined using a solenoidal coil and an inversion recovery sequence (86).

^b determined using a solenoidal coil and an inversion recovery sequence (70).

^c determined using a surface coil and a modified saturation recovery sequence (82) which introduces periodic phase shifts in the saturating pulse. (1).

^d determined using a solenoidal coil with an inversion recovery sequence (101).

An attempt was made within this project to determine the ^{31}P T_1 relaxation times for rat kidney in vivo, which to our knowledge has not yet been reported. However, a number of technical limitations prevented the accurate measurement of in vivo ^{31}P T_1 's. A four turn, 2cm diameter solenoidal coil was constructed and placed around the surgically exposed kidney. A copper sheet was wrapped around the abdomen of the animal such that only the kidney was protruding, in order to minimize contributions to the NMR signal from surrounding tissue. An inversion recovery sequence ($180^\circ - \tau - 90^\circ$) was employed with a delay time of 20 sec. The τ values were varied from 10 msec to 8.0 sec, and the number of scans was 128. On average, the above data set required 8 hours to acquire and therefore required repeated administration of anaesthetic to the animal. In several instances the animal expired prior to completion of the experiment. The possibility of significant changes in metabolite concentrations during the course of the experiment and also due to the differential dose of anaesthetic administered are factors which must be taken into consideration when analysing the resulting data. Resorting to a saturation recovery sequence, $(90^\circ - \tau)_n$, to reduce the time period required to acquire the data set yielded spectra in which the sugar phosphate peak and P_i peak were not always resolved. Regardless of the pulse sequence employed, the

dimensions of the kidney and the length of the vascular pedicle were such that the kidney did not sit exactly in the centre of the solenoidal coil but instead occupied the bottom 1/3 of the coil with the underside of the kidney protruding from the coil. As a result different portions of the kidney may have experienced different tip angles. It is possible that the ^{31}P T_1 's differ for different regions of the kidney (eg. cortex and medulla) as has been reported for ^1H T_1 's (105).

To correct for the saturation effects, the relative amount to which each of the resonances were reduced was determined by recording the signal intensity under non-saturating conditions ($t_r=20$ sec) and comparing them with those measured under the conditions of the experiments ($t_r=1.0$ sec). A saturation factor defined as the ratio of the signal intensity measured with a 20 sec repetition interval (I_{20}) to the signal intensity measured with a repetition interval of 1.0 sec (I_1), was determined for each observable ^{31}P metabolite.

Multiplication of these saturation factors by the peak intensities obtained with the one second repetition interval enabled the changes in the relative concentrations of metabolites to be followed. The mean saturation factors calculated in Table 3.2 were based on results from only 3 animals. A considerable amount of variability between animals was observed in the signal intensities of the different metabolites and also

Table 3.2 Mean and Standard Deviation
For the Saturation Factors

	Ratio (I_{20}/I_1)			$\bar{x} \pm \sigma$
	Rat#1	Rat#2	Rat#3	
SP	2.33	1.22	1.60	1.7 \pm 0.6
Pi	1.27	1.20	1.79	1.4 \pm 0.3
PD	2.29	2.00	1.68	2.0 \pm 0.3
PCr	1.40	2.07	1.94	1.8 \pm 0.4
ATP- γ	1.67	1.33	1.36	1.5 \pm 0.2
ATP- α	1.44	1.13	1.32	1.3 \pm 0.2
ATP- β	1.17	1.07	1.04	1.1 \pm 0.1

between the different repetition times as illustrated in figure 3.8. As a result the calculated saturation factors also exhibit considerable variability. Due to the small sample size standard deviations varied from 0.56 for sugar phosphates, to 0.07 for ATP- β . The observed variability in intensities for a particular repetition rate is probably a reflection of the metabolic variability between animals.

Another source of error when estimating the relative intensity of the various peaks results from phasing of the spectrum. Burt et al have reported that the standard deviation from measurement of peaks derived from metabolites present in vivo at high concentrations is +10%, whereas the variance in the measurement of minor peaks (ex. PCr at late stages of tumor growth) may be as high as +50% (21). Despite the difficulties encountered with accurate quantification, the changes observed in the ^{31}P spectrum reflect metabolically important events. Since accurate T_1 's could not be obtained and we are interested in the changes in the relative concentrations of metabolites, saturation factors were calculated and applied to the ^{31}P spectra to enable us to follow alterations in the metabolic pathways. The saturation factors obtained from NMR measurements on normal healthy kidneys were also applied to the spectra obtained from kidneys implanted with tumor cells.

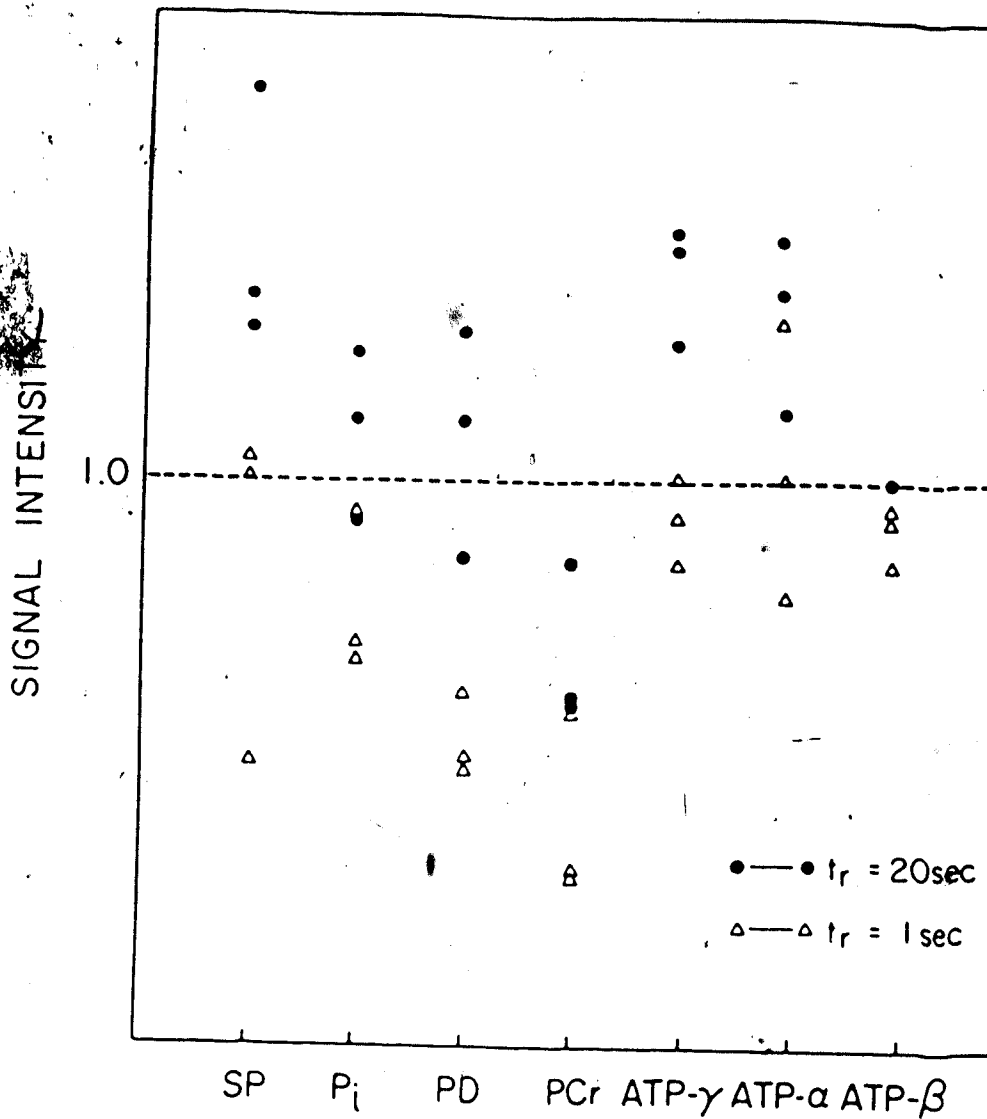


Fig 3.8 Signal intensities obtained for ^{31}P metabolites in the rat kidney employing the depth pulse sequence $\theta/3$; $\theta/5$; $\theta(\pm x)$; $AQ(\pm)$ with repetition intervals of 1.0 and 20 sec. The 90° pulse length was 11 μsec , the number of scans was 256. All signal intensities were normalized to that of the βATP at the 20 sec repetition interval to enable comparisons between animals to be made.

3.4 MONITORING TUMOR GROWTH IN THE RAT KIDNEY BY ^{31}P NMR SPECTROSCOPY

Tumor energy metabolism was monitored by ^{31}P NMR as a function of tumor growth in the rat kidney. Employing the depth pulse sequence $\theta/3;\theta/5;\theta(+X);AQ(+)$, spectra were acquired at a depth of 2-4mm from the surface of the kidney on days 0, 3, 6, 9, and 15 after implantation of the tumor cells. Our results, consistent with those of other groups (50, 51, 94, 70, 1), demonstrated profound changes in the ^{31}P spectrum of the untreated tumor at various stages of growth. Typical changes observed with tumor growth in the ^{31}P metabolites and pH are depicted in Fig 3.9. Although variations existed in the intensities of the different peaks, the spectral trends exhibited were essentially the same.

The control spectrum (day 0), prior to implantation of the tumor cells, indicated intense NTP and PCr resonances, the presence of PD, and elevated levels of PME and Pi. The region in the kidney from which the spectrum was acquired is illustrated in Fig 3.10. Fig 3.10 depicts a histological section of a normal rat kidney. The kidney can be grossly divided into two regions, the cortex (1.3-1.7mm) and the medulla (\approx 6mm), which are surrounded by a fibrous capsule membrane (65). All three cell types are observed in the photograph.

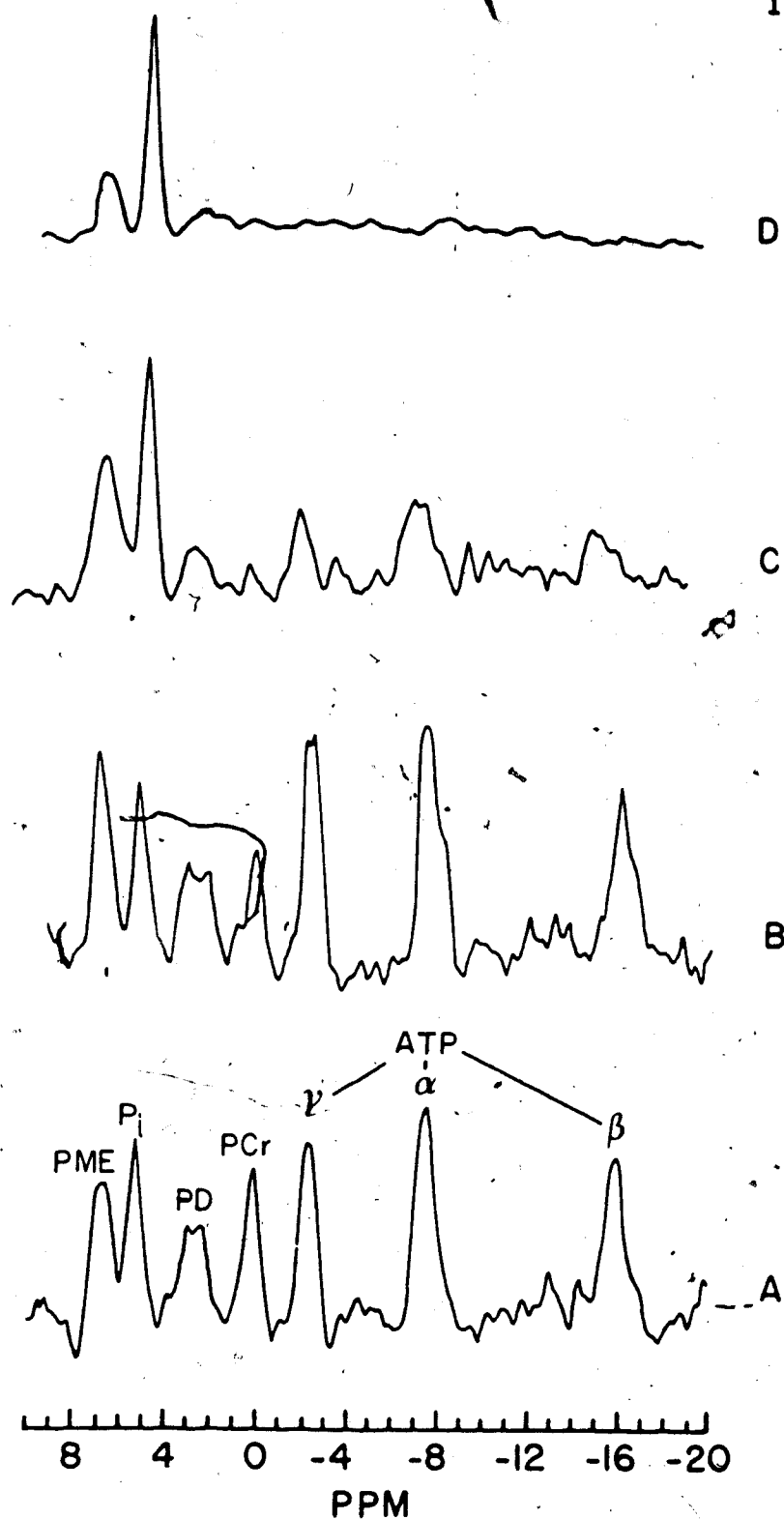
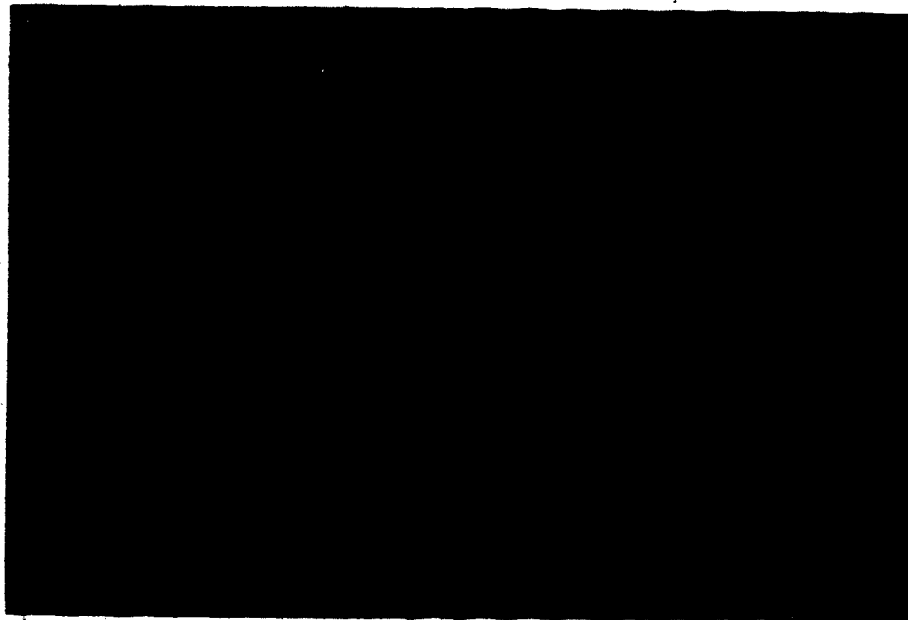
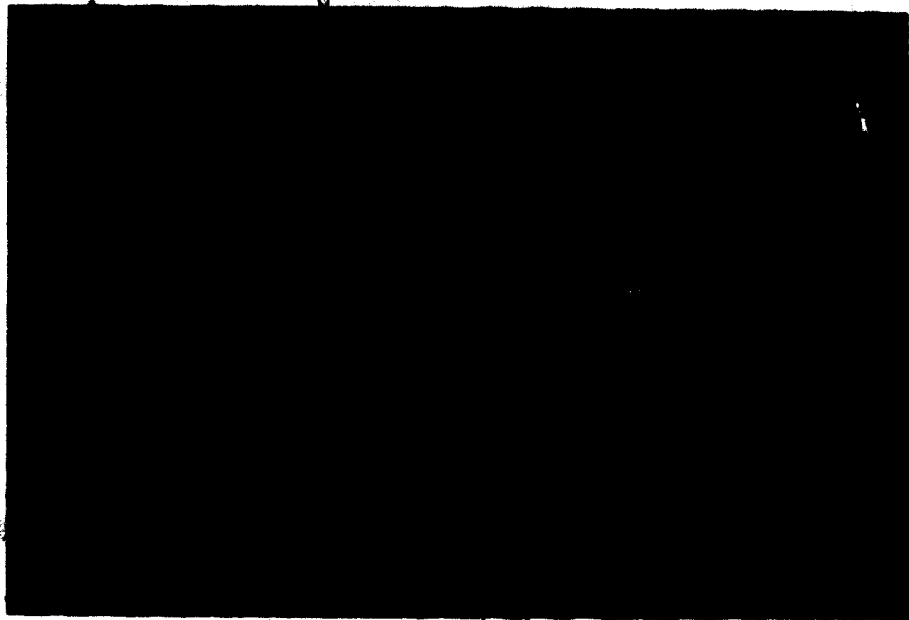


Fig. 3.9 Changes in the ^{31}P metabolites and pH with tumor growth. The 90° pulse was $13 \mu\text{sec}$, the repetition interval was 1.0 sec, the number of scans was 512. (A) Day 3 of tumor growth (pH 7.35); (B) Day 6 of tumor growth (pH 7.31); (C) Day 9 of tumor growth (pH 6.76); (D) Day 15 of tumor growth (pH 5.63).

Fig. 3.10 Histological sections of a normal rat kidney and the rat kidney one day after implantation of tumor cells.

a) Normal rat kidney. Regions of the medulla (upper left hand corner), cortex (middle), and renal capsule (right hand side) can be seen.

b) The rat kidney one day after implantation of tumor cells. The tumor cells are stained blue and appear in the renal capsule. Regions of unaffected cortex and medulla are also observed.



(The dimensions given for the different regions are those for a normal kidney of an adult rat weighing between 180-280g.) Therefore, our control ^{31}P spectra acquired at 2-4mm depth was derived mainly from the kidney medulla. One day after implantation of the tumor cells, histological studies demonstrated the presence of a thin rim of tumor cells growing just under the kidney capsule (Fig 3.10 (b)).

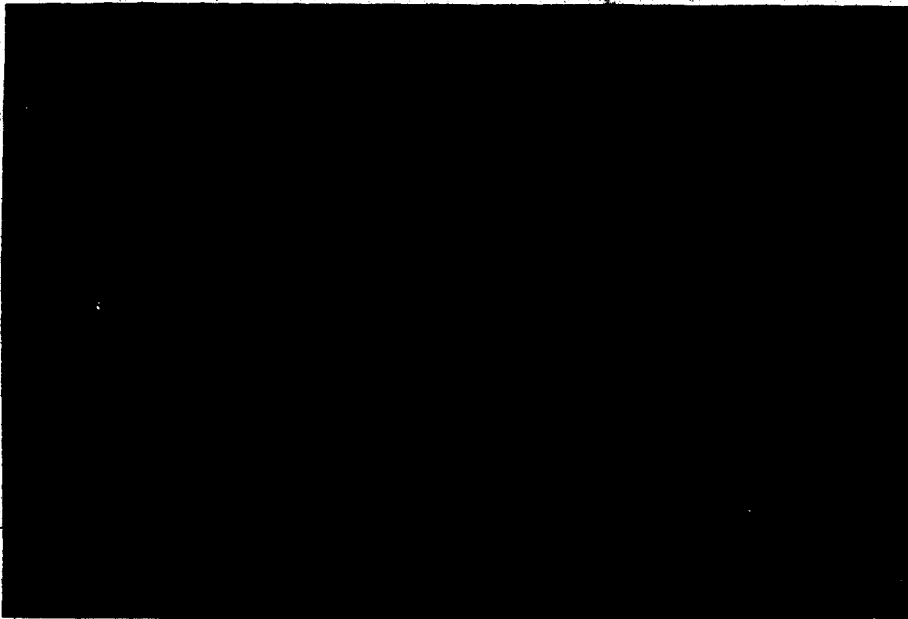
Three days after implantation of the tumor cells, the ^{31}P spectrum remained essentially the same. At this stage of growth tumor formation was not observed macroscopically. Histological studies indicated that most of the tumor cells were growing along the capsule membrane (Fig. 3.11 (a)), and therefore would not contribute significantly to the ^{31}P spectrum. The intracellular pH was estimated to be 7.35.

After six days of growth, the tumor spectrum exhibited a slight decrease in PCr, with an increase in PME and little change in the NTP resonances. A decrease of the tumor pH to 7.31 was observed. Ng et al (94) observed similar changes in the ^{31}P spectrum of a MOPC myeloma. These workers attributed the above spectral changes to decreased vascularization and a consequent increase in the proportion of hypoxic cells in the tumor. An increase in the hypoxic fraction of the tumor would indeed result in an increased demand of the tumor cells on anaerobic glycolysis for energy production.

Fig. 3.11 Histological sections of the rat kidney 3 days and 6 days after implantation of tumor cells.

a) The rat kidney 3 days after implantation of the tumor cells. The slide indicated that the tumor cells (stained blue) were growing along the renal capsule and had not yet penetrated the cortex or medulla.

b) The rat kidney 6 days after implantation of the tumor cells. The tumor cells had penetrated (1-3 mm) from the surface into the cortex.



The observed increase in the PME resonance was therefore attributed by Ng et al, to the accumulation of glycolytic intermediates. The depletion of PCr levels was accounted for by a proposed activation of the enzyme creatine kinase which converts ADP into ATP at the expense of PCr to maintain the high and approximately constant levels of ATP. The decrease in intracellular pH was attributed to the build up of lactic acid which is the end product of anaerobic glycolysis. Although caution must be exercised in comparing different tumor models, the above explanation for the mechanism behind the observed spectral changes may be an overinterpretation of the results. The subcutaneously implanted MOPC myeloma investigated by Ng et al was reported to have a tumor mass of <1g at this stage of growth. Localization techniques were not implemented, neither was the actual extent of tumor growth determined; therefore, it is difficult to assess the possible contribution to the spectrum from normal tissue (ex. muscle). The observed changes in the relative intensity of the PCr peak with tumor growth may be a reflection of a decrease in the relative contribution to the spectrum from other tissue metabolites (ex. muscle). Adams et al (1) noted that despite the similar and well vascularized appearance of some tumor spectra (i.e. high levels of high energy phosphates) histological examination revealed differences in the extent of

necrosis of 10% and 30%.

Histological examination of the Walker sarcoma after six days of growth in the rat kidney revealed a penetration depth of the tumor cells into the cortex of approximately 1-3mm (Fig 3.11 (b)). The tumor spectrum acquired at day 6 (Fig 3.9(b)) therefore contains a considerable contribution to the spectrum from unaffected medulla. The effect of tissue heterogeneity can have a marked effect on the appearance of the ^{31}P spectrum.

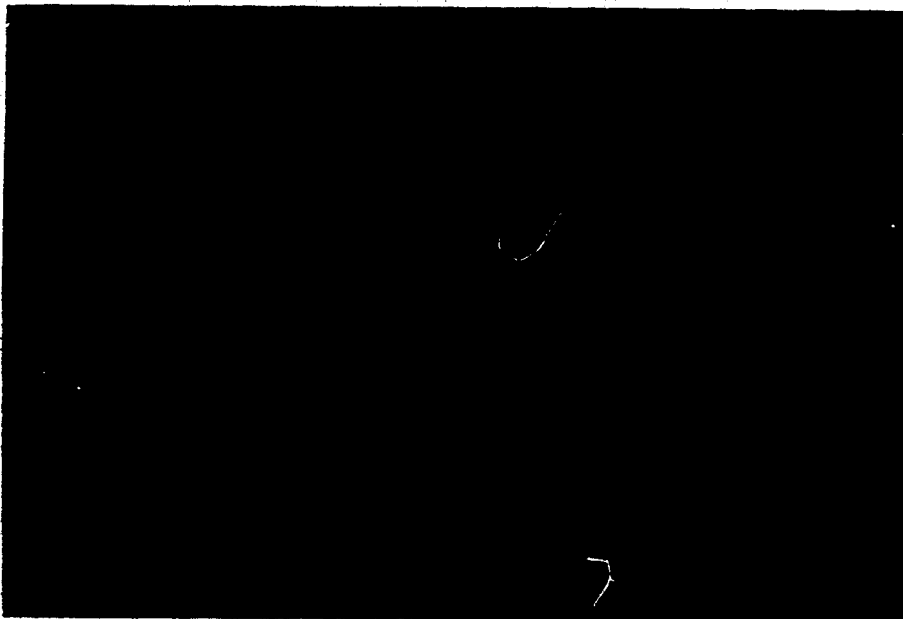
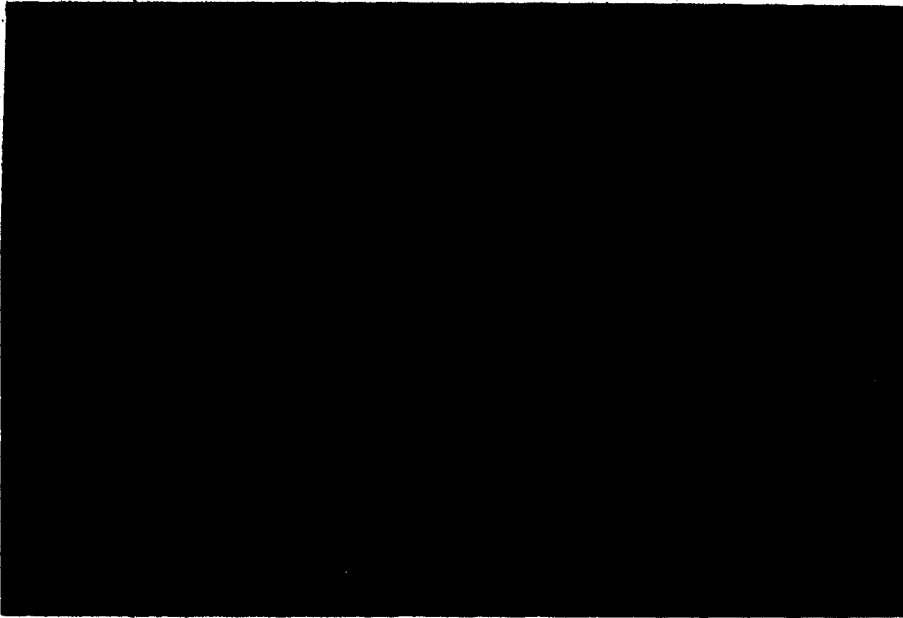
After 9 days growth in the rat kidney the tumor cells had penetrated 5-10mm from the capsule (Fig 3.12 (a)). The corresponding ^{31}P spectrum exhibited a dramatic decrease in ATP levels with a corresponding increase in Pi levels. Phosphodiester and PCr levels were also depleted and the tumor pH decreased to 6.76. In most instances the tumor pH had decreased significantly after 9 days of tumor growth (Fig. 3.13). This decrease appeared to correlate with the decrease in NTP levels at approximately the same stage of tumor growth (Fig 3.14).

At late stages of growth (day 15), the invasive tumor cells had almost completely replaced the kidney tissue (Fig. 3.12(b)). The only resonances observed were those of PME and an intense Pi peak. Hydrolysis of ATP ($\text{ATP} \rightarrow \text{ADP} + \text{Pi}$) probably accounts for the intense Pi resonance. The concentrations of the high energy

Fig. 3.12 Histological sections of the rat kidney 9 days and 15 days after implantation of the tumor cells.

a) The rat kidney 9 days after implantation of the tumor cells. The tumor cells had penetrated 5-10 mm from the surface through the capsule, cortex and medulla.

b) The rat kidney 15 days after implantation of the tumor cells. The slide indicated that at this stage of growth the tumor cells had almost completely replaced the kidney tissue.



U

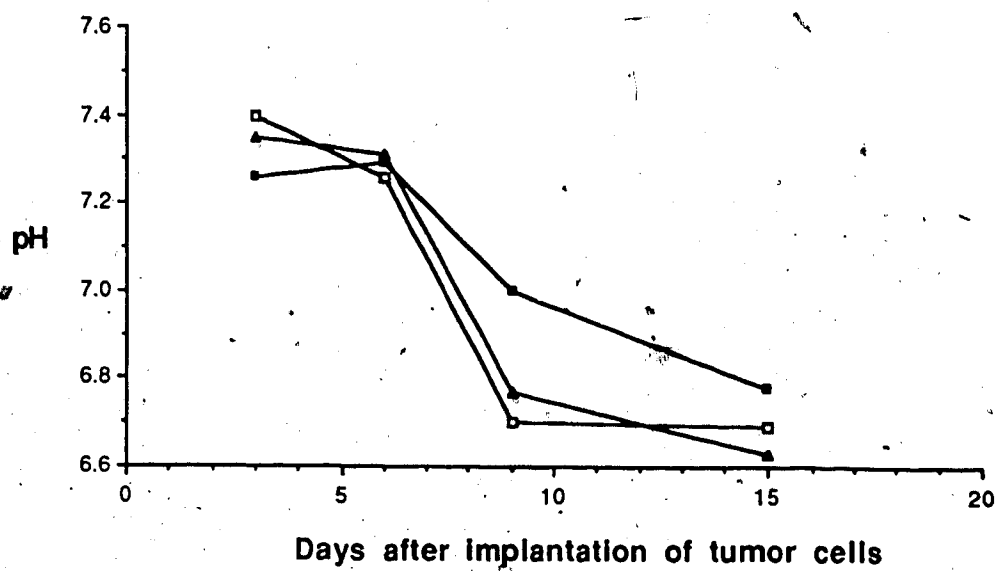


Fig. 3.13 Variation in intracellular pH with tumor growth.

phosphates fell to levels below the level of detection (<1.0mM). The intracellular pH at this stage of growth was 6.63. Dead tissue examined after excision generally exhibited a very intense Pi resonance with residual PME and NAD peaks. Therefore, the Walker sarcoma tumor at this stage of growth was probably comprised of mainly necrotic and metabolically inactive hypoxic cells. The rate of change in the ^{31}P metabolites are affected by those factors that change metabolic rates ex. blood flow, tissue oxygenation, CO_2 tension, anaesthetics and temperature, which may vary from animal to animal.

An apparent peak NTP β /Pi ratio was calculated after correcting for the saturation effects. The intensity of the β -ATP was used for the NTP value since this resonance is unique to NTP (Table 3.3). The data indicated an overall trend toward decreasing NTP/Pi as the tumor grew (Fig. 3.14).

Griffiths et al (50,51), employed topical magnetic resonance to measure the in vivo ^{31}P NMR spectrum of a Walker sarcoma subcutaneously implanted in Wistar rats. The tumor after 14 days growth exhibited intense NTP, Pi and PME resonances, weaker PD, and in contrast to our results, no detectable PCr. A number of investigators have, however, observed PCr in the spectra of a variety of subcutaneously implanted tumors (94,90,31,32,34). The variability in the levels of PCr observed by

Table 3.3 Changes in The NTP/Pi intensity ratio
and pH with tumor growth

Days after implantation	pH	Peak intensity ratio
		NTP/Pi
0	7.33	1.02
3	7.35	0.95
6	7.31	0.95
9	6.76	0.27
15	6.63	/

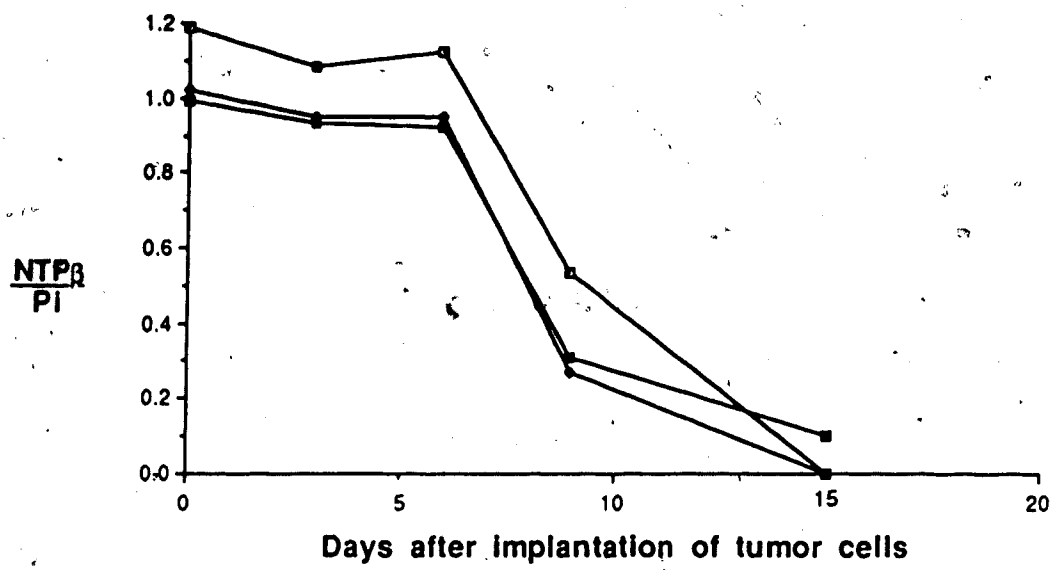


Fig 3.14 Variation in the $\frac{NTP_{\beta}}{Pi}$ ratio of the Walker sarcoma with tumor growth.

in vivo ^{31}P spectroscopy in the above tumors may be the result of a number of factors. The differences may be specific for the type of tumor examined. As Griffiths (51) has pointed out, "the presence of PCr in tumors will vary according to the cell type of origin and the degree of differentiation of the tumor", or they may be a result of the different localization techniques employed. The presence and intensity of the observed PCr resonance may also be dependent on the host and the site of implantation. Tumors implanted subcutaneously are known to be infiltrated by other non-tumor cells. Spectra of tumors in which PCr was not detected were from relatively large tumors and therefore possibly poorly vascularized (ie. hypoxic). In spectra where the PCr resonance was fairly prominent, precautions were not performed to rule out the possibility that this -- resonance resulted from spectral contributions from high levels of PCr in surrounding muscle or skin.

Our results, consistent with those of Adams (1), Evanochko (31) and Ng (94), demonstrate a decrease in the intensity of the PCr peak with increasing tumor growth. Ng and Glickson have postulated that the reduction of PCr levels in the MOPC myeloma with tumor growth reflects a progressive onset of vascular insufficiency and therefore hypoxia in the tumor (33). To examine this hypothesis knowledge of the vascular pattern of the tumor is required. Investigations of the

blood supply and vascularity of the tumor have been the subject of many investigators. Often, solid tumors are poorly vascularized and tend to be circled with a coarse network of large vessels (99). Reliable determination of blood flow in a tumor mass can only be obtained if normal tissues are excluded from the neoplasm. This is not possible with tumors grown as subcutaneous implants (55). The vascular morphology of the subcutaneous tumors examined using ^{31}P NMR spectroscopy by Ng and co-workers was not reported. Since the vascularity of tumors differs for each tumor type and is also dependent on the site of implantation, generalizations cannot be made.

To obtain accurate measurements of the blood flow to the Walker sarcoma, Gullino and Grantham implanted the tumor into the rat kidney, maintained the tumor tissue isolated, and cannulated the vein, draining the implanted organ (55). Employing this method Gullino et al obtained an estimate of the total tumor blood flow. It should be noted that histopathological studies indicated that the tumor implants of the kidney contained varying amounts of normal tissue even at late stages of growth (54). The authors claim that the biological characteristics of the tumor remained the same whether grown as tissue isolated implants in the rat kidney or as subcutaneous implants (54). The tumor blood flow was found to decrease as the tumor increased

in size (55). From studies of subcutaneous implants it is known that tumor blood flow decreases with increasing tumor growth parallel with the development of central tumor necrosis. (99). On day 10 after implantation of the tumor cells Gullino recorded a blood flow rate of 1.5ml/hr/mg N. On day 15 after implantation of the tumor cells this rate had decreased to 0.9-0.12ml/hr/mg N. This slow blood flow in the tumor remained relatively constant during tumor growth (55). The blood flow was calculated to be less than the blood flow of the normal kidney of an adult rat (10ml/hr/mg N) (55).

Assuming a similar blood flow rate to the tumor model employed in our studies, a reduction of blood flow to the tumor could account for the dramatic decrease in high energy phosphates observed in the ^{31}P spectrum after approximately 9 days growth in the rat kidney. (Fig 3.9 (C)). This reduced blood flow may also be responsible for the progressive decrease in tumor pH as lactic acid accumulates and is not cleared as efficiently from the tumor.

In addition to changes in tumor vascularization and tumor blood flow, the actual oxygen uptake per unit weight decreases exponentially during tumor growth (99). The distribution of oxygen to different parts of the tumor is difficult to assess. Using the same tumor kidney model Gullino et al (56) determined the in vivo utilization of oxygen in the Walker sarcoma. The oxygen

delivery was calculated by subtracting from the oxygen content of the blood supply entering, the oxygen content of that leaving the tumor. The tumors examined varied in weight from 5-12 g. The amount of necrosis present was usually small. Their results demonstrated that the Walker sarcoma was able to remove about 50% of the oxygen carried by the afferent blood. ($Q_{O_2} = 3.3 \mu l O_2 / mg \text{ dry tumor} / hr$). This removal rate was as efficient as that of normal tissues. (56). Although Gullino determined that the rate of oxygen delivery remained constant even at advanced stages of growth, examination of the ^{31}P spectrum acquired from a depth of 2-4mm in our study, after 15 days of tumor growth in the kidney, indicated that oxygen consumption by the tumor had decreased. The tumor cells at this stage appeared to be metabolically inactive.

In investigating the relationship between oxygen supply and utilization by the Walker sarcoma, Gullino et al (56) varied the supply of oxygen to the tumor and determined the oxygen consumption. A respiratory quotient (RQ), defined as the carbon dioxide eliminated from the tumor (CO_2 of venous blood - CO_2 of arterial blood) divided by the oxygen consumed per hr, was then determined. When more oxygen was supplied to the tumor (by inhalation of pure oxygen for a period of 30-60 minutes) the oxygen uptake of the tumor remained about 50%, but the oxygen consumption (RQ) increased to

3.5 times the normal level, i.e. the oxygen utilization of the tumor increased. The capacity of the tumor to utilize oxygen could not be saturated under the conditions of the experiment. The method employed by Gullino for determining the oxygen delivery and consumption estimates the total oxygen consumption of the malignant tissue. However it is quite likely that the histologically distinct regions in the tumor utilize oxygen at different rates. Knowledge of the location and extent of these regions in the tumor (which may be reflected in the ^{31}P spectra), is important for effective radiotherapy and chemotherapy.

To evaluate Ng and Glickson's hypothesis that the ^{31}P spectra reflect the state of oxygenation and vascularization of the tumor, it would be interesting to employ the above model and monitor the bioenergetics of the tumor during an increase in oxygen supply to the tumor.

The variability in the relative intensities observed in the in vivo ^{31}P spectrum of the Walker tumor is probably the result of the different rates of tumor growth, the extent to which normal host cells comprise the tumor, the extent of damage to the kidney on injection of the tumor cells, and the heterogeneity in the histological pattern (viable versus necrotic cells) in the tumor. While this biochemical heterogeneity makes it difficult to draw general conclusions from

these studies, it also illustrates the ability of NMR localization techniques to monitor subtle metabolic differences at a particular depth in the same tumor implanted in different animals. In general, the tumors examined all exhibited the same spectral pattern as a function of growth i.e., marked increases in Pi and PME, a decrease in the high energy phosphates and a decrease in tumor pH. The spectral changes appear to reflect the increased demand of the tumor cells on anaerobic glycolysis with tumor growth. At early and late stages of growth, interpretation of the ^{31}P spectrum is relatively straightforward. At intermediate stages the differential contributions from normal tissue and uncertainties on the extent of growth and vascularization of the neoplastic tissue renders identification of the mechanisms underlying the spectral changes difficult to identify.

3.5 MONITORING ISCHEMIA IN NORMAL RAT KIDNEY BY ^{31}P NMR SPECTROSCOPY

In order to interpret the response of the tumor propagated in the rat kidney subjected to metabolic insults, control studies were performed on normal rat kidney. The metabolic insults investigated by ^{31}P NMR were (a) production of ischemia in the rat kidney, and (b) injection of 150mg/kg of cyclophosphamide I.V.

(section 3.7).

The normal kidney of an adult rat weighing 180-280g is approximately 20 mm long, 15 mm wide, 10 mm dorsoventrally and weighs between 0.7 and 1.2 g (65). The kidney is a heterogeneous tissue which can be grossly divided into two regions, the cortex (1.3-1.7mm thick), and the medulla (=6mm thick) which are surrounded by a fibrous capsule (65). The two main functions of the kidney are to regulate the salt and water balance and the acid-base balance of body fluids. Metabolically, it is an active organ; it receives 25% of the cardiac output. Part of this blood flow is necessary for the support of its own activities while part of it is passing through only for processing (64).

A number of investigators have employed ^{31}P NMR spectroscopy to study energy metabolism of perfused and intact animal kidneys (109,110,4,100,7,40,101,79). Many of these studies were concerned with the measurement of ATP content and intrarenal pH in order to assess tissue viability to determine the optimal conditions for preservation of the organ for transplantation. These studies provided a novel method of evaluating the viability of organs and established that depleting ATP levels together with tissue acidosis played a significant role in renal damage (105).

The time course of the changes in ^{31}P metabolites in the normal rat kidney observed during ischemia and

recovery are depicted in Fig 3.15. As expected production of ischemia (5-10min) resulted in a marked decrease in NTP levels with a corresponding increase in Pi and a decrease in renal pH (Fig 3.16). The control spectrum exhibited intense NTP resonances with detectable levels of PCr, PD, Pi and PME peaks. The intracellular pH was 7.18. After 5 minutes of ischemia the pH decreased to 6.87, and the ATP levels were depleted. A residual peak corresponding to the β -P of NDP (-2.5ppm) and a small peak at -7.7ppm corresponding to α -NDP and NAD were observed. An unexpected observation was an increase in the PCr peak during ischemia. The dramatic increase observed in the Pi resonance during ischemia was probably the result of hydrolysis of ATP and not PCr. Ten minutes after the restoration of blood flow, the pH had recovered to 7.15, the NTP levels had increased, together with a corresponding decrease in Pi levels. A difference in the relative intensities of the NTP resonances was observed, the γ -NTP peak being significantly larger than the α or β peaks. This may be a reflection of a change in the relative concentrations of ADP and ATP and/or a change in the local environment of these metabolites. Thirty minutes after the restoration of blood flow, the pH had increased to 7.34, and the levels of NTP and Pi had recovered to values approximately equal to those observed prior to ischemia. In the normal rat kidney

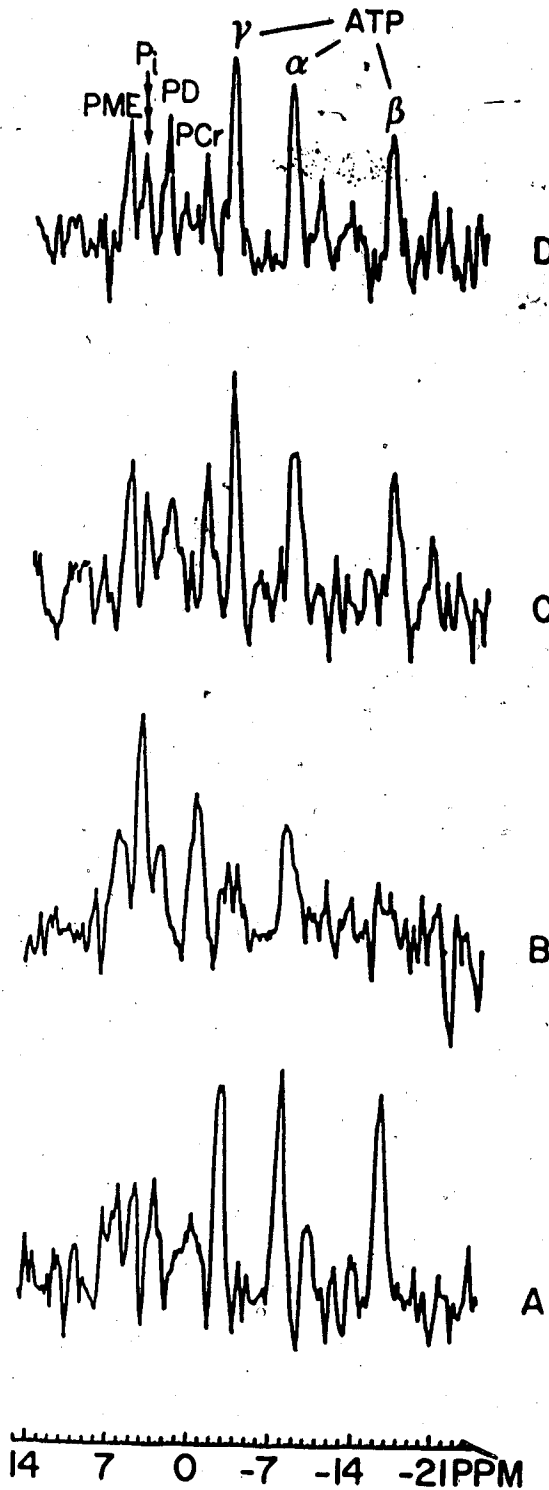


Fig. 3.15 Time course of the changes in ^{31}P metabolites in the rat kidney at 2-4 mm depth during ischemia and recovery. The 90° pulse length was 13 μsec , the repetition interval was 20 sec, the number of scans was 128. (A) Control (pH 7.18); (B) 5 min. ischemia (pH 6.87); (C) 10 min. recovery (pH 7.15); (D) 30 min. recovery (pH 7.34).

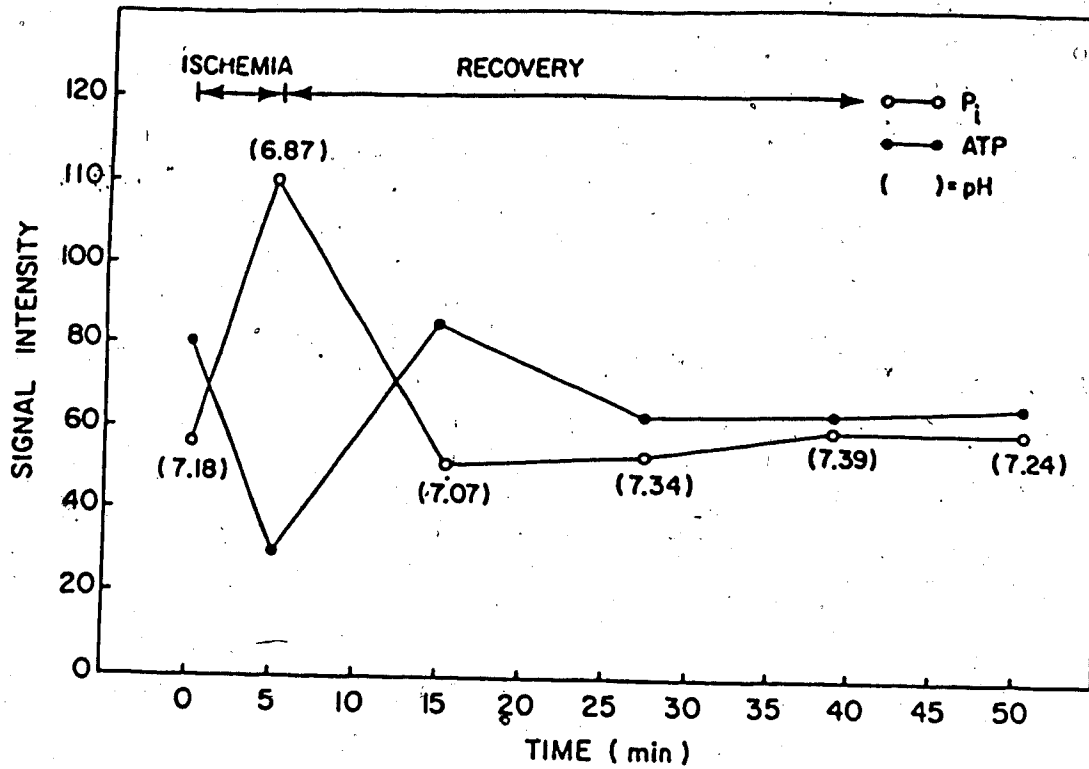


Fig. 3.16 Typical changes in the signal intensity of the ATP_{β} and P_i resonances during ischemia (5 min) and recovery.

the "cut off" period for functional recovery after ischemia is 15 minutes (39). For periods of ischemia less than 15 minutes the ATP levels can be re-established fairly rapidly and a functional organ is revitalized.

The intracellular pH measured by ^{31}P NMR provided an average measure over the region of kidney sampled. Renal pH has been demonstrated by Alder et al to be heterogeneous between the cortex and medulla (2). The Pi resonance in the ^{31}P spectrum was therefore derived from resonances of Pi at a variety of pHs. The changes in the intracellular pH during periods of ischemia and of recovery are depicted in Fig. 3.17. In most cases the pH recovered to control values within 20 minutes after the restoration of blood flow. The pH value observed on recovery was often greater than the control value. This "overshoot" was probably to compensate for the tissue acidosis produced during ischemia.

A relatively intense PME peak was observed in the ^{31}P spectrum of the normal rat kidney, the ischemic kidney, and also at different depths in the kidney. The amount of AMP present in the normal kidney determined enzymatically is below the limits of detection by NMR (105). The PME peak in normal kidney therefore probably receives no contribution from AMP and consists mainly of sugar phosphates.

Significant levels of PD are also observed in all

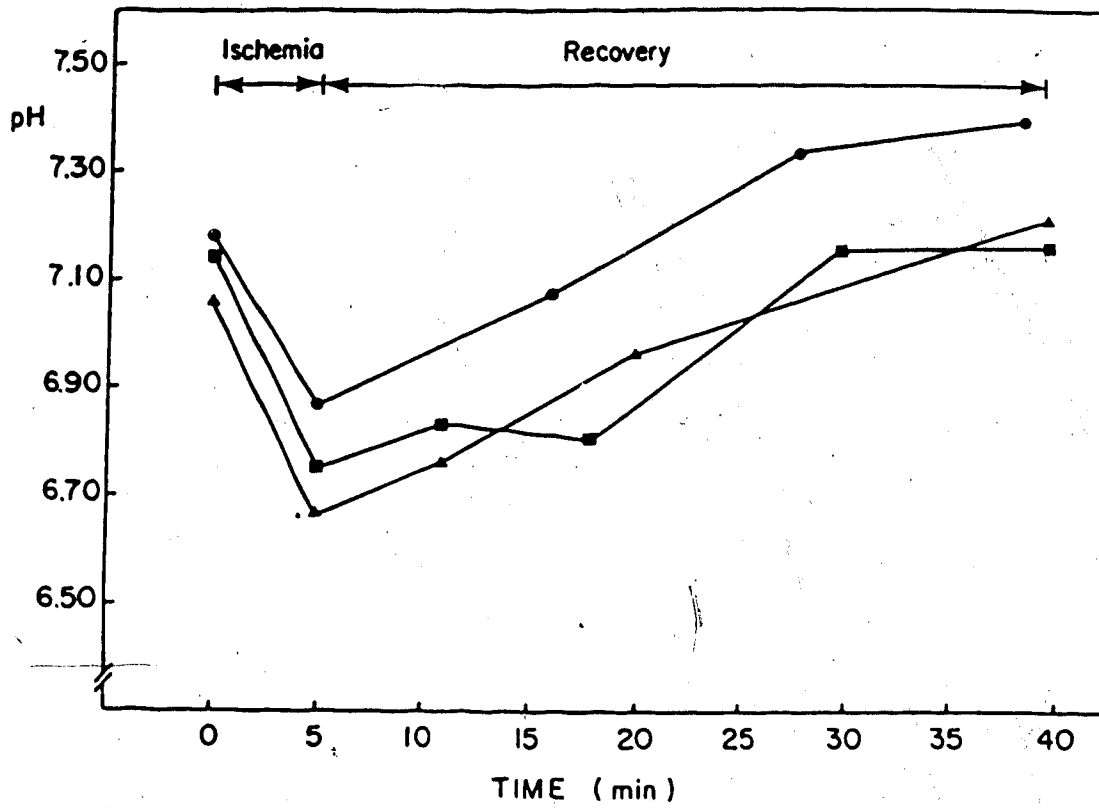


Fig. 3.17

Changes in the intra cellular pH in the rat kidney during periods of ischemia and recovery for 3 animals.

in vivo ^{31}P NMR spectra from rat kidney. This peak, often labelled as a "mystery peak" of renal spectra, has been identified as glycerolphosphorylcholine (GPC) by Balaban (8). Using ^{31}P and ^{14}N NMR spectroscopy, and isolated cells obtained from the cortex and medulla of rabbit kidneys, Balaban determined that the GPC concentration is higher in the medulla than in the cortex, which suggests differences in lipid composition in the two regions (110). Our ^{31}P spectra, obtained at different depths from the surface of the rat kidney (Fig 3.18(D)), also indicate high levels of phosphodiester in the medulla (5-7mm depth). This peak in ^{31}P NMR spectra of kidney may be useful to the study of energetics of the renal medulla since lipid is thought to be the major respiratory fuel for the kidney (105).

In our studies, spectra acquired using depth pulse sequences and with the kidney surgically exposed consistently exhibited detectable PCr signals and varied in intensity with penetration depth. Significant levels of PCr were recorded at 0-2mm depth which decreased to lower but still detectable levels with increasing depth into the kidney (Fig 3.18). In contrast, in the investigations by Freeman (40), Radda (100), and Ackerman (6) on perfused kidneys, the ^{31}P spectra revealed little if any signal from PCr. Balaban et al (7) obtained similar results in an intact kidney using a surface coil and topical magnetic resonance to localize

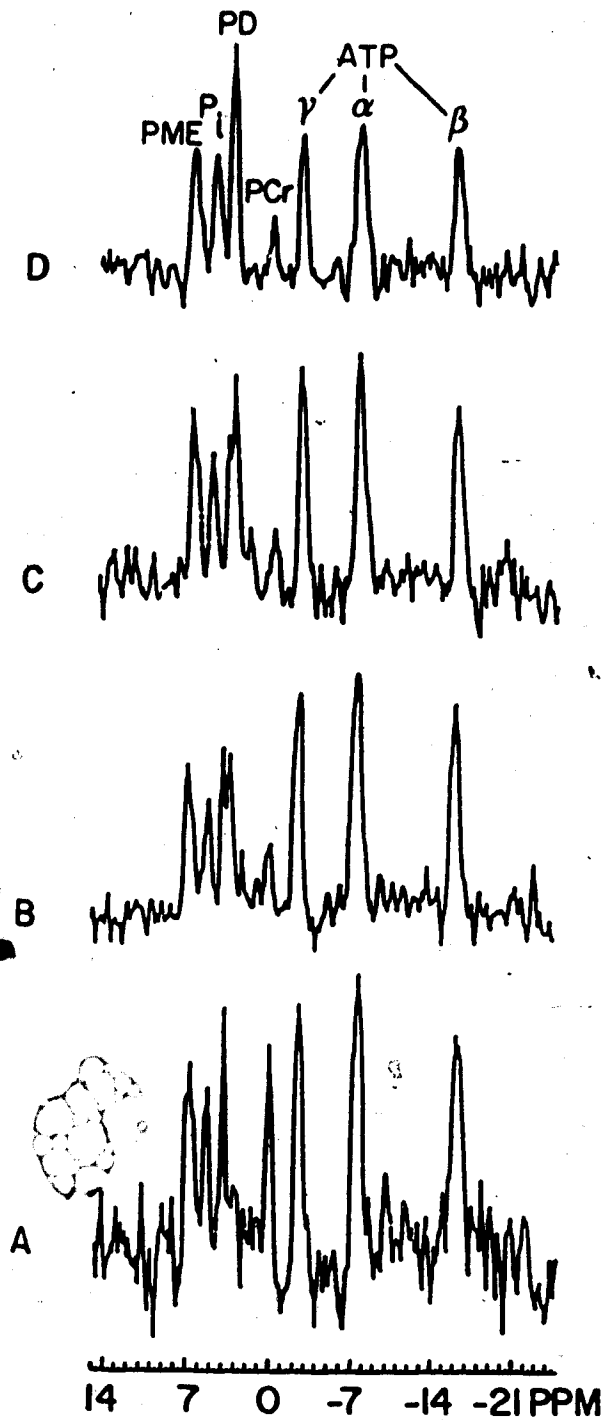


Fig. 3.18 ^{31}P spectra of rat kidney to show changes in metabolite concentrations at different depths from the surface. The repetition interval was 1.0 sec, the number of scans was 256. The spectra are not corrected for saturation effects. (A) 0-2 mm; (B) 2-4 mm; (C) 4-6 mm; (D) 5-7 mm.

the spectrum. In our studies, ^1H images of the sensitive volume provided reassurance that the PCr signal did not arise from surrounding tissue ex. (fig 3.6 and Fig 3.7). The reason for the discrepancy in the observation of a PCr signal is not clear. Freeman (40) reported that the level of PCr is below the limits of detection ($<0.2\text{mM}$) and that the rat kidney does not contain large amounts of the enzyme creatine kinase.

The ^{31}P spectrum of a homogeneous population of renal-cortical-tubular cells obtained from the cortex of rabbit kidneys did not exhibit a PCr signal (2).

Assuming little species difference, if the rat cortex does not contain appreciable amounts of PCr, this would suggest that the PCr signal we observe must have originated primarily from the kidney capsule.

Adenine nucleotides which contribute to the NTP resonances in the ^{31}P spectrum can account for as much as 90% of the total nucleotide pool in skeletal muscle, in kidney they comprise approximately 50-60% of the nucleotide pool, the remaining 40-50% is made up of guanosine, uridine, and cytidine triphosphates. The concentration of ATP in the kidney varies considerably during the period of metabolic stress. Stubbs, Freeman, and Ross (115) measured the adenine nucleotide and Pi content of the kidney by enzymatic assay (after freeze clamping and acid extraction) and by ^{31}P NMR. Both methods gave similar results for ATP in control kidneys

of 6.3 $\mu\text{mol/g}$ dry wt. Knowledge of the ADP concentration within the cell is important since ADP is a key to control of the regulation of metabolism in the cell. An increase in ADP in the micromolar range may control the adenine nucleotide translocator (K_m 1-12 μM), the enzyme which controls the rate of ATP synthesis (105).

The concentration of free (non-bound) inorganic phosphate (Pi) in vivo is an important parameter for both aerobic and anaerobic energy metabolism. A large amount of Pi is generated in renal ischemia. Chemical analysis by Stubbs et al (115) revealed that hydrolysis of ATP yielded a concentration of 44 $\mu\text{mol Pi}$, whereas the NMR method yielded a concentration of 24 $\mu\text{mol Pi}$. The NMR method therefore detects only a fraction (about 50%) of the Pi within the ischemic kidney. It is also possible that the Pi resonance may be overlapped by other unidentified species.

Tissues such as the kidney which have highly developed functions tend to have complex vascular arrangements. For example, the nephron of the kidney has an artery which breaks up into multiple capillaries (the glomerular tuft) and reforms to constitute another artery (64). Considering the structure of the kidney and its blood supply it is possible that the two main regions of the kidney, the cortex and medulla, may respond differently to ischemia.

The ability of the depth pulse sequence to

discriminate between different regions of the kidney, was demonstrated in one experiment where recovery of the metabolite levels and pH after ischemia did not occur as expected. The ^{31}P spectra yielded constant high levels of Pi with no recovery of NTP. On visual examination and from examination of multiecho images of the kidney, the volume of tissue from which spectra were obtained was an infarcted region of the kidney. Spectra were that recorded at several depths in the kidney in order to obtain a spatial profile of the ^{31}P metabolites (Fig 3.19). Progressing deeper into the kidney, away from the infarcted region to healthy tissue, resulted in an increase in the high energy phosphates as well as an increase in renal pH. Damaged regions of tissue can therefore be readily distinguished from healthy regions by ^{31}P NMR using the DEPTH pulse sequences. These results have important clinical potential.

3.6 MONITORING ISCHEMIA IN THE RAT KIDNEY IMPLANTED WITH TUMOR CELLS BY ^{31}P NMR SPECTROSCOPY.

The time course for the changes in the relative concentrations of ^{31}P metabolites in the rat kidney implanted with tumor cells were monitored during a period of ischemia and recovery. Due to the fact that small tumors can be a mixture of neoplastic cells and host cells, and to ensure that the response measured was

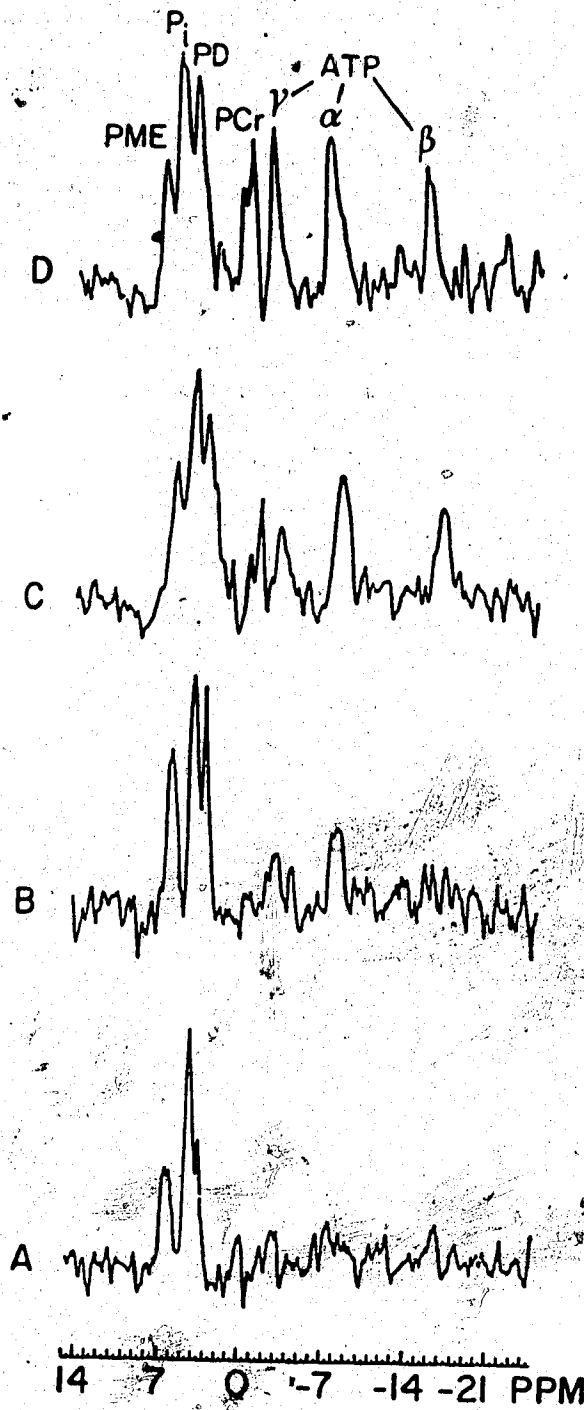


Fig. 3.19 ^{31}P spectra of rat kidney at different depths below the surface of the kidney following infarction. The repetition interval was 1.0 sec, the number of scans was 512. (A) 0-2 mm; (B) 1-3 mm; (C) 2-4 mm; (D) 3-5 mm.

primarily due to the tumor, tumors chosen for study were at a relatively late stage of growth (9-12 days after tumor cell implantation). For the monitoring of ischemia, tumors which produced similar control spectra, i.e., detectable levels of high energy phosphates and intense Pi and PME resonances, were selected. Fig 3.20(A) illustrates a typical control spectrum and the changes in the relative concentrations of ^{31}P metabolites during ischemia (10 min) and recovery. In order to obtain adequate signal to noise the number of scans was increased to 512 with a repetition interval of 1.0 sec, from the 128 scans employed in the ischemia experiments on the normal rat kidney. In contrast to the effect of ischemia on normal rat kidney, the ^{31}P spectrum of the kidney implanted with tumor cells when rendered ischemic demonstrated a decrease in pH (from 7.3 to 6.7), a depletion of the NTP levels (to levels below the limits of detection) and a decrease in PME. There was no subsequent recovery to control values for any of the metabolites or pH (Fig. 3.21). Despite the renewed blood flow and re-oxygenation of the tumor, there is no re-synthesis of ATP. Recovery was monitored at 10 min, 20 min, 30 min, 1 hr and 2 days after production of ischemia. No change was observed in the ^{31}P spectrum. The metabolic stress had altered the bioenergetic state of the tumor such that the spectra now reflect a metabolically inactive hypoxic tumor,

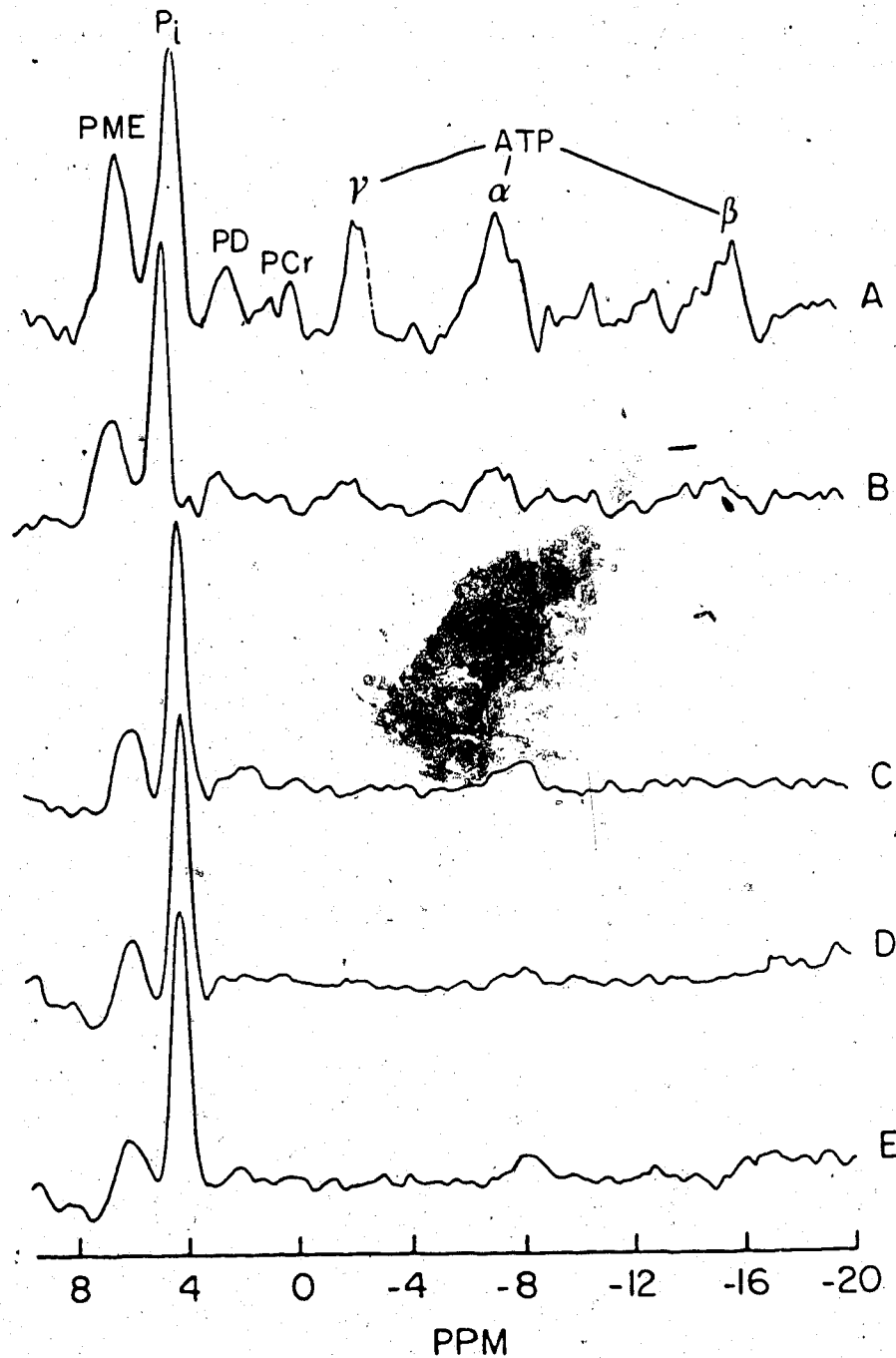


Fig. 3.20 Changes in the ^{31}P metabolites in rat kidney implanted with tumor cells during ischemia and post ischemia at 2-4 mm depth. The repetition interval was 1.0 sec, the number of scans was 512. (A) Control (day 9 of tumor growth); (B) 10 min. ischemia; (C) 10 min. post ischemia; (D) 30 min. post ischemia.

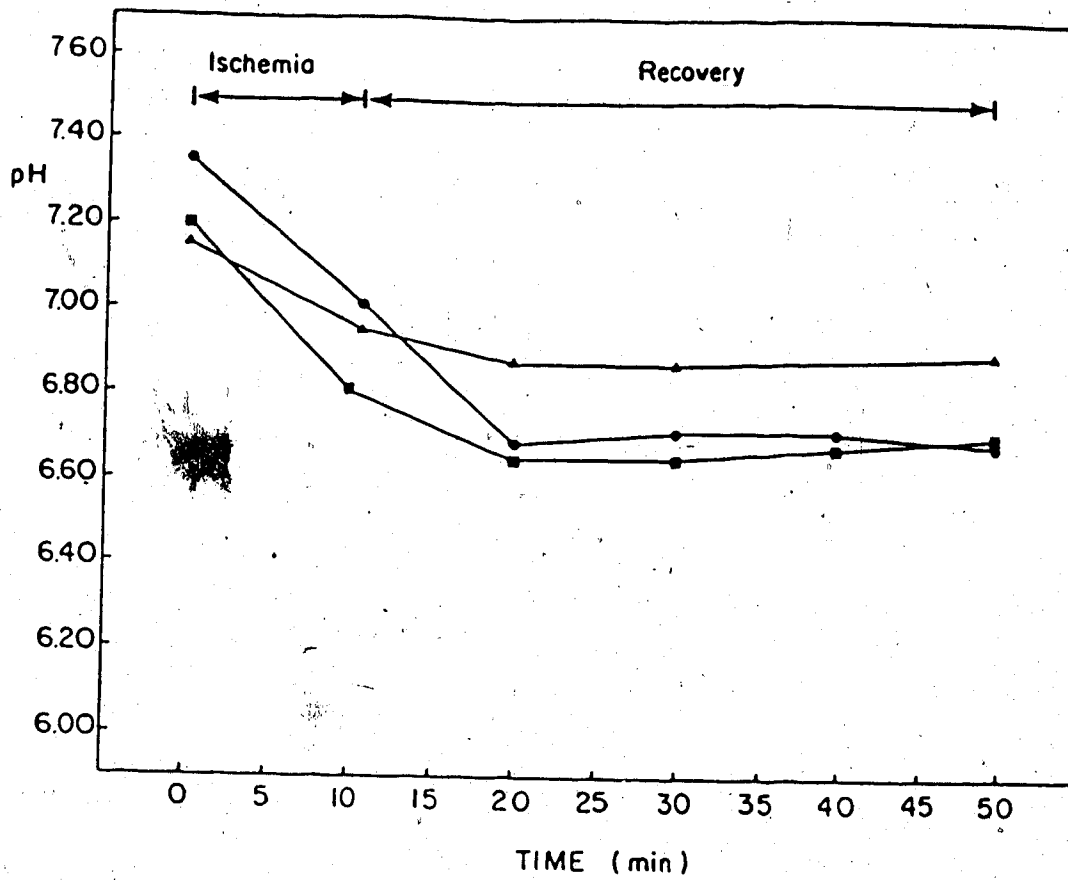


Fig. 3.21 Changes in the intracellular pH in rat kidney implanted with tumor cells during ischemia and recovery.

similar to that observed at very late stages of tumor growth in the rat kidney, as illustrated in Fig. 3.9 (D).

The spectrum prior to ischemia exhibits relatively high concentrations of PME (presumably sugar phosphates) indicating a reliance of the tumor cells on glycolysis. During 5-10 min ischemia the supply of nutrients (glucose) decreased, resulting in a reduction of the intensity of the PME peak. A lack of re-synthesis of ATP and low levels of PME also indicate a reduction of the supply of oxygen and nutrients to the tumor. The absence of recovery of pH to control values suggests an inability to remove the lactate produced. Presumably 5-10 min ischemia has resulted in irreversible destruction or impairment of the tumor vasculature.

The supply of oxygen and nutrients to the tumor depends on supply through the vascular system and the removal capacity of the tissue (57). Gullino et al demonstrated that the oxygen removal by tumors is as efficient as normal tissue (56). The vascular system of the tumor undergoes continuous changes as the tumor mass increases and the volume of vascular network decreases. Therefore, as the tumor grows, oxygen supply per unit mass decreases, as does the oxygen consumption (57). Gullino also demonstrated that during an acute shortage of oxygen to the Walker sarcoma (produced by removal of erythrocytes in the animal), oxygen delivery to the

tumor was improved (56). The effect of ischemia on blood flow was investigated by Mattsson et al (83). Blood flow rates in a tumor implanted in the hindpaw of a rat were found to decrease after 10 minutes of ischemia. Considering these results and the fact that new vessels formed in the tumor are composed of only a single endothelial layer further substantiates the possibility that vascular damage has occurred.

Employing techniques such as depth pulse spectral editing on the proton resonances the levels of lactate produced during tumor growth and during production of ischemia could be monitored and correlated with the changes in intracellular pH determined from the ^{31}P spectra. One would expect to observe an increase in the concentration of lactate with decreasing pH.

3.7 MONITORING TUMOR RESPONSE TO CHEMOTHERAPY BY ^{31}P NMR SPECTROSCOPY

Cyclophosphamide is an antineoplastic agent used clinically in the treatment of cancer and for prevention of recurrences and the appearance of metastases (30). Cyclophosphamide is an alkylating agent which is thought to act by alkylating and cross-linking guanine and possibly other bases in deoxyribonucleic acid thereby arresting cell division. (26). The antineoplastic effect is dependent on a cytotoxic action which is not

selective for malignant cells but may affect all rapidly dividing cells.

Experimentally the drug displays a wide spectrum of antitumor activity. At high dose it causes regression of Walker sarcoma (30). Administration of cyclophosphamide at 5.0 mg/kg/day for 9 days to rats injected with 10^6 cells/ml of Walker sarcoma cells offered complete protection from the lethality of the tumor cells (63). The LD_{50} administered I.V. in rats is 160mg/kg (85).

Cyclophosphamide (150mg/kg I.V.) was administered as a single dose at a relatively late stage of tumor growth (day 9-12 after implantation of tumor cells). Control spectra, prior to administration of the drug exhibited detectable levels of high energy phosphates and intense Pi and PME resonances, ex. Fig 3.22(A). Since the tumor's only blood supply is via the vascular pedicle this mode of administration of the anti-neoplastic agent ensured a uniform distribution of the drug to the tumor. Cells in solid tumors that are distant from functional blood vessels (and hence hypoxic) may be resistant to chemotherapy since drug concentrations in their vicinity may be low due to limited diffusion from blood vessels, and drug uptake by intervening cells (116). There have been few studies of drug distribution within tumors.

A time course for the changes in ^{31}P metabolites

was followed 2 hrs, 2 days, 4 days, and 5 days after administration of the drug (Fig 3.22). The ^{31}P spectra were recorded from the same volume and depth into the tumor as for the study on untreated tumor growth (2-4mm). A significant increase in the relative concentration of ATP and PME was observed within 2 hours post injection. These levels remained elevated up to day 5 post injection. The NTP_p/Pi ratio exhibited a progressive increase after treatment with the drug. (Fig 3.23) PCr and PD levels increased slightly. Fluctuation in phosphodiesterases (GPC and GPE) during tumor growth and as a response to chemotherapy indicate alterations in the phospholipid fragments and/or precursors of the tumor cells. The intracellular pH demonstrated a progressive increase from day 0 to day 2 post injection and remained elevated up to day 5 post injection (Fig 3.24). The observed reversal to a more "aerobic-like" state may be the result of improved blood flow in the tumor. This would account for the rapid increase in pH and ATP levels. It is quite likely that we were observing the combined response to the drug of both aerobic and hypoxic cell populations within the tumor.

In contrast, first to the response of an in vivo RIF-1 tumor (94) to cyclophosphamide (injected I.P.) which exhibited a complete disappearance of the Pi resonance, and second to the response of a MOPC myeloma

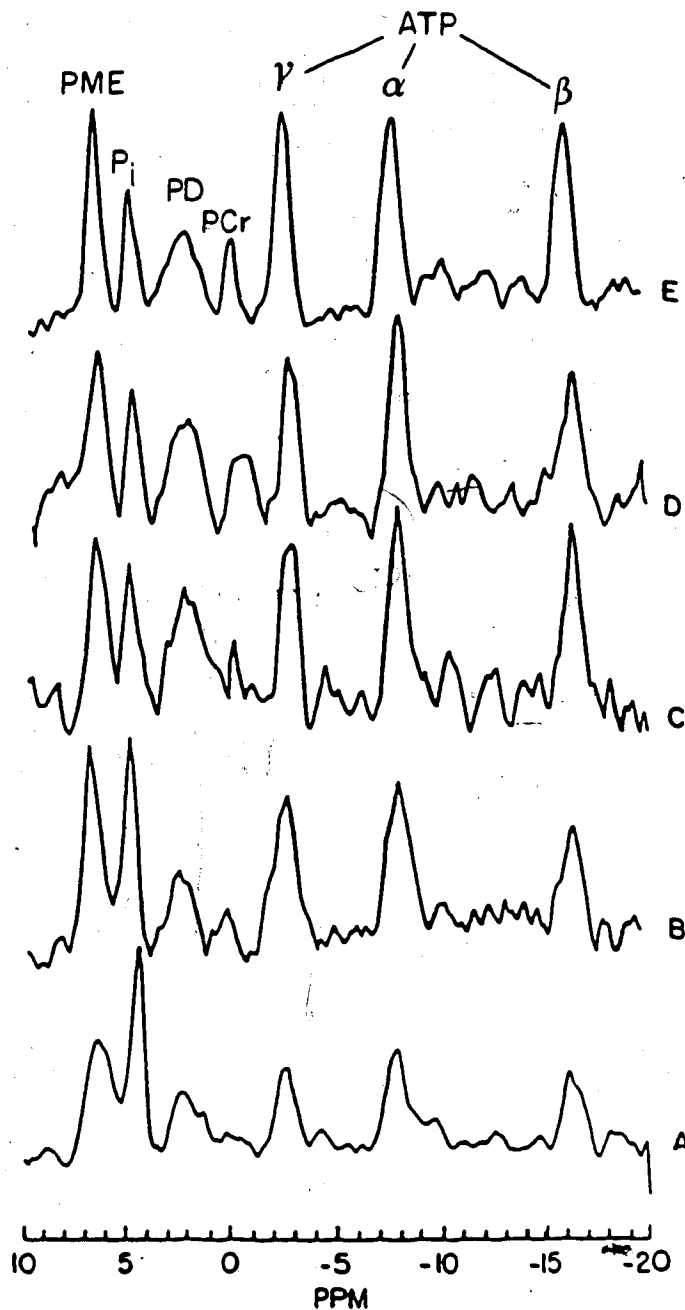


Fig. 3.22

Time course of the changes in ^{31}P metabolites in the rat kidney implanted with tumor cells after administration of a single dose of cyclophosphamide (150 mg/kg I.V.). $t_r=1.0$ sec, $\text{NS}=1024$. The spectra are not corrected for saturation effects. (A) day 0, before drug (pH 6.76); (B) 2 hrs after drug (pH 7.20); (C) day 2 after drug (pH 7.35); (D) day 4 after drug (pH 7.25); (E) day 5 after drug (pH 7.31).

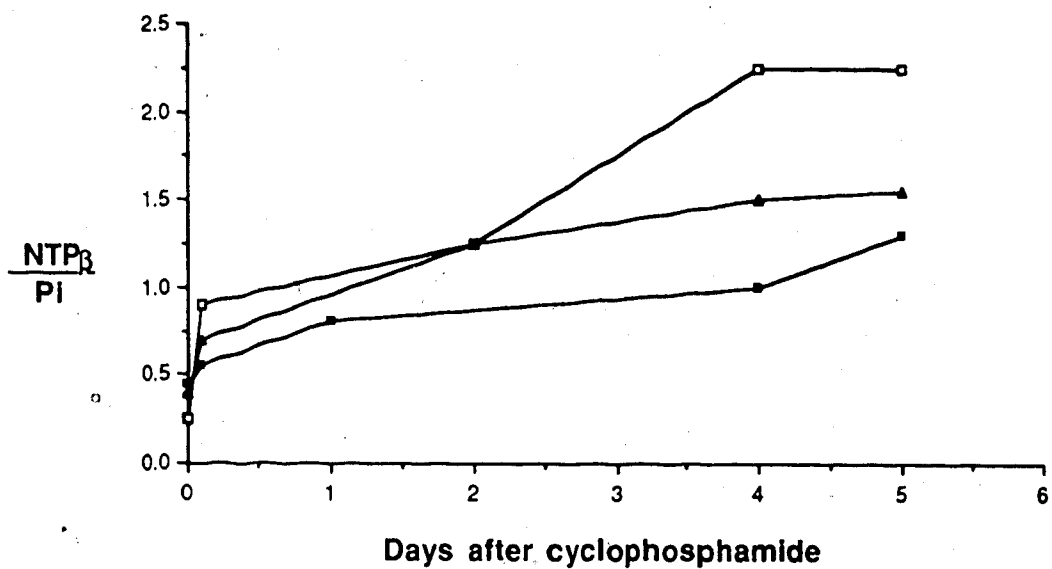


Fig. 3.23 The NTP β /Pi ratio of Walker sarcoma as a function of time after treatment with cyclophosphamide (150 mg/kg I.V.).

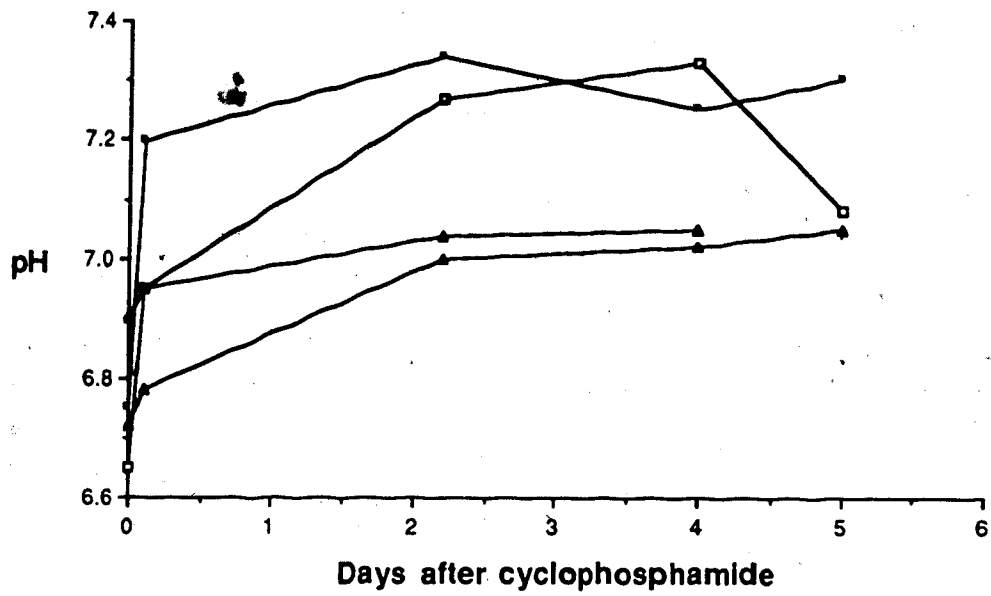


Fig. 3.24 Variation in pH of the tumor after treatment with cyclophosphamide.

which revealed a striking increase in PCr (33), the Walker sarcoma exhibited only a slight decrease in Pi and a slight increase in PCr. The presence of an intense Pi peak is indicative of metabolically inactive cells. The disappearance of the Pi observed by Ng et al after treatment with the drug in the RIF-1 tumor may be due to removal of the dead tumor cells, leaking of Pi out of the cells, or association of Pi with macromolecules. Localization techniques were not implemented in this study. The fact that only a slight decrease is observed in the ^{31}P spectra of the Walker sarcoma suggests that processes such as lysis and phagocytosis which remove dead tumor cells are not as efficient in the Walker sarcoma as compared to the RIF-1 tumor. The tumor mass was not determined, but did not appear on visual examination to regress.

The ^{31}P spectra of normal rat kidney and muscle were not affected by the drug. This result is consistent with that of Naruse et al (90) and suggests preferential activity of the drug against the tumor.

Naruse et al (90), (91) examined the effects of cyclophosphamide on the ^{31}P spectra of a number of neuroectodermal tumors of rat and human origin subcutaneously implanted in rats. The tumors were studied at a late stage of growth and doses approximating the LD_{50} were administered intravenously. The spectra of the living tumors were rapidly

transformed to give the spectral characteristics of dead tumors. The ATP resonances decreased in intensity with a corresponding increase in Pi exactly the opposite effect to that which we have observed in the Walker sarcoma.

It appears that the spectroscopic response of different tumors to cyclophosphamide varies widely and may be the result of the metabolic response of the tumor, differences in or the absence of the spatial localization techniques employed, and/or the dose, time and mode of administration of the antineoplastic drug.

With hindsight, histological studies of the tumor at different stages post-injection should have been performed to estimate any reduction in the extent of tumor growth, as a result of administration of the drug.

Investigations of the state of oxygenation and vascularization of the tumor during untreated growth and following chemotherapy would provide an index with which to compare the observed spectral changes. Moreover, dose response curves for the drug could be determined and correlated with the therapeutically induced spectral changes.

To determine if the spectral changes reflect the action of the drug on the DNA, alterations in the rate of DNA synthesis could be determined by monitoring the uptake of ^3H thymidine in the tumor cells.

Depth pulse spectral editing techniques could be

employed to monitor the changes in the relative concentrations of lactate before and after treatment with the drug. These values could then be compared with the observed changes in tumor pH.

Our studies have demonstrated that the response of a particular region of a tumor can be monitored by ^{31}P NMR. A major requirement in clinical oncology is a non-invasive technique for monitoring tumor metabolism and tumor response to therapy. Studies in animals (31,32,33) and in a few patients (52,124) indicate that the response of tumors to chemotherapy is accompanied by distinct and rapidly detectable changes in its ^{31}P spectral properties. The mechanisms underlying these spectroscopic changes remains to be elucidated.

4. CONCLUSIONS

Magnetic resonance applications to biological and clinical problems have grown steadily in recent years. The advantages of the application of NMR to investigations of metabolism are that the method is non-destructive, non-invasive, and measurements can be made on the tissues in situ in their normal living state.

The spectra of in vivo tumors illustrate the sensitivity of the ^{31}P NMR spectrum to detect progressive changes in the bioenergetic state of tumor tissue. The spectra yield information on the cellular metabolite levels, changes in the metabolic pathways, and the intracellular pH. The presence and intensity of the detected resonances depends on the characteristics of the cell type from which the tumor originated, on its degree of growth, and the extent of its vascularization.

NMR studies of tumors are still in their initial stages. Previous investigations of tumor metabolism were performed on tumors implanted subcutaneously in animals. The NMR signals were excited using a single radiofrequency pulse and were therefore acquired from a region localized solely by placement of the coil, by its diameter, and by control of the pulse length. This method has been used in the vast majority of in-vivo NMR

metabolic studies but in no way does it provide adequate localization. The resulting ^{31}P spectrum represents a spatial average over the total volume of the tissues sampled, a volume which contains both tumor and surrounding tissues, each of which contributes to the overall signal.

We have improved on the previous experimental technique by making use of surgical exposure on the one hand, and depth pulse localization techniques on the other, in order to ensure the accurate assignment of the spectrum to a specific region within the tumor. This has enabled us to evaluate the response of the tumor to metabolic insults in a far more precise way than had previously been possible. Moreover, by generating images of the sensitive volume we were able to provide the reassurance (lacking in previous studies) that the spectra obtained did not contain unwanted contributions from surrounding tissue (Fig 3.6 and Fig 3.7).

Employing the depth pulse sequences we were able to discriminate between different regions of the kidney (Fig. 3.18), and between healthy and damaged tissue (Fig. 3.19). Because the time required for a measurement was 5 minutes, we could make serial measurements every 5 minutes, therefore, we were able to monitor metabolic processes occurring over periods greater than 5 minutes.

Our results on the effects of a modest ischemic

insult to the normal rat kidney indicated a decrease in ATP levels with a corresponding increase in Pi and a decrease in renal pH followed by a recovery to control values within 30 minutes (Fig. 3.15). This shows that we were able to monitor a precise region of tissue with an acquisition time of 5 minutes, and thereby follow the metabolic changes that occur over this period greater than 5 minutes. The kidney implanted with tumor cells when rendered ischemic demonstrated a similar decrease in pH and ATP levels but with no subsequent recovery to control values. These results indicate a disruption of the vascular system of the tumor.

Because of our ability to implement precision localization we were able to observe the serial expansion of a tumor through the predefined region and show that progressive tumor growth typically resulted in an acidotic shift in pH, an increase in Pi and a decrease in the high energy phosphates. This confirms Warburg's hypothesis that tumor cells are more hypoxic than normal tissue and are characterized by a high rate of lactate formation (99). *Again, by observing the same precise tumor region following treatment with cyclophosphamide, we were able to demonstrate that this therapy resulted in a reversal of the spectral characteristics to a more "aerobic like" state, i.e., an increase was observed in tumor pH and in the relative concentrations of ATP, PCr, and PME, together with a slight decrease in Pi when

compared with spectra obtained prior to the treatment. This shows the response of a particular region of the Walker sarcoma to the antineoplastic agent.

In spite of its considerable promise for monitoring phosphate containing metabolites in vivo, ^{31}P spectroscopy does however suffer from some technical limitations. As an analytical technique it is relatively insensitive and quantitative information is limited to only a few of the more abundant metabolites. In addition to signal to noise problems, the ability of ^{31}P NMR to accurately quantify the amplitudes of the resonances, a prerequisite for the monitoring of the absolute NMR visible concentrations of the ^{31}P metabolites, is also hampered by the variations in T_1 between metabolites and between different environments in a heterogeneous sample. Additional work is clearly required to improve both of these situations.

Although the ^{31}P spectra are relatively simple and the resonances readily assigned, the interpretation of the changes in the ^{31}P spectra is often sometimes quite difficult to make. This is due in part to the number of contributing mechanisms which may be responsible for the observed changes and also to the experimenters inability to manipulate many of the in vivo variables which can control these contributory mechanisms.

Ideally, to obtain an accurate account of metabolic processes, metabolism of the tissue should be monitored

in vivo without surgical intervention. ^1H images (Fig 3.5) have demonstrated the ability of the depth pulse sequences to suppress surface layer signals. For the non-invasive monitoring of metabolism, the depth pulse sequences should be employed without surgical exposure of the tumor and the resulting ^{31}P spectrum compared to that obtained with surgical exposure. Such experiments will provide validation required for future in vivo work.

REFERENCES

- 1 Adams, D.A., Denardo, G.L., Denardo, S.J.,
Conboy, C.B., Bradbury, E.M., (1985)
 ^{31}P surface coil NMR analysis of metabolic
studies in KHJJ tumors. *Mag. Res. in Med.*
2 (5) 419-427.
- 2 Alder, S., Shoubridge, E., Radda, G., (1984)
Estimation of Cellular pH gradients with
 ^{31}P NMR in intact rabbit renal tubular
cells. *Am.J. Physiol.* 247 C188-196.
- 3 Allen, P.S., (1983) Imaging by nuclear magnetic
resonance. *Sci. Prog. Oxf.* 68 487-501.
- 4 Ackerman, J., Bore, P., Gadian, D., (1980)
NMR studies of metabolism in perfused
organs. *Phil. Trans. R. Soc. Lond.*
289 425-
- 5 Ackerman, J.J.H., Grove, T.H., Wong, G.G., Gadian,
D.G., Radda, G.K., (1980) Mapping of
metabolites in whole animals by ^{31}P
NMR using surface coils. *Nature* 283
167-170.
- 6 Ackerman, J., Lowry, M., Radda, G., Ross, B., Wong,
G., (1981) The role of intracellular pH
in regulation of ammoniogenesis: ^{31}P NMR
studies of the isolated perfused rat
kidney. *J. Physiol.* 319 65-79.
- 7 Balaban, D., Gadian, D., Radda, G., (1981)
Phosphorus NMR study of the rat kidney in
vivo. *Kidney International.* 20 575-579.
- 8 Balaban, R.S., Knepper, M.A., (1983) Nitrogen
 ^{14}N NMR spectroscopy of mammalian tissues.
Am.J. Physiol 245 C439-444.
- 9 Barany, M., Glonek, T., (1984) Identification of
diseased states by ^{31}P NMR. In: *Phosphorus
 ^{31}P principles and applications.* ed. D.G.
Gorenstein. 512-544, Academic Press, New
York.
- 10 Battocletti J., (1984) Medical Applications of
NMR Spectroscopy. 1. Clinical applications
of ^{31}P NMR. *CRC Reviews in Biomed.
Engin.* 10 (1) 1-25.

- 11 Bendall, M.R., (1984) Surface coils and depth resolution using the spatial variation of radiofrequency field. In. Biological Magnetic Resonance ed. T. James and A. Margulis. p.99-126. Radiology Research and Education Foundation, San Francisco.
- 12 Bendall, M.R., (1984) Elimination of high flux signals near surface coils and field gradient sample localization using depth pulses. J. Mag. Res. 59 406-429.
- 13 Bendall, M.R., Gordon, R.E., (1983) Depth and refocusing pulses designed for multipulse NMR with surface coils. J. Mag. Res. 53 365-385.
- 14 Bore, P.J., Chan, L., Gadian D., Radda, G., Ross, B., Styles, P., Taylor D. (1982) Non-invasive pH measurements of human tissue using ^{31}P NMR. In Intracellular pH its measurement, regulation and utilization in cellular functions. p. 527-535 ed. R. Nuccitelli and D. Deamer. p. 527-535 Liss Inc., New York.
- 15 Bottomley, P., Kogure, K., Namon, R., Alonso, O. (1982) Cerebral energy metabolism in rats studied by ^{31}P NMR using surface coils. Mag. Res. Imag. 1 81-85.
- 16 Bottomley, P., Foster, T., Darrow, R., (1984) Depth-resolved Surface Coil Spectroscopy (DRESS) for in vivo ^1H , ^{31}P and ^{13}C NMR. J. Mag. Res. 59 338-342.
- 17 Boulanger, Y., Vinay, P., Viet, M.T.P., Guardo, R., Desroches, M., (1985) An improved Perifusion System for NMR Study of Living Cells 495-500.
- 18 Boyd, W., (1970) A textbook of Pathology pg 218 Leu and Febiger, Philadelphia.
- 19 Berger, W.A., Henderson, J.F., (1983) Cell ATP. vol 5 in the Wiley Series Transport The Life Sciences. ed. E. Bittar John Wiley and Sons, 114-144, New York.
- 20 Burt, C.T., Glonek, T., Baranay, M., (1976) Analysis of phosphate metabolites, the intracellular pH and state of ATP in intact muscle by NMR. J. Biol Chem. 251 2584-91.

- 21 Burt, C.T., Cohen S.M., Barany, M., (1979) Analysis of intact tissue with ^{31}P NMR. Ann. Rev. Biochem. 8 1-25.
- 22 Burt, C.T., (1985) Phosphodiesterases and NMR a tale of rabbits and chickens. TIBS 10 (10) 404-406.
- 23 Carpinelli, G., Maddaluno, G., Podo, F., Proietti, L., Santurbando, F., Belardelli, F., (1983) ^{31}P NMR studies on subcutaneous tumors in mice injected with friend erythroleukemia cells. from the San Francisco meeting of the Society of Magnetic Resonance in Medicine pg 77.
- 24 Chan, L., Radda, B., Ross, B. (1983) ^{31}P NMR of Renal Cell Carcinoma In Intact Ischemic Human Kidney. Soc. Mag. Res. In Med. 3rd Annual meeting, San Francisco. pg 89
- 25 Cohen, J.S. (1985) ^{31}P NMR studied of Cell Metabolism. Magnetic Resonance in Biology And Medicine. ed. G. Govil, C. Khetrapol, A. Saran. Tata Mc Graw Hill Publ. Co. New Delhi.
- 26 Currie, G., Currie, A., (1982) Cancer: the biology of malignant tissue. Edward Arnold Publishing Co. Ltd. 60-78, London.
- 27 Damadian, R., (1971) Tumor detection by NMR. Science 171 1151-1153.
- 28 Dawson, J., Gadian, D., Wilkie, D., (1977) Studies of living, contracting muscle by ^{31}P NMR. In: NMR in Biology. ed. Dweck, Campbell, Richards, and Williams Academic Press, 703-735.
- 29 Degani, H., Petroff, O.A., Prichard, J.W., Alder, J.R., Shulman, R.G., (1985) In vivo ^{31}P Magnetization Transfer studies of creatine kinase in rabbit brain. Soc. of Mag. Res. In Med. 4th Annual meeting, Aug. 19-23. London, pg 457.
- 30 Emanuel, N.M., (1982) Kinetics Of Experimental Tumor Processes. Pergamon Press, New York.
- 31 Evanochko, W., Ng, T.C., Glickson, J., Durrant, J., Corbett, T., (1982) Human tumors as examined by in vivo ^{31}P NMR in athymic

mice. BBRC 109 1346-1352.

- 32 Evanochko, W., Ng, T.C., Lilly, N., Lawson, A., Corbett, T., Glickson, J., (1983) In vivo ^{31}P NMR study of the metabolism of murine mammary 16/c adenocarcinoma and its response to chemotherapy and x-radiation and hyperthermia. PNAS 80 224.
- 33 Evanochko, W.T., Ng, T.C., Glickson, J.D., (1984) Application of in vivo NMR spectroscopy to cancer. Mag.Res. In Med. 1 508-534.
- 34 Evanochko, W.T., Sakai, T.T., Ng, T.C., Krishna, N.R., Kim, H.D., Zeidler, R.B., Ghanta, V.K., Brockman, R.W., Schiffer, L.M., Braunschweiger, P.G., Glickson, J.D., (1984) NMR studies of in vivo RIF-1 tumors. Analysis of perchloric acid extracts and identification of ^1H , ^{31}P , and ^{13}C resonances. B.B.A. 805 104-116.
- 35 Evans, F., Kaplan, N., (1977) ^{31}P NMR studies of HeLa cells. Proc. Natl. Acad. Sci. 4909-4913.
- 36 Evelhoch, J.L., Crowley, M.G., Ackerman, J.J.H., (1984) Signal to noise optimization and observed volume localization with circular surface coils. J. Mag.Res. 56 110-124.
- 37 Evelhoch, J.L., Sapareto, S.A., Nussbaum, G.H., Ackerman, J.J.H., (1986) Substrain dependence of RIF-1 tumor composition in C3H mice. In: Magnetic Resonance In Cancer. ed. P.Allen, D. Boisvert, B. Lentle. Pergamon Press, 93-94. Toronto.
- 38 Farrar, T.C., Becker, E.D., (1971) Pulse and Fourier Transform NMR. Introduction to theory and methods. Academic Press N.Y.
- 39 Foster, M.A., (1984) Magnetic Resonance in Medicine and Biology. Pergamon Press 108-135, New York.
- 40 Freeman, D., Bartlett, S., Radda, G., (1983) Energetics of sodium transport in the kidney by saturation transfer ^{31}P NMR. B.B.A. 762 325-336.
- 41 Gadian, D., Radda, G., Dawson, M.J., Wilkie, D.,

- (1982) pH measurements of cardiac and skeletal muscle using ^{31}P NMR. In: Intracellular pH its measurement, regulation, and utilization in cellular functions. ed. R.Nuccitelli and D.Deamer p. 61-77, Liss Inc., New York.
- 42 Gadian D.G. (1982) Nuclear Magnetic Resonance And Its Application To Living Systems. Clarendon Press, Oxford.
- 43 Gadian, D.G., Radda, G.K., Richards, R.E., Seeley P.J., (1979) ^{31}P NMR in living tissue: the road from a promising to an important tool in biology. In: Biological Applications Of Magnetic Resonance. ed. R.G. Shulman, Academic Press, New York.
- 44 Gillies, R.J., Ogino T., Shulman, R.G., Ward, D.C., (1982) ^{31}P NMR evidence for the regulation of intracellular pH by Ehrlich Ascites Tumor cells. *J. Cell. Biol.* 95 24-28.
- 45 Gillies, R., Alger, J., den Hollander, J., Shulman, R., (1982). Intracellular pH measured by NMR methods and results. In: Intracellular pH its measurement, regulation, and utilization in cellular functions. ed. R.Nuccitelli and D.Deamer. p.79-104, Liss Inc., New York.
- 46 Glickson, J.D., Evanochko, W.T., Sakai, T.T., Ng, T.C., (1986) In vivo NMR studies of RIF-1 tumors. In: Magnetic Resonance in Cancer ed. P.S. Allen, D.P. Boisvert, B.C. Lentle, 71-82, Pergamon Press, Toronto.
- 47 Goldacre, R.J., Sylven, B., (1962). On the access of blood-borne dyes to various tumor regions. *Br. J. Cancer* 16 306-322.
- 48 Gordon, R., Hanley, P., Shaw, D., Gadian, D., Radda, G., Styles, P., Bore, P., Chan, L., (1980) Localization of metabolites in animals using ^{31}P Topical Magnetic Resonance. *Nature* 287, 736-738.
- 49 Gordon, R., Topical Magnetic Resonance (1982) *Biosci. Rep.* 2 (9) 701-706.
- 50 Griffiths, J.R., (1981) ^{31}P NMR investigation of solid tumors in the living rat. *Biosci. Reports.* 1 319-325.

- 51 Griffiths, J.R., (1982) NMR studies of Tumors. Biosci. Reports 2 (9) 719-725.
- 52 Griffiths, J., Cady, E., Edwards, R., M^cCready, V., Wilkie, D., Wiltshaw, E., (1983) ³¹P NMR studies of a human tumor in situ. Lancet. 1435 June 25, 1983.
- 53 Grove, T., Ackerman, J., Radda, G., Bore, P., (1980) Analysis of rat heart in vivo by phosphorus NMR. PNAS 77 299-302.
- 54 Gullino, P., Grantham, F.H., (1961) Studies on the exchange of fluids between host and tumor. A method for growing tissue isolated tumors in laboratory animals. Journ. of the Natl. Cancer Inst. 27 (8) 679-689.
- 55 Gullino, P.M., Grantham, F.H., (1961) Studies on the exchange of fluids between host and tumor. The blood flow of Hepatomas and other tumors in rats and mice. J. Natl. Cancer Inst. 27 1465-1491.
- 56 Gullino, P.M., Grantham, F.H., Courtney, A.H., (1967) Utilization of oxygen by transplanted tumors in vivo. Cancer Res. 1020-1030.
- 57 Gullino, P. (1976) In vivo utilization of oxygen and glucose by neoplastic tissue. In: Advances In Experimental Medicine and Biology. 75. Oxygen transport to tissue II ed. J. Grote, D. Repeau, G. Theus. 521-536. Plenum Press. New York.
- 58 Gullino, P.M., (1980) Influence of blood supply on thermal properties and metabolism of mammary carcinomas. Annals of the New York Academy of Sciences. 335 ed. R.K. Jain, P. Gullino. 1-18, Publ. New York Academy of Sciences.
- 59 Gupta, R., Yushok, W., (1980) Non-invasive ³¹P NMR probes of free Mg²⁺, MgATP, and MgADP in intact ehrlich ascites tumor cells. Proc. Natl. Acad. Sci. 77 2487-2491.
- 60 Hanstock, C.C., Bendall, R.M., Heatherington, H.P., Boisvert, D.P., Allen, P.S., (1986) Localized in vivo ¹H spectroscopy using DEPTH pulse spectral editing.

J. Mag. Res. (in press)

- 61 Harris, B., (1962) Biochemistry of the cancer cell. pg 4-11. Academic Press, New York.
- 62 Harris, R.K., (1983) Nuclear Magnetic Resonance Spectroscopy. Pitman Books Ltd. London.
- 63 Harrison, E.F., Fuquay, M.E., Hunter, H.L., (1983) Effect of N-acetylcysteine on the anti-tumor activity of cyclophosphamide against Walker 256 carcinosarcoma in rats. Seminars in Oncology 10 1, 25-28.
- 64 Harrison, R.J., Holmes, R.L., (1981) ed. Progress in Anatomy. Cambridge Univ Press, London.
- 65 Hebel R., Stromberg, M., (1976) Anatomy of the laboratory rat. The Williams and Wilkins Co. Baltimore. pg 62.
- 66 Hoult, D.I., Busby, S.J.W., Gadian, D.G., Radda, G.K., Richards, R.E., Seeley, P.J. (1974) Observations of tissue metabolites of tissue metabolites using ^{31}P NMR. Nature 252 285-287.
- 67 Iles, R.A., Stevens, A.N., Griffiths, J.R., (1982) NMR studies of metabolites in living tissue. Prog. in NMR Spec. 15 49-200.
- 68 Illingworth, J.A. (1981) A common source of error in pH measurements. Biochem J. 195 259-262.
- 69 Ingwall, J.S., Kobayashi, K., Bittl, J.A., (1984) Creatine kinase kinetics in muscle measured with ^{31}P NMR magnetization transfer. Society of Mag. Res. in Med. 3rd annual meeting. Aug 13-17. New York pg 369.
- 70 Irving, M.G., Simpson, S.J., Field, J., Doddrell, D.M., (1985) Use of high resolution ^{31}P labelled topical magnetic resonance spectroscopy to monitor in vivo tumor metabolism in rats. Cancer Res. 45 481-486.
- 71 Jacobus, W., Pores, I., Lucas, S., Kallman, C., Weisfeldt, M., Flaherty, J. (1982) The role of intracellular pH in the control of normal and ischemic myocardial contractility; A ^{31}P NMR and mass spectrometry study. In Intracellular pH: its

160
measurements, regulation, and utilization
in cellular functions. ed. R. Nuccitelli
and D. Deamer. p. 537-565, Liss Inc, N.Y.

- 72 Kido, C., (1970) Angiography of experimental
transplantable tumors. Invest. Radol.
5 341-347.
- 73 Koeze, T.H., Lantos, P.E., Iles, R.A., Gorden,
R.E. (1984) In vivo NMR spectroscopy of
a transplanted brain tumor. BR. J. Cancer
49 357-361.
- 74 Koretsky, A.P., Wang, S., Murphy-Boesch, J.,
Klein, M.P., James, T.L., Weiner, M.W.,
(1983) ^{31}P NMR spectroscopy of rat organs
in situ using chronically implanted
rf coils. PNAS 80 7491-7495.
- 75 Koretsky, A., James, T., Weiner, M., (1984).
Measurement of ATP turnover in the rat
kidney in vivo by ^{31}P NMR. Kid. Internal.
25 (1) 1984. Abstract.
- 76 Lehninger, A.L., (1976) Biochemistry The
molecular basis of cell structure and
function. pg 417ff. Worth Publishers, Inc.
New York.
- 77 Lilly, M.B., Ng, T.C., Evanochko, W.T.,
Katholi, C.R., Kumar, N.G., Elgavish, G.A.,
Durrant, J.R., Hiramoto, R., Ghanta, V.,
Glidkson, J.D., (1984) Loss of high energy
phosphates following hyperthermia
demonstrated by in vivo ^{31}P NMR
spectroscopy. Cancer Research 44 633-638.
- 78 Luyten, P., Marien, J.H., Sijtsma, B., Den
Hollander J. (1986) Solvent-Suppressed
Spatially Resolved Spectroscopy. An
approach to High Resolution NMR on a
Whole Body MR system. J. Mag. Res. 67
148-155.
- 79 Manganaro, M., Miccheli, A., Delfini, M.,
Gaudio, E., Narinozzi, G., Conti, F.,
(1985) ^{31}P Metabolites and organ
preservation. ^{31}P NMR study on rat
kidney. Cellular and Molec. Biol.
31 (2) 89-96.
- 80 Maris, J., Evans, A., McLaughlin, A., D'Angio, G.,
Bolinger, L., Manos, H., Chance, B., (1985)
 ^{31}P NMR spectroscopic investigation of

human neuroblastoma *in situ*. New England
Journal of Medicine 1500, June 6, 1985.

- 81 Mathews, P.M., Bland, J.L., Gadian, D.G., Radda,
G.K., (1981) The steady state rate of ATP
synthesis in the perfused rat heart
measured by ^{31}P NMR saturation transfer.
BBRC 103 1052-1059.
- 82 Matson, G.B., (1984) Measurement of Longitudinal
Relaxation times using surface coils.
J. Mag. Res. 56 200-206, 1984.
- 83 Mattsson, J., Applegren, L., Hamberger, B.,
Peterson, H.I., (1979) Tumor vessel
innervation and influence of vasoactive
drugs on tumor blood flow. In: Tumor Blood
Circulation. H.I. Peterson ed. CRC Press
129-135. Florida.
- 84 Milne, E.N.C., Margulis, A.R., Noonan C.D.,
Stroughton, J.T., (1967) Histologic type
specific vascular patterns in rat tumors.
Cancer 20 1635-1646.
- 85 Merck Index, 8th edition (1968) pg 313
Merck and Co Inc. New York.
- 86 Meyer, R.A., Brown, T.R, Kushmerick, M.J.,
(1985) Phosphorus nuclear magnetic
resonance of fast and slow twitch muscle.
Am. J. Physiol. 248 279-287.
- 87 Miller, B.E., Miller, F.R., Heppner, G.H., (1981)
Interactions between tumor subpopulations
affecting their sensitivity to the anti-
neoplastic agents cyclophosphamide and
methotrexate. Cancer Res. 41 4378-4381.
- 88 Moon, R.B., Richards, J.H., (1973) Determination
of intracellular pH by ^{31}P magnetic
resonance. J. Biol. Chem. 248 7276-7278.
- 89 Muller, S., Abe, W.P., Seelig, J., (1985) NMR
imaging and volume selective spectroscopy
with a surface coil. J. of Mag. Res.
63 530-543.
- 90 Naruse, S., Hirakawa, K., Horikawa, Y., Tanaka,
C., Higuchi, T., Ueda, S., Nishikawa, H.,
Watari, H., (1985) Measurements in *in vivo*
neuroectodermal tumors for the evaluation
of the effects of chemotherapy. Can. Res.
45 2429-2433.

- 91 Naruse, S., Horikawa, Y., Tanaka, T., Higuchi, T., Ueda, S., Hirakawa, K., Nishikawa, H., Watari H., (1985) Observations of energy metabolism in neuroectodermal tumors using in vivo ^{31}P NMR. Mag. Res. Imig. 3 117-123.
- 92 Navon, G., Ogawa, S., Shulman, R., Yamane, T., (1977) ^{31}P NMR studies of Ehrlich ascites tumor cells. Proc. Nat. Acad. Sci. 74 87-91.
- 93 Navon, G., Navon R., Shulman, R., Yamane, T., (1978) Phosphate metabolites in lymphoid friend erythroleukemia and HeLa cells observed by high resolution ^{31}P NMR. PNAS 75 891-895.
- 94 Ng, T.C., Evanochko, W., Hiramoto, R., Ghanta, T., Carbett, T., Glickson, J.D., (1982) ^{31}P NMR spectroscopy of in vivo tumors. J. Mag. Res. 49 271-286.
- 95 Ng, T.C., Glickson, J.D., Bendall, M.R., (1984) Depth pulse sequences for surface coils: spatial localization and T₁ measurements. Mag. Res. In Med. 1 450-462, 1984.
- 96 Nuccitelli, N., Heiple, J., (1982) Summary of the evidence and discussion concerning the involvement of pH in the control of cellular functions. In Intracellular pH its measurement, regulation and utilization in cellular functions. ed. R.Nuccitelli and D.Deamer. 567-586 Liss Inc. New York.
- 97 Ordidge, R.J., Bendall, M.R., Gordon, R.E., Connolly, A., (1983) Volume selection for in-vivo biological spectroscopy. Magnetic Resonance In Biology and Medicine. ed. G.Govil, A.Saran., C.Khetrapol, p. Tata McGraw Hill Pub. Co., New Delhi.
- 98 Ordidge, R.J., Connelly, A., Loham, J.A.D., (1986) Image selected in vivo spectroscopy A New Technique For Spatially Selective NMR Spectroscopy. Mag. Res. In Med. 3
- 99 Peterson, H.I. Tumor Blood Circulation. Angiogenesis, Vascular morphology and Blood flow of experimental and human tumors. CRC Press Inc. Florida 1979.

- 100 Radda, G., Ackerman, J., Bore, P., Sehr, P., Wong, G., (1980) ^{31}P NMR studies on kidney intracellular pH in acute renal acidosis. *J. Bioch* 12 277-281.
- 101 Rhodes, A., Jentoft, J., Barr, R., Robinson, A., (1983) ^{31}P NMR studies of energy metabolism in perfused rat kidney. *J. of Surgical Res.* 35 373-382.
- 102 Rosenoer, V.M., Mitchley, B.C.V., Roe, F.J.C., Connors, T.A. (1966) Walker carcinosarcoma 256 in study of anticancer agents; method for simultaneous assessment of therapeutic value and toxicity. *Cancer Res.* 26 937-941.
- 103 Ross, B., Marshall, V., (1984) ^{31}P NMR examination of perfused human renal carcinomas. *Kidney international* 25 (1) 268.
- 104 Ross, B., Marshall, V., Smith, M., Bartlett, S., Freeman, D., (1984) Monitoring response to chemotherapy of intact human tumors by ^{31}P NMR. *Lancet* 8378 641-646.
- 105 Ross, B., Freeman, D., Chan, L., (1986) Contributions of nuclear magnetic resonance to renal biochemistry. *Kidney International* 29 131-141.
- 106 Ruddon, R.W., (1981). *Cancer Biology*. Oxford University Press.
- 107 Schleich, T., Matson, G.B., Garwood, M., Acosta, G., (1984) Spatial localization of tissue metabolites by ^{31}P NMR rotating frame zeumatography. *Biophys. Journal* 45 321a.
- 108 Scott, K., (1984) Localization techniques for non-proton imaging or nuclear magnetic resonance spectroscopy *in vivo*. *Biological Magnetic Resonance*. ed. T. James and A. Margulis. p.79-97. Radiology Research and Education Foundation, San Francisco.
- 109 Sehr, P., Radda, G., Bore, P., Sells, R., (1977) A model kidney transplant studied by ^{31}P NMR. *BBRC* 77 195-
- 110 Sehr, P., Bore, P., Papatheofanis, J., Radda, G., (1979) Non-destructive measurements of metabolites and tissue pH in the kidney by ^{31}P NMR. *Br. J. of Exptl. Pat.* 60 632-641.

- 111 Seo, Y., Murakami, M., Watari H., Imai, Y., Yoshizaki, H., Nishikawa, Morimoto, T., (1983) Intracellular pH determination by a ^{31}P NMR technique. The second dissociation constant of phosphoric acid in a biological system. J. Biochem. 94 729-734.
- 112 Shaw, D., (1981) In vivo chemistry with NMR Nuclear Magnetic Resonance Imaging In Medicine L. Kaufman, L. Crooks, A. Margulis p.147-183 Igaku-Shoin, Tokyo.
- 113 Shoubridge, E., Briggs, R., Radda, G., (1982) ^{31}P NMR saturation transfer measurements of the steady state rates of creatine kinase and ATP synthetase in the rat brain. FEBS LETTS. 140 288.
- 114 Sostman, H.D., Armitage, I.M., Fisher, J.J., (1984) NMR in cancer: High resolution spectroscopy of tumors. Magnetic Resonance Imaging 2 265-278.
- 115 Stubbs, M., Freeman, D., Ross, B.D., (1984) Formation of NMR invisible ADP during renal ischemia in rats. Biochem J 224 241-246.
- 116 Tannock, I., (1982) Response of aerobic and hypoxic cells in a solid tumor to adriamycin and cyclophosphamide and interaction of the drugs with radiation. Cancer Res. 4921-4926.
- 117 Tew, K.D., (1982) Comparative cytotoxic properties of Ifosfamide and cyclophosphamide in rat solid tumor and normal tissues. Seminars in Oncology 9 (4) Suppl 1 24-27.
- 118 Warren, B.A., (1970) The ultrastructure of the microcirculation at the advancing edge of Walker sarcoma. Microvascular Res. 2 443-453.
- 119 Weber, G., Enzymology of Cancer Cells. (1977) (second of two parts) The New England Journal Of Medicine 541-551.
- 120 Wehrli, F.W., (1985) Localization methods for NMR spectroscopy in vivo. Circulation 72 (suppl iv) 97-102.
- 121 Weisman, I., Bennett, L., Maxwell, L., Woods, M.,

- Burk, D., (1972) Recognition of cancer in vivo by NMR. Science 178 1288.
- 122 Yushok, W., Gupta, R., (1980) Phosphocreatine in Ehrlich ascites tumor cells detected by non-invasive ^{31}P NMR spectroscopy. Biochem. Biophys. Res. Commun. 95 73-81.
- 123 Zaner, K., Damadian, R., (1975) ^{31}P as a nuclear probe for malignant tumors. Science 189 729-731.
- 124 Zimmerman, R.A., Bottomley, P.A., Edelstein, W.A., Hart, H.R., Redington, R.W., Bilal, L.T., Grossman, R.I., Goldberg, H.I., Bello, L., Kressel, H., (1985) Proton imaging and phosphorus spectroscopy in a malignant glioma. A.J.N.R. 6 109-110.
- 125 Deutz, N.E., Bovee, W.M., Chamuleau, R.A., (1986). Brain ^{31}P NMR spectroscopy in the conscious rat. J. Neuroscience Methods 16 157-161.